Ultra-High Speed Switching Functionalities using none-linear fibres

Galili, Michael; Jeppesen, Palle; Oxenløwe, Leif Katsuo; Clausen, Anders

Publication date:
2007

Document Version
Publisher's PDF, also known as Version of record

Ultra-High Speed Switching Functionalities using Non-Linear Fibres

160 - 640 Gbit/s all-optical signal processing

Ph.D. Thesis
by
Michael Galili

July 23 2007

COM•DTU
Department of Communications, Optics & Materials
Technical University of Denmark
Building 343
2800 Kgs. Lyngby
DENMARK

Abstract

This thesis deals with optical signal processing of high-speed optical data signals at 160 – 640 Gbit/s. By exploiting non-linear effects in optical fibres several signal processing functionalities are implemented. This includes wavelength conversion of intensity modulated and phase modulated data signals, conversion between intensity and phase modulation, clock recovery for synchronising a receiver to an incoming data signal and finally reduction of timing sensitivity in such high-speed systems. All of the signal processing tasks are performed directly on the optical signal i.e. without converting it into an electrical signal first. In this way it is possible to manipulate signals at much higher speeds, than can be done electronically. All of the investigated signal processing operations are shown to work in high-speed system demonstrations at bit rates up to 640 Gbit/s.

Resumé

Denne afhandling behandler optisk signal-behandling af optiske høj-hastigheds datasignaler ved 160 – 640 Gbit/s. Ved at udnytte ulineære effekter i optiske fibre er adskillige signalbehandlings funktionaliteter implementeret. Dette inkluderer bølgelængdekonvertering af intensitetsmodulerede og fasemodulerede data signaler, konvertering mellem intensitets- og fasemodulation, klokkegenskabelse til at synkronisere en modtager til et indkommende data signal og endelig reduktion af følsomheden overfor timing i sådanne højhastigheds-systemer. Alle signalbehandlings funktionerne bliver udført direkte på det optiske signal dvs. uden at omdanne det til et elektrisk signal først. På denne måde er det muligt at behandle signaler ved meget højere hastigheder, end det er muligt at gøre elektronisk. Det er vist, at alle de undersøgte signalbehandlings funktioner virker i højhastigheds-system demonstrationer ved bit-rater op til 640 Gbit/s.

Acknowledgements

I would like to thank my colleagues in the systems group at COM for many fruitful discussions, and my supervisors Palle Jeppesen, Leif K. Oxenløwe and Anders T. Clausen for their valuable assistance and guidance through this Ph.D. project. A special thank to Hans Christian Hansen Mulvad, Darko Zibar and Leif Oxenløwe for their invaluable assistance during the late nights spent in the lab, and for their constructive input to my thesis work.

I also thank Professor Hans-Georg Weber, Bernd Huettl, Carsten Schmidt-Langhorst, Colja Shubert, Reinhold Ludwig and Alexandre Gual for welcoming me into the systems group at the Heinrich Hertz Institute (HHI) in Berlin, and for helping to make my stay there very enjoyable as well as stimulating and productive. My stay at the HHI was one of the most productive periods during my Ph.D. project. This was primarily due to the unique scientific and technical insight shared with me by all the members of the systems group. An additional and very special thank to Professor Hans-Georg Weber for his very kind assistance during the last days of my stay at the HHI.

I would like to thank Shigeki Watanabe for his series of inspiring and insightful lectures at COM during the fall of 2005. These lectures and the related discussions were a great source of inspiration for many aspects of this work.

On a more personal note, I would like to thank my wife for her great support, especially during the last months of the project. And I would like to thank my daughter for sleeping through the night, almost every night for the last couple of months. Finally I would like to thank all my family for their help and support during the project.

The project Ultra-high speed data rates for future generation internet (UltraNet) (project number 2059-03-0006), which was the frame for my Ph.D. project was sponsored by the Danish research council program

committee for IT-Research under the NABIIT (Nanotechnology, Biotechnology and Information technology) framework. OFS Fitel Denmark and Tellabs Denmark kindly provided some of the equipment needed for the experiments.

I would like to acknowledge the contribution of the external collaborators involved in this work. The long period gratings (LPGs) used for pulse shaping in demultiplexing in chapter 6 were developed in a collaboration between the Institute of Photonics and Electronics in Prague in the Czech Republic and the Institut National de la Recherch Scientifique in Québec in Canada. In particular I would like to thank Radan Slavík for his collaboration and input to this part of the work.

The fibre bragg gratings (FBGs) used for pulse shaping in the retiming demonstration in chapter 6 were manufactured by the Optics Research Centre in Southampton in the United Kingdom. I would like to thank Francesca Parmigiani for her key role in the retiming experiments in chapter 6.

Ph.D. Publications

The following publications have been produced during this Ph.D. project.

[i] M. Galili, L. K. Oxenløwe, D. Zibar, A. T. Clausen, and P. Jeppesen. "160 Gb/s Raman-assisted SPM wavelength converter", in *Proceedings of the European Conference on Optical Communication, ECOC'04*, Stockholm, Sweden, pp. 28–29, Paper Th4.3.1, September 2004 - *post-deadline*

[ii] M. Scaffardi, P. A. Andersen, L. K. Oxenløwe, M. Galili, D. Larsson, K. Yvind, P. Jeppesen, A. Bogoni, P. Ghelfi, and L. Potì. "Performance evaluation of a highly non-linear fibre based NOLM for regeneration up to 160 Gb/s", in *Technical Digest of the IEEE Lasers and Electro-Optics Society Annual Meeting, LEOS'04*, Sydney, Australia, pp. 979–980, Paper ThBB4, November 2004

[iii] M. Galili, L. K. Oxenløwe, D. Zibar, A. Clausen, and P. Jeppesen. "Characterisation of Systems for Raman-Assisted High-Speed Wavelength Conversion", in *Technical Digest of the Conference on Lasers and Electro-Optics, CLEO'05*, Baltimore, Maryland, U.S.A., pp. 288–290, Paper CMQ2, May 2005

[iv] D. Zibar, J. Mørk, L. K. Oxenløwe, M. Galili, and A. T. Clausen. "Timing jitter analysis for clock recovery circuits based on an opto-electronic phase-locked loop (OPLL)", in *Technical Digest of the Conference on Lasers and Electro-Optics, CLEO'05*, Baltimore, Maryland, U.S.A., pp. 458–460, Paper CMZ4, May 2005

[v] L. K. Oxenløwe, D. Zibar, M. Galili, A. T. Clausen, L. J. Christiansen, and P. Jeppesen. "Clock recovery for 320 Gb/s OTDM data using

filtering-assisted XPM in an SOA", in *Technical Digest of the European Conference on Lasers and Electro-Optics, CLEO Europe'05*, Munich, Germany, p. 486, Paper CI3-4-MON, June 2005

[vi] M. Galili, L. K. Oxenløwe, D. Zibar, A. T. Clausen, H.-J. Deyerl, N. Plougmann, M. Kristensen, and P. Jeppesen. "160 Gb/s notch-filtered Raman-assisted XPM wavelength converter", in *Proceedings of the European Conference on Optical Communication, ECOC'05*, Glasgow, Scotland, pp. 113–114, Paper Mo4.5.3, September 2005

[vii] L. K. Oxenløwe, D. Zibar, M. Galili, A. T. Clausen, L. J. Christiansen, and P. Jeppesen. "Filtering-assisted cross-phase modulation in a semiconductor optical amplifier enabling 320 Gb/s clock recovery", in *Proceedings of the European Conference on Optical Communication, ECOC'05*, Glasgow, Scotland, pp. 485–486, Paper We3.5.5, September 2005

[viii] D. Zibar, L. K. Oxenløwe, J. Mørk, M. P. Sørensen, M. Galili, A. T. Clausen, B. M. Sørensen, and P. Jeppesen. "Detailed modelling and experimental characterisation of an ultra-fast optoelectronic clock recovery circuit", in *Proceedings of the European Conference on Optical Communication, ECOC'05*, Glasgow, Scotland, pp. 723–724, Paper We4.P.111, September 2005

[ix] J. Seoane, A. T. Clausen, L. K. Oxenløwe, M. Galili, T. Tokle, and P. Jeppesen. "Enabling technologies for OTDM networks at 160 Gbit/s and beyond", in *Technical Digest of the IEEE Lasers and Electro-Optics Society Annual Meeting, LEOS'05*, Sydney, Australia, pp. 81–82, Paper MG1, October 2005 - *invited*

[x] M. Galili, L. K. Oxenløwe, H. C. H. Mulvad, D. Zibar, A. T. Clausen, and P. Jeppesen. "160 Gb/s Raman-assisted notch-filtered XPM wavelength conversion and transmission", in *Technical Digest of the Optical Fiber Communication Conference, OFC'06*, Anaheim, California, U.S.A., Paper OWW2, March 2006

[xi] D. Zibar, L. K. Oxenløwe, H. C. H. Mulvad, J. Mørk, M. Galili, A. T. Clausen, and P. Jeppesen. "The impact of gating timing jitter on a

160 Gb/s demultiplexer", in *Technical Digest of the Optical Fiber Communication Conference, OFC'06*, Anaheim, California, U.S.A., Paper OTuB2, March 2006

[xii] R. Kjær, M. Galili, L. K. Oxenløwe, C. G. Jørgensen, and P. Jeppesen. "Raman-assisted transmission of 16x10 Gbit/s over 240 km using post-compensation only", in *Technical Digest of the Conference on Lasers and Electro-Optics, CLEO'06*, Long Beach, California, U.S.A., Paper CThP4, May 2006

[xiii] L. K. Oxenløwe, M. Galili, H. C. H. Mulvad, A. T. Clausen, D. Zibar, and P. Jeppesen. "Solutions for ultra-high speed optical wavelength conversion and clock recovery", in *Proceedings of the International Conference on Transparent Optical Networks, ICTON'06*, Nottingham, UK, Paper Tu.D2.3, June 2006 - *invited*

[xiv] L. K. Oxenløwe, M. Galili, H. C. Mulvad Hansen, A. T. Clausen, and P. Jeppesen. "Reduced timing sensitivity in all-optical switching using flat-top control pulses obtained by the optical fourier transform technique", in *International Conference on Photonics in Switching*, Heraklion, Greece, Paper O9.3, October 2006

[xv] M. Galili, L. K. Oxenløwe, H. C. H. Mulvad, A. T. Clausen, and P. Jeppesen. "Raman-assisted XPM wavelength conversion at 320 Gb/s", in *Proceedings of the European Conference on Optical Communication, ECOC'06*, Cannes, France, pp. 333–334, Paper We3.P.106, September 2006

[xvi] C. Schmidt-Langhorst, R. Ludwig, M. Galili, B. Huettl, F. Futami, S. Watanabe, and C. Schubert. "160 Gbit/s all-optical OOK to DPSK inline format conversion", in *Proceedings of the European Conference on Optical Communication, ECOC'06*, Cannes, France, Paper Th4.3.5, September 2006 - *post-deadline*

[xvii] L. K. Oxenløwe, M. Galili, A. T. Clausen, and P. Jeppesen. "Generating a square switching window for timing jitter tolerant 160 Gb/s demultiplexing by the optical Fourier transform technique", in *Proceedings of the European Conference on Optical Communication, ECOC'06*, Cannes, France, pp. 73–74, Paper We2.3.4, September 2006

[xviii] H. C. H. Mulvad, M. Galili, L. K. Oxenløwe, A. T. Clausen, P. Jeppesen, and L. Grüner-Nielsen. "Simultaneous add-drop multiplexing of 80 Gbit/s data in a non-linear optical loop mirror", in *Proceedings of the European Conference on Optical Communi- cation, ECOC'06*, Cannes, France, pp. 505–506, Paper We4.3.5, September 2006

[xix] H. C. H. Mulvad, L. K. Oxenløwe, M. Galili, A. T. Clausen, P. Jeppesen, and L. Grüner-Nielsen. "Simultaneous 160 Gb/s add-drop multiplexing in a non-linear optical loop mirror", in *Technical Digest of the IEEE Lasers and Electro-Optics Society Annual Meeting, LEOS'06*, Montreal, Quebec, Canada, Paper ThP5, October 2006

[xx] M. Galili, L. K. Oxenløwe, H. C. Hansen Mulvad, A. T. Clausen, and P. Jeppesen. "Cross phase modulation wavelength conversion of 320 Gb/s data", in *Proceedings of the European Optical Society Topical Meeting on Extreme Optics, EOS-TOM2*, Paris, France, pp. 62–64, October 2006

[xxi] M. Galili, B. Huettl, C. Schmidt-Langhorst, A. G. i Coca, R. Ludwig, and C. Schubert. "320 Gbit/s DQPSK All-Optical Wavelength Conversion Using Four Wave Mixing", in *Technical Digest of the Optical Fiber Communication Conference, OFC'07*, Anaheim, California, U.S.A., Paper OTuI3, March 2007

[xxii] M. Galili, B. Huettl, C. Schmidt-Langhorst, R. Ludwig, F. Futami, S. Watanabe, and C. Schubert. "All-Optical Combination of DPSK and OOK to 160 Gbit/s DQPSK Data Signals", in *Technical Digest of the Optical Fiber Communication Conference, OFC'07*, Anaheim, California, U.S.A., Paper OThI5, March 2007

[xxiii] H. C. H. Mulvad, L. K. Oxenløwe, A. T. Clausen, M. Galili, L. Grüner-Nielsen, and P. Jeppesen. "Error-free 320 Gb/s simultaneous add-drop multiplexing", in *Technical Digest of the Optical Fiber Communication Conference, OFC'07*, Anaheim, California, U.S.A., Paper OTuI5, March 2007

[xxiv] M. Galili, H. C. H. Mulvad, L. K. Oxenløwe, A. T. Clausen, and P. Jeppesen. "Low-penalty Raman-Assisted XPM Wavelength Conversion at 320 Gb/s", in *Technical Digest of the Conference on Lasers*

and Electro-Optics, CLEO'07, Baltimore, Maryland, U.S.A., Paper CThF4, May 2007

[xxv] L. Oxenløwe, M. Galili, H. Mulvad, P. Jeppesen, and R. Slavik. "Using a newly developed long-period grating filter to improve the timing tolerance of a 320 Gb/s demultiplexer", in *Technical Digest of the Conference on Lasers and Electro-Optics, CLEO'07*, Baltimore, Maryland, U.S.A., Paper CMZ5, May 2007

[xxvi] L. K. Oxenløwe, R. Slavik, M. Galili, H. Mulvad, Y. Park, J. Azana, and P. Jeppesen. "Flat-top pulse enabling 640 Gb/s OTDM de-multiplexing", in *Technical Digest of the European Conference on Lasers and Electro-Optics, CLEO Europe'07*, Munich, Germany, Paper CI8-1, June 2007

[xxvii] L. K. Oxenløwe, F. Parmigiani, M. Galili, D. Zibar, A. T. Clausen, M. Ibsen, P. Petropoulos, D. J. Richardson, and P. Jeppesen. "160 Gb/s retiming using rectangular pulses generated using a superstructured fibre Bragg grating", in *Proceedings of the OptoElectronics and Communications Conference, OECC'07*, Yokohama, Japan, July 2007

[xxviii] M. Galili, L. K. Oxenløwe, A. T. Clausen, and P. Jeppesen. "320 Gbit/s Simultaneous Clock Recovery and Channel Identification", in *Proceedings of the European Conference on Optical Communication, ECOC'07*, Berlin, Germany, September 2007

[xxix] L. K. Oxenløwe, M. Galili, R. Slavík, H. C. H. Mulvad, A. T. Clausen, Y. Park, J. Azaña, and P. Jeppesen. "400 fs flat-top pulse for error-free timing jitter tolerant 640 Gb/s demultiplexing using a long-period grating", in *Proceedings of the European Conference on Optical Communication, ECOC'07*, Berlin, Germany, September 2007

[xxx] F. Parmigiani, L. Oxenløwe, M. Galili, M. Ibsen, D. Zibar, P. Petropoulos, D. Richardson, A. Clausen, and P. Jeppesen. "All-optical 160 Gbit/s RZ data retiming system incorporating a pulse shaping fibre Bragg grating", in *Proceedings of the European Conference on Optical Communication, ECOC'07*, Berlin, Germany, September 2007 - *invited*

Contents

List of Figures

Chapter 1

Introduction

1.1 Perspectives and background for high-speed serial data

The demand for increased bandwidth for optical data transmission has driven the increase in single channel bit-rates to 10-40 Gbit/s in today's commercially available systems. In deployed systems these single channel bit-rates are often implemented in a wavelength division multiplexing (WDM) configuration, where several channels at different wavelengths are co-propagated through the fibre. In this way the high bandwidth of the optical fibre is better exploited, compared to having only one such signal propagate in the fibre.

An alternative approach for increasing the amount of transmitted data, is to increase the bit-rate of each wavelength channel instead of adding more WDM channels. This can potentially be done by increasing the speed of the electronic signal generation (electrical time division multiplexing (ETDM)), the electro-optic data modulators and the detectors. Alternatively, it can be done by interleaving several low-rate optical data channels in time - optical time division multiplexing (OTDM). In both cases, the result is a high-speed serial data signal.

High-speed serial data communications is presently regaining a position as a focus area in the optical communications community. An example of this trend is the strong efforts put in 100 Gbit/s ETDM and Ethernet research worldwide e.g. [1] and several others. High-speed serial data may be particularly beneficial for e.g. metro networks or for serial interconnects between computer nodes. At this moment of writing, the data rates obtainable by ETDM are limited to ∼100 Gbit/s. In contrast, using the

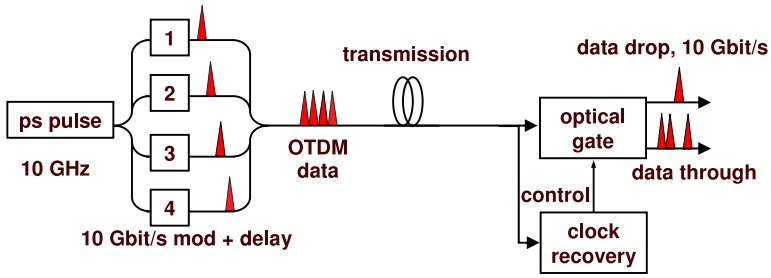

Figure 1.1: OTDM scheme for time interleaving data channels to generate high speed aggregated signal.

OTDM scheme, data rates up to 640 Gbit/s have been reported [2]. Combining OTDM with polarisation multiplexing the bit-rate has been doubled to 1.28 Tbit/s [3]. The current record for single channel data transmission was achieved by further adding a multilevel modulation format (DQPSK) to the scheme, achieving a total bit-rate for a single wavelength channel of 2.56 Tbit/s [4]. The demonstrated potential for very high per-channel bit-rates has been one of the main driving forces in pursuing research on OTDM and OTDM-related technologies.

Whether OTDM will evolve into a viable commercial technology for data transmission is uncertain. However, at the present time OTDM technology is sufficiently developed to be a useful tool for characterising systems at very high bit-rates. In turn, the ability to investigate and develop systems for very high data rates may contribute to maturing the OTDM technology, by adding new or improved functionality. In this way e.g. demultiplexers are continuously being improved, which is also addressed in this work.

1.2 Optical time division multiplexing

The basic scheme for optical time division multiplexing, is illustrated in figure 1.1. In this scheme, time interleaving of low-rate (or base-rate) optical data signals is performed in order to achieve aggregated data rates far above what is achievable using electronic signal generation and direct electro-optic data modulation. The pulse source used for OTDM is required to generate a stable train of narrow optical pulses (typically a few ps) at the base-rate of the system - here 10 GHz. The pulse train is then split up into a number of branches and individually data modulated. Applying appropriate differential delays between the branches, the base-rate data signals are temporally

interleaved to form one high-speed signal. This signal can then be transmitted, including appropriate compensation for transmission impairments like chromatic dispersion and polarisation mode dispersion (PMD). In the receiver, a fast switch synchronised by a clock recovery (CR)-circuit, demultiplexes the signal, extracting a base-rate channel from the high-speed signal. The switch is required to have a temporal switching window, which is sufficiently narrow to avoid interference from neighboring pulses, when demultiplexing a data channel.

In a laboratory environment the OTDM system is often modified to reduce the required equipment. This is done by data modulating the pulse train in a single data modulator. The data modulated base-rate pulses are then split into several arms, delayed, and recombined. In this way an OTDM signal with the desired number of channels can be generated using only one data modulator and a number of passive delays (typically fibre delay lines). However, all of the tributary channels in an OTDM signal generated in this way will carry the same data content.

1.3 Scope and structure of the Thesis

In this thesis, OTDM technology is used as a framework for investigating several optical signal processing functionalities. Presently, this allows for characterisation and demonstration of signal processing at bit-rates up to 640 Gbit/s. In the context of OTDM, optical signal processing is frequently used to facilitate some of the needed functionalities. One of the appealing features of optical signal processing, is the potential for very high speed operation which is associated with many optical signal processing schemes. The optical signal processing functionalities addressed in separate chapters of this thesis are: wavelength conversion (OOK and phase modulated data), data format conversion, clock recovery and channel identification (ID), and timing tolerant demultiplexing. Most of these processes are relevant and applicable to any high-speed serial data signal regardless of its origin. Optical temporal demultiplexing is, however, mainly relevant in an OTDM system.

In chapter 2, wavelength conversion of an on-off keying (OOK) data signal by cross-phase modulation (XPM) in a highly non-linear fibre (HNLF) is investigated. The regenerative properties of the wavelength conversion are characterised by introducing noise in the signal. The wavelength converter is seen to have data reshaping properties, improving the performance of a noisy signal after conversion. In-line wavelength conversion in a trans-

mission line is demonstrated at 160 Gbit/s. Virtually penalty free wavelength conversion at 320 Gbit/s is demonstrated. Potential for 640 Gbit/s operation is indicated. Additionally, wavelength conversion by spectral broadening and filtering is addressed here. The wavelength converter is demonstrated at 160 Gbit/s, and data reshaping capabilities are observed.

In chapter 3, wavelength conversion by four-wave mixing (FWM) is characterised for conversion of phase modulated data signals. Wavelength conversion of 160 Gbit/s differential phase shift keying (DPSK) data and 320 Gbit/s differential quadrature phase shift keying (DQPSK) is demonstrated. The effect of the applied stimulated brillouin scattering (SBS) suppression scheme based on phase modulation is evaluated, and is seen to cause a limitation on the DQPSK performance.

In chapter 4, the process of XPM is investigated for phase modulation of optical data signals. This is done in an optical format converter, where XPM maps the data of an OOK signal as phase modulation on a pulse train. In this way an OOK to DPSK conversion is performed. This is demonstrated for 160 Gbit/s format conversion halfway in a transmission line. Additionally the scheme is demonstrated for adding phase modulation to a previously modulated signal, combining two data signals. The combination of an 80 Gbit/s OOK data signal and an 80 Gbit/s DPSK signal into a 160 Gbit/s DQPSK signal is demonstrated.

In chapter 5, a scheme for combined clock recovery and channel identification is proposed and demonstrated. The scheme relies on XPM to impose a phase modulated label on one data channel in the transmitter. In the receiver, the label is detected by sideband-filtering and used for clock recovery and channel identification. The scheme is demonstrated for 320 Gbit/s transmission and further characterised at 160 Gbit/s. The contrast in filtered power between the labeled channel and the remaining channels confirms the reliability of the channel identification.

In chapter 6, the issue of timing sensitivity of optical switches for demultiplexing is addressed. Three different approaches to creating flat-top optical pulses for switching are characterised. The optical fourier transform (OFT)-technique is used to convert a rectangular shaped optical spectrum into a pulse with an equivalent temporal shape. Using these pulses as control pulses when demultiplexing a 160 Gbit/s signal in a non-linear optical loop mirror (NOLM) increases the timing tolerance of the demultiplexer. A super-structured fibre bragg grating (SSFBG) is also used to create flat-top pulses which are implemented in a 160 Gbit/s wavelength maintaining optical re-timer. A significant timing jitter reduction is observed after signal

re-timing. Finally, a long period grating (LPG)-based optical differentiator is used to create narrow flat-top pulses. The pulses are implemented as control pulses for 640 Gbit/s demultiplexing in a NOLM. The flat-top control pulses introduce a tolerance to timing jitter, which significantly improves the bit error rate (BER) performance of the demultiplexed signal.

Chapter 2

Wavelength Conversion by XPM and SPM

2.1 Introduction

In this chapter two different schemes for all-optical wavelength conversion are investigated. Both schemes rely on introducing a Kerr mediated phase shift to generate frequency shifts in an optical signal.
The first scheme to be addressed relies on cross-phase modulation (XPM) between strong data pulses and a weaker co-propagating continuous wave (CW) probe signal in an optical fibre. XPM-based wavelength conversion of optical time division multiplexing (OTDM) signals was originally proposed by Olsson et al in [5] and has been further developed by L. Rau and W. Wang in [6, 7]. In [7] XPM conversion of a 40 Gbit/s OTDM signal was performed with ∼1 dB penalty in receiver sensitivity, while conversion of a strongly degraded 80 Gbit/s signal produced ∼2 dB sensitivity improvement, demonstrating the capability of regeneration. In [6] XPM conversion was performed at 160 Gbit/s with a penalty in receiver sensitivity of ∼3 dB.
In section 2.2, the operating principle behind XPM based wavelength conversion is described, and some of the main considerations when implementing such a system are indicated. A novel filtering scheme for extracting the converted signal is introduced in section 2.3 suggesting the use of a fibre bragg grating (FBG) based notch filter to supplement the conventional filtering. The effect of varying the suppression of XPM sidebands is investigated.
XPM-based wavelength conversion of OTDM data signals from 80 Gbit/s to 320 Gbit/s using the proposed filtering scheme is demonstrated in this

work. The effect of combining XPM with Raman gain during conversion is characterised. In section 2.4, regenerating properties of the XPM wavelength converter are demonstrated at 80 Gbit/s with a sensitivity improvement up to ∼4.5 dB. In-line XPM conversion in a 130 km transmission line is demonstrated at 160 Gbit/s in section 2.5, indicating the potential for using the XPM based conversion scheme in a wavelength converting network node. Finally, in section 2.6, XPM conversion of a 320 Gbit/s OTDM data signal is demonstrated with a record-low penalty of ∼0.2 dB. This penalty is ∼10 dB lower than the only other reported demonstration of wavelength conversion at 320 Gbaud [8]. Preliminary results for 640 Gbit/s wavelength conversion have also been obtained, confirming the prospect of extending this scheme to even higher bit-rates.
The second wavelength conversion scheme covered in this chapter is conversion by spectral broadening of data pulses, mainly through self phase modulation (SPM), and subsequent optical filtering at the target wavelength for the wavelength conversion. This scheme was originally proposed by P. Mamyshev in [9] and is often referred to as the *Mamyshev regenerator*. In section 2.7, the principle of SPM based wavelength conversion is discussed. Wavelength conversion is demonstrated at 160 Gbit/s in section 2.8, and some regenerative properties of the conversion are observed.

2.2 Principle of XPM wavelength conversion

In this section the principle of wavelength conversion by XPM will be described. The operating principle is illustrated in figure 2.1. A data signal and a CW probe are launched together into a non-linear medium, in this case a highly non-linear fibre (HNLF). The data signal is amplified to achieve sufficient peak power in the data marks to cause XPM in the fibre. XPM will then broaden the spectrum of the CW probe where a mark has co-propagated with it through the fibre. At the output of the HNLF the sidebands on the CW probe can be isolated by spectral filtering to form a wavelength converted copy of the original data signal.

The process of XPM is described by a set of coupled wave equations given in equations 2.1 and 2.2 from [10].

$$\frac{\partial A_1}{\partial z} + \frac{1}{v_{g1}}\frac{\partial A_1}{\partial t} + \frac{i\beta_{21}}{2}\frac{\partial^2 A_1}{\partial t^2} + \frac{\alpha}{2}A_1 = i\gamma(|A_1|^2 + 2|A_2|^2)A_1 \qquad (2.1)$$

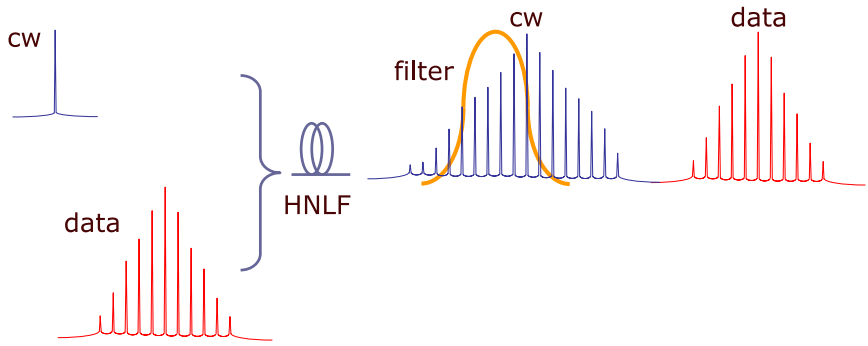

Figure 2.1: Principle of wavelength conversion by XPM.

$$\frac{\partial A_2}{\partial z} + \frac{1}{v_{g2}}\frac{\partial A_2}{\partial t} + \frac{i\beta_{22}}{2}\frac{\partial^2 A_2}{\partial t^2} + \frac{\alpha}{2}A_2 = i\gamma(|A_2|^2 + 2|A_1|^2)A_2 \tag{2.2}$$

This describes the case of two interacting optical fields (A_1 and A_2) in a fibre where polarisation effects and the differences in transverse fibre modes of the two fields have been ignored. A_j is the slowly varying (variation much slower than the optical frequency) envelope of the electric fields, v_{gj} is the group velocity of field j, β_{2j} is the group-velocity dispersion (GVD) coefficient, α is the propagation loss and γ is the non-linear coefficient.

For the purpose of illustrating wavelength conversion by XPM it is assumed that only one of the two fields - signal 2 - is strong enough to introduce significant non-linear effects in the fibre. Furthermore the fibre loss, the GVD and the group-velocity mismatch between the two fields are all assumed to be negligible. These approximations correspond to the practical configuration of having a strong and a weak signal traveling through a short length of HNLF (α typically ~ 0.2 dB) with the zero-dispersion wavelength between the two signal wavelengths, minimising the group-velocity mismatch. Additionally, a very low dispersion slope in the fibre will ensure negligible GVD at the signal wavelengths. With these approximations the expressions become

$$\frac{\partial A_1}{\partial z} = i\gamma_1(2|A_2|^2)A_1 \tag{2.3}$$

$$\frac{\partial A_2}{\partial z} = i\gamma_2(|A_2|^2)A_2 \tag{2.4}$$

This set of equations is easily solved giving

$$A_1(z,T) = e^{i2\phi(z,T)} A_1(0,T) \tag{2.5}$$

$$A_2(z,T) = e^{i\phi(z,T)} A_2(0,T) \tag{2.6}$$

where

$$\phi(z,T) = \gamma |A_2|^2 z, \qquad |A_2|^2 = P_2 e^{-\frac{T^2}{T_0^2}} \tag{2.7}$$

represents the non-linear phase shift, accumulated by traveling the distance z through the fibre. P_2 is the peak power of the pulses in signal 2 assuming a Gaussian pulse shape, and T_0 is the initial $1/e$ pulse width. The time T is in a frame of reference moving with the signals at the group velocity v_g. The dispersion length is given by

$$L_D = \frac{T_0^2}{|\beta_2|} \tag{2.8}$$

Assuming that the GVD is negligible, the SPM experienced by signal 2 will not affect its temporal shape and thus will not affect the XPM imposed on signal 1. We set signal 1 to be a CW at 1544 nm and signal 2 is a 2 ps full width at half maximum (FWHM) Gaussian pulse at 1557 nm. The fibre has a non-linear coefficient of $\gamma = 10\ W^{-1}km^{-1}$, the zero-dispersion wavelength is $\lambda_0 = 1551\ nm$, the dispersion slope is $S = 0.017\ ps\ nm^{-2}km^{-1}$, and the length is 500 m. The dispersion length for the pulse is in this case $L_D \approx 11\ km$ which is significantly larger than the length of the fibre justifying neglecting the GVD in the calculation. The local phase and frequency modulation of signal 1 due to XPM can thus be calculated, and are shown in figure 2.2. The frequency chirp is simply found as the time derivative of the phase modulation in equation 2.7. As seen in figure 2.2, XPM introduces a wavelength shift in the CW probe. This shift is localised to the part of the probe that has co-propagated with a strong pulse through the fibre. In this way, if the strong pulses represent an on-off keying (OOK) data signal, the shifts in wavelength of the probe, will represent the same data logic as the original pulses. Isolating either the red- or the blue shifted part of the probe will thus give a wavelength converted copy of the original data signal. In figure 2.1 the setup for XPM wavelength conversion using this

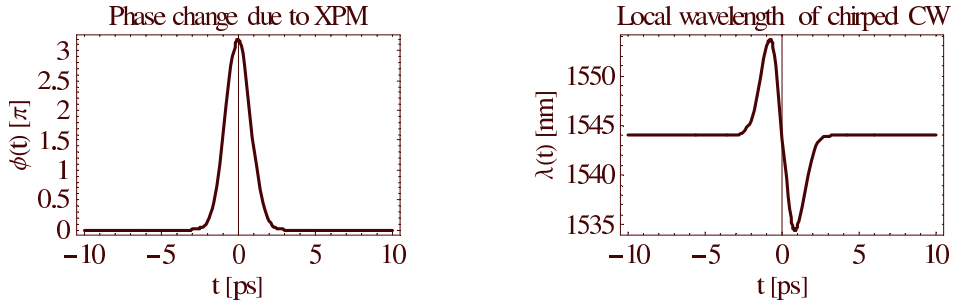

Figure 2.2: Calculated phase change and frequency chirp caused by XPM in a 500 m HNLF with$\gamma \sim 10 W^{-1} km^{-1}$ by a 2 ps Gaussian pulse with peak power of 1 W.

scheme is sketched. The two signals are combined at appropriate power levels, and injected into a HNLF. Here, XPM generates red- and blue shifted sidebands on the CW probe. One of these sidebands are extracted using optical filtering. In order to extract as much power as possible from a sideband, a filter with large bandwidth and a very steep edge is desirable to allow filtering close to the CW probe.
In the following section some properties of this XPM based scheme for wavelength conversion will be presented and discussed.

2.3 Characteristics of XPM conversion

This section discusses some of the considerations to be done in order to achieve XPM wavelength conversion at high bit-rates up to 320 Gbit/s.
The first issue to be addressed is the filtering scheme for extracting the wavelength converted signal from the side band of the CW probe. Here a trade-off exists between increasing the power in the converted signal, and minimising the CW probe present in the converted signal. To increase the converted signal power a band pass filter with a large bandwidth is desirable as this will extract a larger fraction of the power available in the sideband, and allow for the extraction of narrow pulses. On the other hand strong suppression of the CW is required, as power at the CW probe wavelength will appear as a DC background level in the converted signal. Additionally the sideband that will not be used as the wavelength converted output must also be suppressed. The two sidebands are temporally separated as seen in figure 2.2 and therefore in order to prevent splitting of the optical pulse, only one sideband must be present in the converted output signal [11]. Figures 2.3 and 2.4 show the effect of varying the suppression of one side-

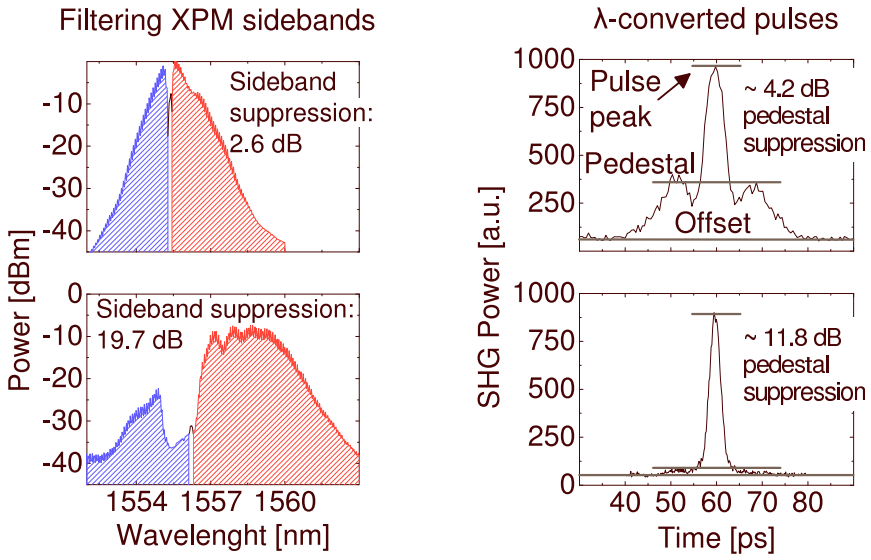

Figure 2.3: Experimental results of the effect of varying the sideband suppression when extracting the wavelength converted signal. Left: Spectra with different degrees of sideband suppression. Right: Corresponding temporal profile, in the shape of autocorrelation traces.

band in measurements and in numerical simulations, respectively. The sideband suppression is defined as the ratio between the power in the two CW sidebands after filtering. For the experimental measurements in figure 2.3, it is seen that the pulse pedestals observed in autocorrelations of the output signal depend strongly on the sideband suppression, and the pulse pedestal suppression is increased by increasing the sideband suppression. In order to achieve this variation of the sideband suppression, several different combinations of optical filters and FBGs were used. Two different FBG notch filters were used, one had a spectral FWHM of ∼0.1 nm and the other was ∼2 nm. Two concatenated bandpass filters were subsequently tuned to achieve different spectral sideband suppressions. These changes in filter configuration are expected to have some impact on the results, as the chirp introduced by filtering, would vary. This applies to the FBGs in particular. In the numerical simulations in figure 2.4 the trend from the experiments is confirmed. The trailing pulse generated in the conversion is reduced by increasing the sideband suppression. Contrary to the experiments the same filter functions were applied for all sideband suppressions. The filtering was implemented using a narrow notch filter (0.1 nm) and a 3 nm bandpass filter. The results are summarised in figure 2.5, where a

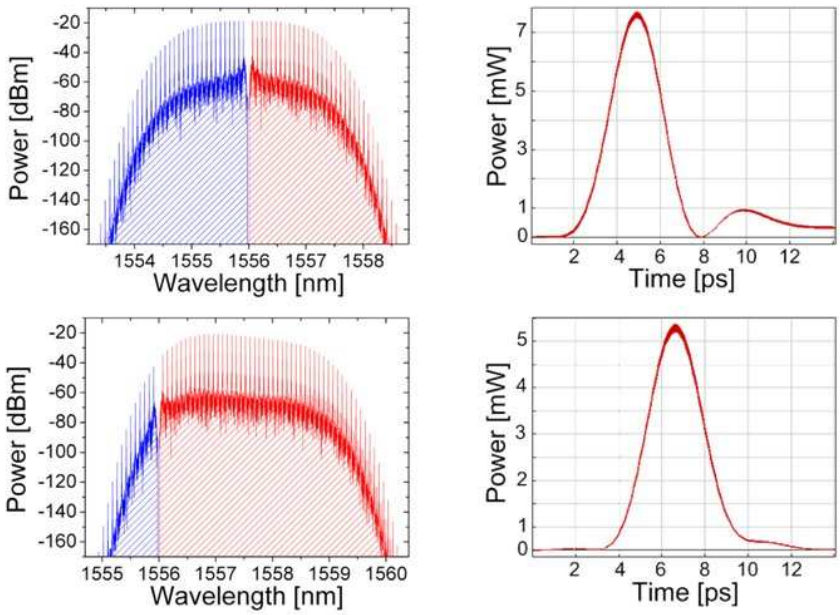

Figure 2.4: Numerical simulation results of the effect of varying the sideband suppression when extracting the wavelength converted signal. Left: Optical spectral. Right: Corresponding temporal profiles.

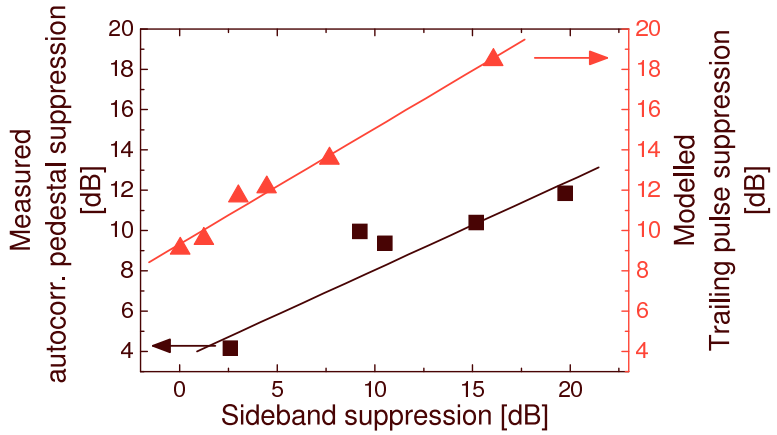

Figure 2.5: Relationship between the spectral sideband suppression and the trailing pulse suppression of the XPM converted output, experimental and numerical results.

range of different sideband suppressions are investigated in simulations and in experiments. In both cases there is a clear tendency towards increased suppression of pulse pedestals / trailing pulses, as the sideband suppression is increased. In order to make a more direct comparison of the modeled and measured results it would be necessary to simulate the actual autocorrelation process as well as the XPM conversion. The autocorrelator used for the experiments has an unspecified internal gain, which gives rise to a background level in the obtained autocorrelation traces. This limits the range of the discernable pulse pedestal suppression to ∼13 dB. However the overall relationship between spectral sideband suppression and temporal pulse shape, is clearly confirmed by the simulation results. The exact pulse widths and separation between main- and trailing pulse, are strongly affected by the dispersion properties of the fibre. In this regard the simulations do not match the experiments very well. It is expected that this could be improved by better matching the dispersion in the simulations to the experimental setup.

Based on the results discussed above it is concluded that a filtering scheme needs to be devised which allows filtering close to the CW wavelength with low loss, while at the same time strongly suppressing the CW and one sideband. This scheme has been realised here using a combination of two different types of optical filters. The sharp edge for filtering close to the CW is realised using a chirped FBG in transmission configuration. The FBG is chirped to increase its bandwidth to ∼2 nm. Light falling within this bandwidth is reflected, while light outside this range is transmitted,

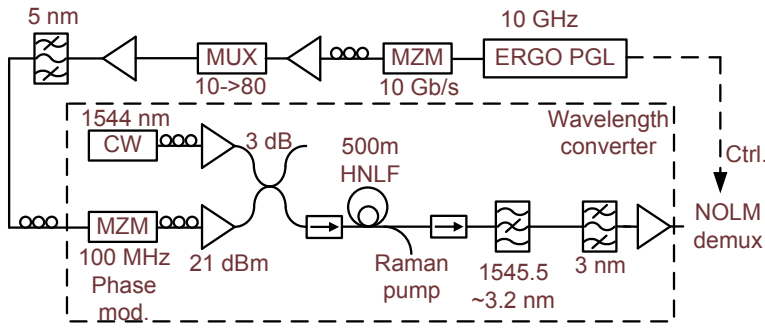

Figure 2.6: Setup for 80 Gbit/s XPM wavelength conversion.

largely unaffected by the grating. In practice this grating is applied to reflect the CW and the 'unwanted' sideband, while transmitting the sideband which is intended as the wavelength converted output. The second filter used to extract the XPM sideband is a conventional optical bandpass filter with a bandwidth appropriate for the desired pulse width at the wavelength converter output.

2.4 80 Gbit/s Raman assisted XPM conversion and regeneration

In this section the performance of the XPM wavelength converter will be demonstrated at 80 Gbit/s. Furthermore regenerating properties of the wavelength conversion will be characterised.
In the previous section the filtering scheme for XPM wavelength conversion was described. This scheme is applied in the system shown in figure 2.6. The optical signal is based on pulses generated by an erbium glass oscillator (ERGO) pulse source supplying a 10 GHz pulse train at a wavelength of 1557 nm and with a pulse width of 2 ps FWHM. The pulse train is data modulated in a Mach-Zehnder modulator (MZM) encoding a 2^7-1 pseudo random bit sequence (PRBS) on the pulse train. The 10 Gbit/s optical data signal is then multiplexed to 160 Gbit/s in a passive fibre delay multiplexer (MUX). The MUX is polarisation maintaining for increased stability and to ensure a truly single-polarisation state of the signal. At $2^7 - 1$ the MUX is PRBS maintaining meaning that the output of the MUX will have the same PRBS data logic as the input 10 Gbit/s signal. This is the case regardless of the chosen output bit rate from the MUX up to 640 Gbit/s. Phase modulation of the multiplexed data signal is per-

formed by a symmetrically driven MZM at 100 MHz to suppress stimulated brillouin scattering (SBS) from the narrow spectral components of the multiplexed high-speed signal [11] (see appendix A). The signal is amplified by an erbium doped fibre amplifier (EDFA) to ∼21 dBm and combined with a CW probe before it is injected into the HNLF. The CW probe is amplified to 14.6 dBm before the signals are combined. In order to reduce SBS in the HNLF the linewidth of the probe has been broadened to ∼ 500 MHz by introducing a weak frequency modulation in the CW laser source. The two signals are launched into 500 m of HNLF which has a non-linear coefficient of ∼ 10 $W^{-1}km^{-1}$. The zero dispersion is at λ_0 =1551 nm and the fibre has a very flat dispersion profile with a slope of 0.017 ps/nm^2km. The wavelengths of the CW probe and the data signal are placed nearly symmetrically around λ_0 to reduce the group velocity dispersion induced walk-off between the two signals to ∼0.1 ps in the HNLF. At the output of the HNLF, a wavelength selective coupler is used to couple a counter-propagating Raman pump into the HNLF while letting the output signal pass with low loss (∼1 dB). Four Raman pump wavelengths are applied (1423 nm, 1435 nm, 1445 nm and 1455 nm) with a total pump power of 200 mW. The Raman pump helps to provide gain to the XPM sidebands, thus enhancing the conversion performance. The blue shifted XPM sideband generated on the CW probe is filtered out using a combination of a chirped FBG and a 3 nm bandwidth bandpass filter. The FBG is applied in the transmission configuration with the Bragg wavelengths reflected into an isolator, giving an almost rectangular shaped notch filter. This notch filter is then used to suppress the CW probe and the red shifted XPM sideband, while the bandpass filter suppresses the original data signal and the residual power in the red shifted sideband. The FBG has centre wavelength at 1545.5 nm and a 3-dB bandwidth of ∼ 2 nm. After filtering, the wavelength converted signal is amplified and then demultiplexed in a non-linear optical loop mirror (NOLM) to the 10 Gbit/s base rate. This is done using 2 ps control pulses from the 10 GHz 1557 nm pulse source to generate XPM in the HNLF in the NOLM. The HNLF in the NOLM is virtually identical to the one used for wavelength conversion meaning that walk-off between the control pulses and the data signal to be demultiplexed is negligible. Thus the width of the switching window will be given largely by the width of the control pulse, giving a switching window with FWHM ∼ 2 ps. Since the control pulses for demultiplexing are at the same wavelength as the original data signal it is not possible to demultiplex the original data signal. The 10 Gbit/s data signal before multiplexing will therefore be used as reference

for the performance of the wavelength converter.

The effect of applying the Raman pump during wavelength conversion is seen in figure 2.7. Adding Raman gain to the conversion process alters one of the features of the non-linear interaction - namely that the power of the interacting signals decrease as they propagate through the HNLF. When Raman gain is present the signals will grow stronger from propagating through the HNLF. In [7] this is described as an increase in the effective length (L_{eff}) of the interaction, increasing the accumulated phase shift for a given signal power level in equation 2.7. The accumulated phase shift at the output of the HNLF is then given by

$$\Delta\phi(T) = \gamma P_2 e^{-\frac{T^2}{T_0^2}} L_{eff} \tag{2.9}$$

where L_{eff} accounts for the loss in the fibre. The traditional form of L_{eff} from e.g. [10] is

$$L_{eff} = (1 - e^{-\alpha L})/\alpha \tag{2.10}$$

However, in the presence of gain in the fibre, this can be introduced into the expression for L_{eff} [7], giving

$$L_{eff} = (1 - e^{(-\alpha+g)L})/(\alpha - g) \tag{2.11}$$

where g is the gain in the fibre - in this case caused by the Raman pump, which is assumed to be constant throughout the length of the fibre. Increasing the non-linear phase shift in this way improves the optical signal to noise ratio (OSNR) of the converted output by allowing more efficient generation of XPM sidebands. In this way less amplified spontaneous emission (ASE) noise is generated when the converted signal is amplified at the output of the converter. This is seen in figure 2.7, where the noise level after filtering and amplification is lowered by 3.5 dB while the signal power is increased by ∼2 dB. Adding Raman gain to the conversion also allows for a shorter physical length of fibre to be used to achieve a given non-linear phase shift.

After wavelength conversion, the signal is demultiplexed as described above and the quality of the signal is evaluated by bit error rate (BER) measurements. Figure 2.8 shows the BER results for wavelength conversion of an 80 Gbit/s data signal. The performance of the wavelength converted and demultiplexed data signal is compared with the BER performance of the 10 Gbit/s base rate signal. It is seen that the performance of the wavelength converter varies significantly depending on the configuration of the wavelength converter i.e. with and without application of Raman gain. In

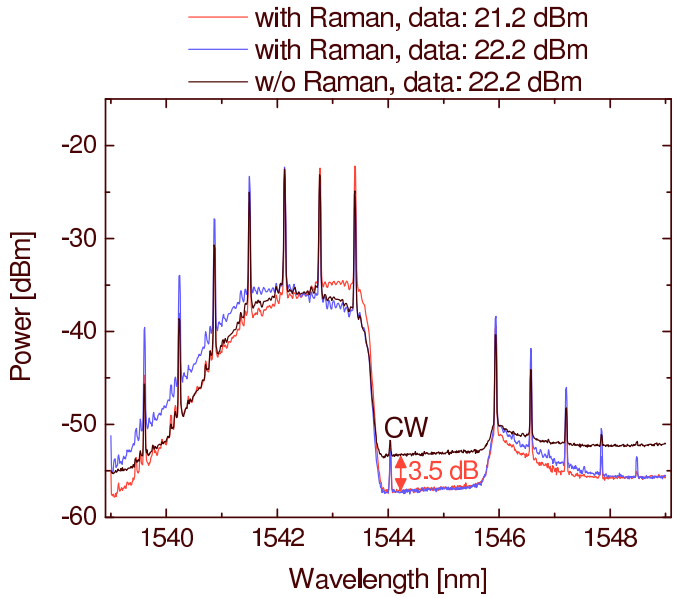

Figure 2.7: The effect of adding Raman gain to the XPM conversion process for an 80 Gbit/s data signal.

the case of doing the wavelength conversion without the presence of Raman gain, the receiver sensitivity at BER 10^{-9} is $\sim$ 0.5 dB better than the 10 Gbit/s reference. This improvement in sensitivity is attributed to the fact that the modulated 10 Gbit/s signal has a small amount of unsuppressed optical power in the logic '0's. This imperfect 0-level is suppressed in the wavelength conversion as the transfer function for the XPM conversion is non-linear having very weak transfer of low power levels in the input data signal [7]. Adding Raman gain to the conversion initially degrades the performance notably introducing 0.6 dB penalty compared to the 10 Gbit/s reference. The optimum performance of the converter when applying the Raman pump is achieved by reducing the average power of the 80 Gbit/s signal into the HNLF by 1 dB. This changes the performance drastically resulting in a 1.6 dB improvement compared to the 10 Gbit/s. This illustrates the effect of the Raman pump to not only increase the power of the interacting signals, but to alter the power profile of the signals passing through the HNLF by substituting the fibre loss with a net Raman gain and thus lowering the required input data power.

As mentioned above the wavelength conversion exhibits some regenerating effect on an imperfect input signal. In figure 2.9 the input data signal has

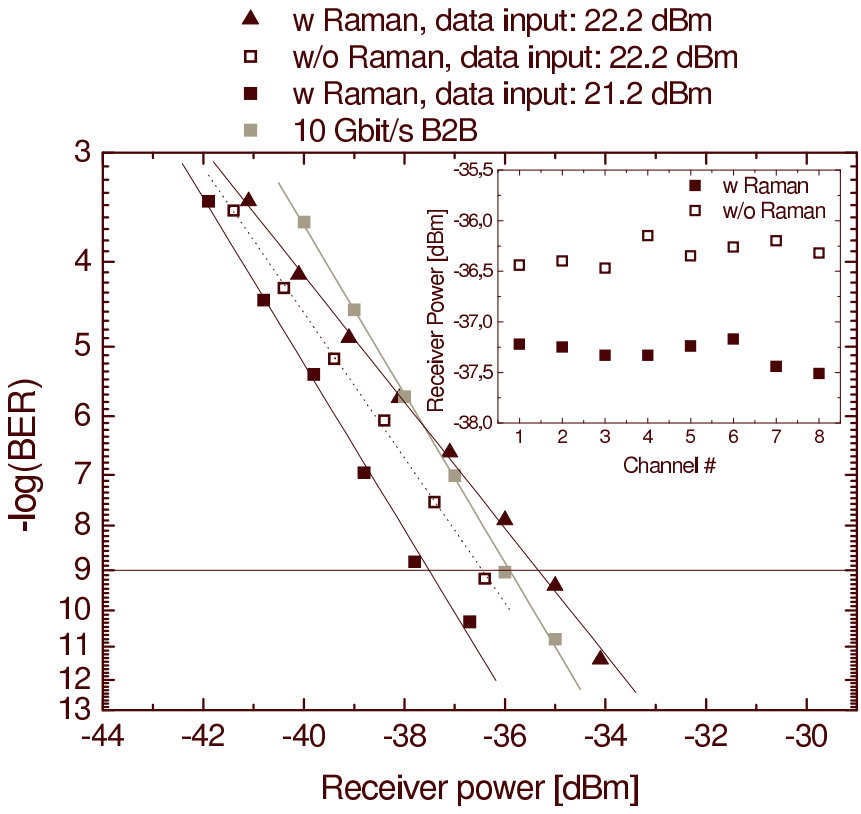

Figure 2.8: BER performance of the wavelength conversion with and without Raman gain for an 80 Gbit/s data signal.

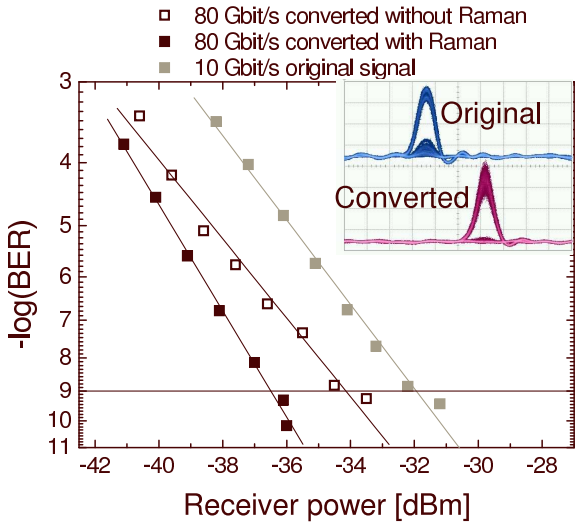

Figure 2.9: BER performance of the wavelength conversion with and without Raman gain for a degraded 80 Gbit/s data signal. The inset shows the original data signal before multiplexing and the wavelength converted demultiplexed data signal.

been deliberately degraded by altering the biasing of the MZM used for data modulation. This introduces noise in the '0' level and some in the '1' level, as seen in the eye diagram in figure 2.9. The 10 Gbit/s reference suffers a penalty of 3.9 dB compared to the one in figure 2.8 with only very weak '0' level noise. In figure 2.9 the wavelength converted and demultiplexed signal is shown for 80 Gbit/s conversion with and without Raman gain. Without Raman gain the converted signal has a sensitivity improvement of ∼2.2 dB. However adding Raman gain to the conversion the sensitivity improvement increases to ∼4.6 dB compared to the 10 Gbit/s reference. Compared to the case in figure 2.8, the wavelength converted signal has only suffered a 1 dB penalty from degrading the input signal.

In figure 2.10 the input signal has been degraded even further as shown in the eye diagram in the figure. This imposes a penalty of ∼7.6 dB on the 10 Gbit/s reference compared to the case in figure 2.8. After Raman assisted wavelength conversion and demultiplexing of the signal, the sensitivity is improved by 4.8 dB. It is seen that the improvement is virtually the same as for the previous case, indicating a saturation of the regenerative effect when the noise is increased beyond a certain level. Some residual noise is also seen in the '0' level of the wavelength converted eye.

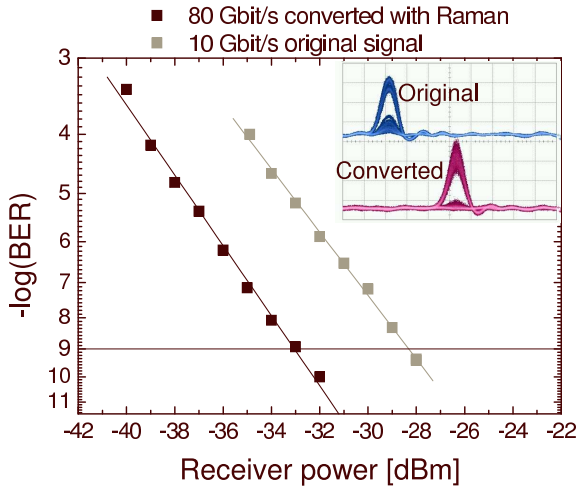

Figure 2.10: BER performance of the wavelength conversion when the input is further degraded. The inset shows the original data signal before multiplexing and the wavelength converted demultiplexed data signal.

2.5 160 Gbit/s wavelength conversion and transmission

In this section, experiments will be presented demonstrating XPM wavelength conversion at 160 Gbit/s [12]. This is also demonstrated for in-line wavelength conversion half way through a transmission link [13].

The experimental setup for 160 Gbit/s XPM wavelength conversion is identical to the setup in figure 2.6 used for conversion at 80 Gbit/s. The 160 Gbit/s bit rate is achieved by introducing an additional stage in the OTDM multiplexer doubling the bit rate to reach 160 Gbit/s. The pulse widths are unchanged from the previous section. The average power of the data signal before combination with the CW probe is increased by 3 dB to 24 dBm in order to maintain the same pulse peak power in the HNLF after doubling the bit rate.

Figure 2.11 (left) shows the spectra of the original data signal and the XPM broadening of the CW spectrum recorded at the output of the HNLF before filtering. Strong 160 GHz modulation peaks can be seen in the XPM broadened spectrum indicating a significant stabilisation of the phase in the converted signal compared to the input signal. This feature of the XPM conversion can be understood by looking again at figure 2.2. The sidebands on the CW probe are generated by phase modulation of the field

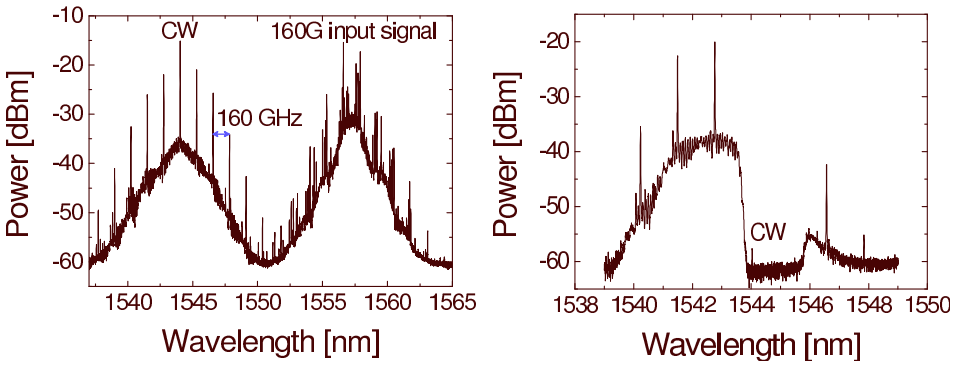

Figure 2.11: The left figure shows the spectrum at the output of the HNLF before any filtering is performed. The right figure shows the filtered wavelength converted 160 Gbit/s output signal.

of the probe. Assuming adequate initial coherence in the probe, the additional optical frequencies forming the sidebands will maintain the high coherence of the probe as they are generated by XPM induced local frequency modulations of the probe. The modulation peaks in the sidebands originate from the fact that the sidebands are only present when a data pulse co-propagates with the CW probe in the HNLF. This means that each of the sidebands represent a signal with the phase properties of the CW probe and the temporal intensity profile of the co-propagating data signal. This is ultimately the reason why the sidebands can be used as a wavelength converted copy of the data signal. In comparison, the original data signal from the multiplexer has no stable phase relation between consecutive pulses in the signal, and hence the spectrum does not show the same clear modulation peaks. The phase properties of XPM wavelength conversion have been further characterised by Rau et al. in [6]. In Figure 2.11 (right) the spectrum of the converted signal after filtering is seen. The CW and part of the red sideband are suppressed more than 40 dB by the FBG and the strong 160 GHz spectral components are retained after filtering. The spectral shape of the FBG is clearly seen in the filtered spectrum. Even though the bandpass filter is tuned to select the blue shifted sideband, a small indication of the red shifted sideband can still be identified in the output signal. Figure 2.12 shows autocorrelations of the input data pulses and the wavelength converted pulses (left and center respectively). The input data channels have some very small differences in power. The converted pulses are slightly broadened by the conversion but still take up less than 40% of the 6.25 ps time slot for a 160 Gbit/s signal. There

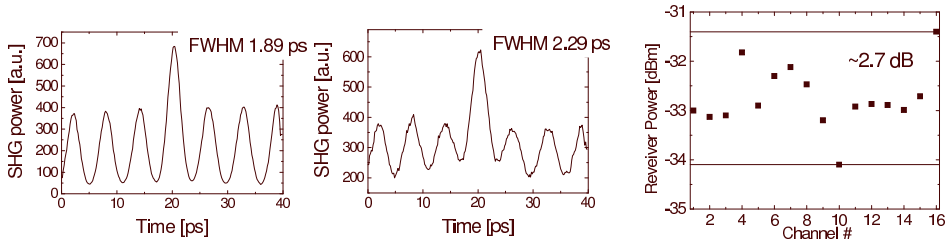

Figure 2.12: Autocorrelations of the original and converted signal and channel sensitivities of the converted 160 Gbit/s signal.

is only negligible broadening of the original and converted pulses due to group velocity dispersion, and the pulse walk-off in the HNLF between the two signals during conversion is ~ 0.1 ps. The major source of the pulse broadening is therefore expected to be the filtering applied to the HNLF output. This significantly changes the spectral shape of the signal compared to the original data signal, which is believed to cause the change in pulse shape. The variation between the OTDM channels is also seen in the measured BER sensitivities shown in figure 2.12 (right). The figure shows receiver sensitivities of the 16 demultiplexed channels in the multiplexed and wavelength converted 160 Gbit/s signal at BER 10^{-9}. All 16 channels are error free, however the receiver powers for BER 10^{-9} are spread over a range of ~ 2.7 dB. The variation in sensitivity between the channels is due to amplitude variations between the channels in the multiplexed signal. This gives rise to a varying XPM performance and a varying effect of the Raman amplification. The average sensitivity is -32.75 dBm.

BER measurements for a typical demultiplexed channel after wavelength conversion at 160 Gbit/s compared to the 10 Gbit/s reference signal are shown in figure 2.13. It is seen that error free performance for a typical channel is achieved at a sensitivity penalty of around 0.36 dB compared to the 10 Gbit/s reference, which has a sensitivity of -33.4 dBm. The best channel represents a 0.64 dB sensitivity improvement compared to the 10 Gbit/s reference. On average though, the converted 160 Gbit/s signal suffers a 0.7 dB penalty compared to the reference. This penalty includes the penalty for multiplexing and demultiplexing the 160 Gbit/s signal and is not the isolated penalty of the wavelength conversion.

In Figure 2.13 (inset) the input and converted eye diagrams are shown for the 10 Gbit/s input signal before multiplexing (top) and 10 Gbit/s converted and demultiplexed (bottom). It is seen from the eye diagrams that the unsuppressed noise at the '0'-level from insufficient extinction of

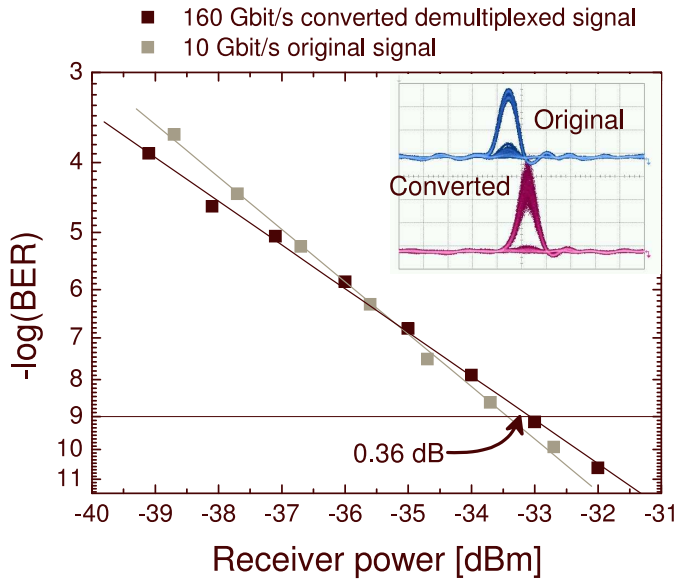

Figure 2.13: BER performance of 160 Gbit/s wavelength conversion. The inset shows the original data signal before multiplexing and the wavelength converted and demultiplexed data signal.

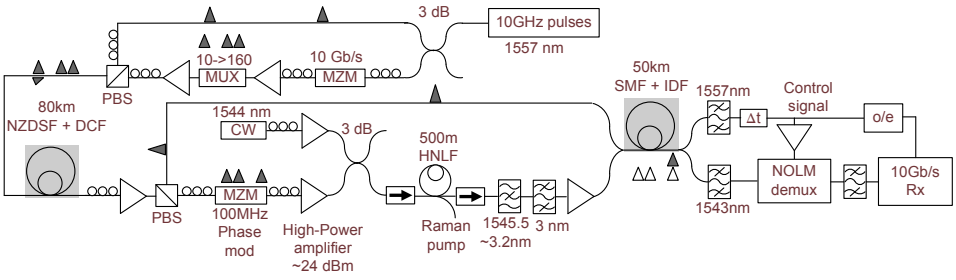

Figure 2.14: Setup for in-line 160 Gbit/s wavelength conversion.

pulses in the MZM is suppressed by the conversion as shown previously at 80 Gbit/s.

The 160 Gbit/s XPM wavelength conversion has been applied for in-line wavelength conversion in a 130 km transmission setup [13]. The experimental setup for in-line wavelength conversion is shown in figure 2.14. The setup for wavelength conversion is almost the same as in figure 2.6. The only difference is a change of Raman pump to a single 1450 nm pump giving up to 31 dBm pump power into the HNLF. Furthermore, the trans-

mitter and receiver are modified in order to support transmission. In the transmitter the 10 GHz pulse train at 1557 nm is split into two before data modulation. One of the 10 GHz pulse train outputs is used to create the 160 Gbit/s data signal. The other pulse train is to be used as control pulses for demultiplexing and for synchronisation of the receiver. This pulse train is combined with the 160 Gbit/s transmitter output in a polarisation multiplexing scheme, where the data signal and the control pulses are combined at orthogonal polarisations in a polarisation beam splitter (PBS). In this way, even though they are at the same wavelength, the two signals can be separated after transmission based on their polarisation. After transmission through 80 km of non-zero dispersion shifted fibre (NZDSF) compensated by dispersion compensating fibre (DCF), the data signal and control pulses are separated in a second PBS. The data signal is then wavelength converted to 1543 nm and optionally retransmitted through a 50 km span of single mode fibre (SMF) and inverse dispersion fibre (IDF) along with the control pulses still at 1557 nm.[1] After wavelength conversion and retransmission, the converted data signal is demultiplexed in a NOLM using the transmitted control pulses, which are also used to generate an electrical clock signal for synchronising the receiver electronics to the transmitted data. In this way the setup for characterising the XPM wavelength converter in a transmission system has been realised using a single pulse source and a simple demultiplexer.
Figure 2.15 shows the spectrum of the wavelength converted 160 Gbit/s signal (after the first transmission span) after applying the notch filter and the band pass filter to suppress the CW probe and the red shifted sideband, along with the original data signal. The spectrum is shown for wavelength conversion with and without Raman gain in the HNLF. The spectra clearly show a reduction in the noise level of ∼5 dB when applying Raman gain to the conversion process. Compared to the results in figure 2.7 this represents an improvement of 1.5 dB, obtained by increasing the Raman pump power. Changing the Raman pump to the single wavelength high power pump sacrifices the flat gain spectrum obtained with the multi-wavelength pump. However at a wavelength shift of 97 nm (∼ 12.5 THz) from the Raman pump, the signal is only ∼ 6 nm from the Raman gain peak, and thus well within the gain bandwidth of the single wavelength Raman pump.

Two different configurations for transmission have been investigated. In one case the 160 Gbit/s data was transmitted 80 km and then wavelength converted before it was demultiplexed and detected in the receiver. In the

[1] The choice of transmission fibre was mainly a practical one, based on availability.

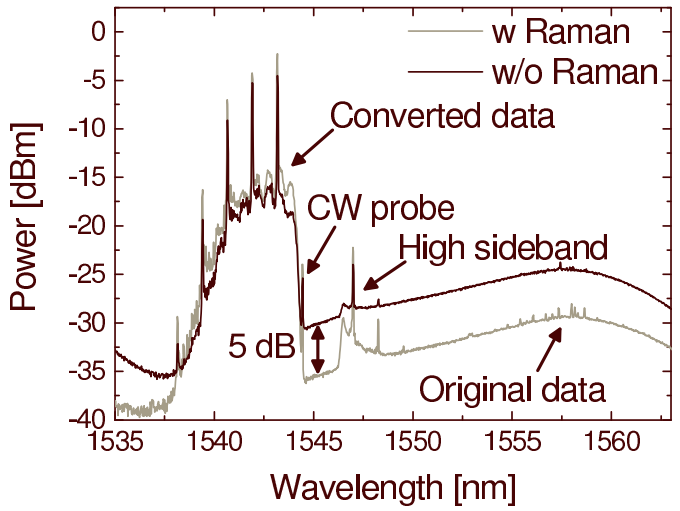

Figure 2.15: Optical spectrum at the output of the wavelength converter, after filtering - with and without Raman gain to assist the conversion.

other case the converted signal was re-transmitted another 50 km, i.e. for a total transmission of 130 km, before it was received. Figure 2.16 shows the BER measurements of the transmitted signals. For the 80 km transmission, BER curves are shown for both cases of wavelength conversion with and without Raman gain to assist the XPM process. The measurements show a ∼0.6 dB improvement in the BER sensitivity when using Raman gain in the conversion. Still, after transmission and wavelength conversion the 160 Gbit/s data signal has suffered ∼ 2.7 dB penalty in receiver sensitivity compared with the 10 Gbit/s reference measurement. The transmitted and converted 160 Gbit/s data signal has clear structure and visible openings in the eye diagram in figure 2.17 ((a) upper) and the 10 GHz electrical sine clock extracted from the transmitted control pulses contains very little noise, as seen in the upper trace. All the 16 10 Gbit/s tributary channels are seen in figure 2.17 ((a) lower) to achieve error free performance after wavelength conversion, within a 3.1 dB range of receiver powers. When the dispersion is compensated channels 1 and 2 in the figure overlap partially in time with the transmitted control signal. This is believed to be the cause of the reduced sensitivity compared to the remaining channels due to transfer of power between the two polarisations and limited isolation in the PBS (∼20 dB) used to separate the data and the control signals after transmission. Transmitting the converted signal an additional 50 km be-

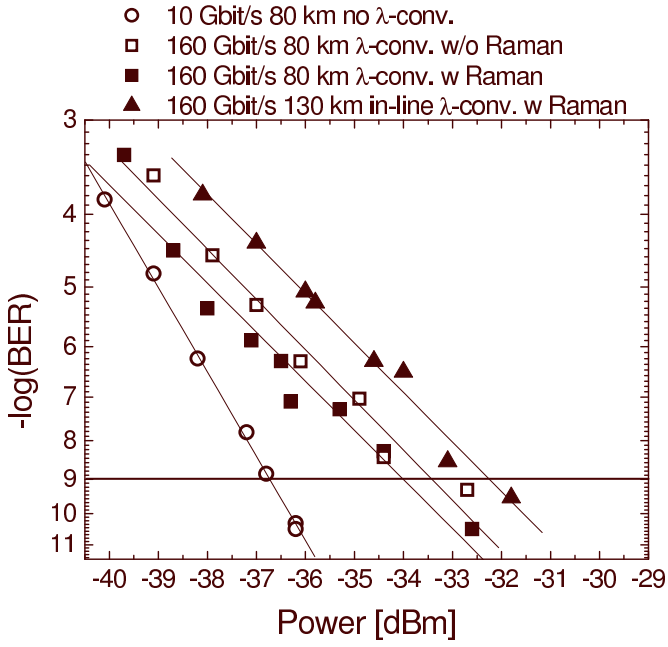

Figure 2.16: BER results for in-line 160 Gbit/s wavelength conversion.

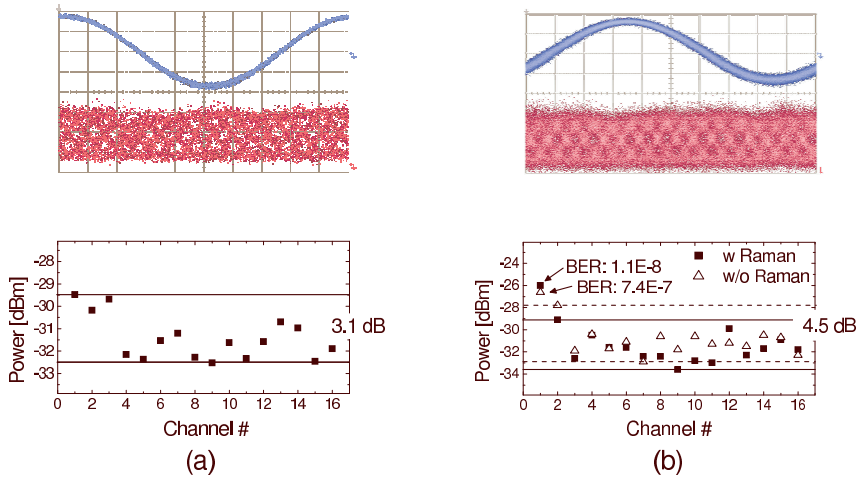

Figure 2.17: Eye diagrams and receiver sensitivities for the 16 channels for (a) transmission and wavelength conversion (b) transmission, wavelength conversion and further transmission.

fore demultiplexing and detecting it induces an additional ∼2 dB sensitivity penalty as seen in figure 2.16. Figure 2.17 ((b) upper) shows that both the 160 Gbit/s eye and the extracted electrical 10 GHz clock contain more noise than in the case of no transmission after conversion. The additional noise observed after retransmission of the signals is believed to be due to interactions between the control pulses and the data signal during transmission - mainly XPM and four-wave mixing (FWM). Despite the added noise, 15 of the 16 transmitted channels show error free performance within 4.5 dB receiver power range as seen in the sensitivity measurements in figure 2.17 ((b) lower). The channel having the largest temporal overlap with the transmitted control pulse could no longer achieve error free operation. From the sensitivity measurements it is also seen that applying Raman gain to assist the XPM conversion improves the receiver sensitivity of 11 of the 16 channels. The optimum filter configuration for wavelength conversion is very sensitive to the strength of XPM in the HNLF. This means that imperfections in the channel equalisation when multiplexing the high speed data signal will result in varying performance of the converter for the different OTDM channels depending on how ideal the filter is for the amount of XPM induced by that specific channel. The same reasoning applies to the effect of adding Raman gain to the conversion. As seen in figure 2.8, adding Raman gain to the conversion does not automatically improve the performance of the system. The benefit from applying Raman gain is only seen when the signal power is adjusted. Similarly, when the channels have unequal power, the effect of Raman gain will vary depending on the power of each individual channel. While most of the channels experience a positive effect from the addition of Raman gain, a few channels may have a power causing the Raman gain to actually deteriorate the performance. It is believed that this is the cause for the varying benefit of Raman gain in the channel sensitivities.

Figure 2.18 (a) shows an autocorrelation of the wavelength converted data signal after 80 km transmission. No pulse broadening is seen in the transmitted and converted signal compared to the 2 ps input pulses and only a very small pulse overlap can be seen. Transmitting another 50 km after conversion (figure 2.18 b) causes ∼0.5 ps pulse broadening and this in turn causes increased pulse overlap between the OTDM channels as seen in the autocorrelation. This pulse broadening is expected to be due to imperfect compensation of dispersion in the second section of the transmission. The broadening is not caused by the converter, but the chirped output signal from the converter may be more sensitive to residual dispersion from

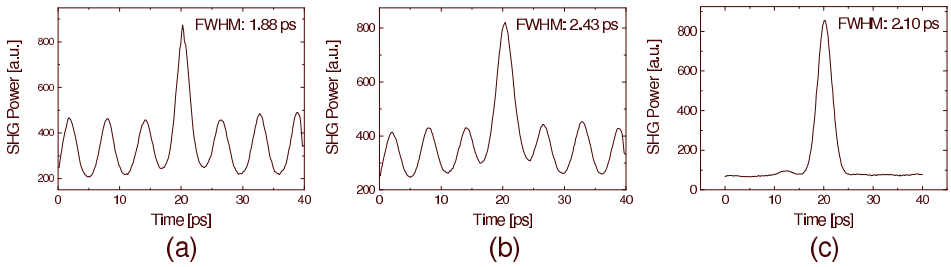

Figure 2.18: Autocorrelations for: (a) 160 Gbit/s signal after 80 km transmission and conversion, (b) signal is transmitted an additional 50 km after conversion, (c) 10 GHz control pulses after the full 130 km transmission.

the transmission. The transmitted control signal shown in figure 2.18(c) experiences virtually no pulse broadening after 130 km transmission and retains its 2.1 ps pulse width, which is suitable for demultiplexing in the receiver.
There are several likely sources for the additional BER penalty caused by transmission. Non-linear effects in the transmission fibre will degrade the performance of the data signal e.g. through intra channel interactions [14]. Furthermore the lack of a proper clock recovery to synchronise the demultiplexer and the receiver to the incoming data signal, will introduce noise mainly in the demultiplexer which is most sensitive to timing imperfections. The transmitted clock after transmission will not be completely well synchronised to the data signal as the clock and data are both affected by transmission effects.

2.6 320 Gbit/s wavelength conversion

In this section the XPM wavelength converter will be extended to 320 Gbit/s constituting the first fibre based wavelength conversion at this symbol rate [15]. The only other wavelength conversion demonstration reported at 320 Gbit/s was performed in an semiconductor optical amplifier (SOA) with a penalty in receiver sensitivity of $\sim$ 10 dB compared to the demultiplexed non-converted signal and a penalty of $\sim$ 18 dB compared to the base rate channel [8]. Furthermore, SOAs have an inherent slow response, making this technique mainly suitable for short PRBS sequences (or equivalent real data), something a fibre switch is not limited by.
320 Gbit/s wavelength conversion by Raman assisted XPM is demonstrated with a penalty in receiver sensitivity of $\sim$ 0.2 dB compared with the non-

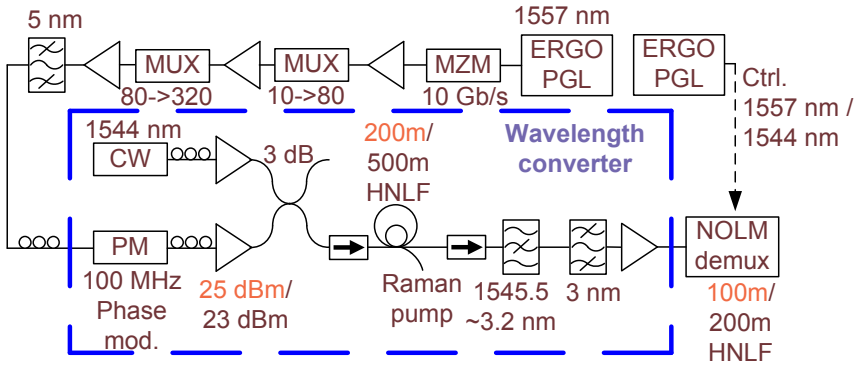

Figure 2.19: Setup for 320 Gbit/s XPM wavelength conversion.

converted signal and a penalty of $\sim$ 1.7 dB compared with the base rate channel.

The experimental set-up for 320 Gbit/s XPM conversion is basically the same as has been used previously. However in order to achieve low penalty the length of the HNLF is changed. The setup is shown in figure 2.19. Contrary to the previous setups, two separate ERGO pulse sources are used for these experiments. This gives the opportunity to demultiplex the non-converted signal at 1557 nm by tuning the control pulses for the NOLM demultiplexer to $\sim$ 1544 nm. In this way the non-converted 320 Gbit/s signal can be used as reference for evaluating the performance of the wavelength converter. For these experiments a fully polarisation maintaining transmitter is used. All components from the pulse source and until the output of the last multiplexer stage in the transmitter, are polarisation maintaining. This strongly reduces temporal variations in the channel equalisation and spacing, in the multiplexed output signal. The output pulses from the ERGO pulse sources are slightly chirped. Compensating this chirp using DCF reduces the pulse width to $\sim$ 1.4 ps FWHM which is adequate for 320 Gbit/s operation. This change in pulse width also affects the necessary average power of the 320 Gbit/s data signal in order to achieve sufficient XPM in the HNLF. For the 500 m HNLF which was also used previously, the 320 Gbit/s data signal is amplified to $\sim$ 23 dBm before combining it with the CW probe at 17 dBm. Substituting a HNLF of 200 m increased the required signal power to 25 dBm. The properties of the shorter HNLF are identical to those of the fibre used previously with respect to zero-dispersion wavelength, non-linearity and dispersion slope. This means that as the fibre is shorter the threshold for SBS will be correspondingly higher [10]. With

the shorter HNLF it is thus possible to amplify the CW probe to 21 dBm before combination with the data signal. This in turn means that more power is available in the filtered sideband at the output of the HNLF. The Raman pump, used to enhance the wavelength conversion, is applied in a counter-propagating scheme with a pump power of ∼29 dBm. The filtering scheme for extracting the wavelength converted signal from the blue shifted sideband is unaltered. However, the bandpass filter is tuned slightly further away from the CW to achieve a broader wavelength converted spectrum. The 320 Gbit/s signal is demultiplexed to the 10 Gbit/s base rate using control pulses at 1557 nm for the wavelength converted signal and 1544 nm for the non-converted signal. In this way the effect of walk-off between the two signals in the demultiplexer is assumed to be the same in the two cases, making them as comparable as possible.

Figure 2.20 shows the spectrum at the output of the HNLF before any filtering is performed. The XPM induced sidebands on the CW are clearly seen, having a 20 dB bandwidth of 9 nm, which is sufficient for extracting a 320 Gbit/s signal from one sideband. The spectrum of the input signal has been broadened due to SPM. This limits the amount of optical power that can be launched into the HNLF, as spectral overlap between the SPM broadening and the XPM sideband to be filtered out will contribute significant noise to the converted signal. As the input signal propagates in the anomalous dispersion regime in the HNLF, soliton effects are expected. From [10], the requirement for a pulse to propagate as a soliton in the absence of loss is

$$\frac{\gamma P_0 T_0^2}{|\beta_2|} = N^2 \tag{2.12}$$

where $\beta_2 < 0$ (anomalous dispersion), T_0 is the 1/e-width of the hyperbolic-secant pulse and P_0 is the peak power. N is the soliton order. The period over which the soliton evolves, the *soliton period*, is given by [10]

$$z_0 = \frac{\pi}{2} L_D \tag{2.13}$$

where the dispersion length is found in equation 2.8. This gives a soliton period $z_0 \approx 17\ km$, for the HNLF used in these experiments. The peak power of a 1.5 ps pulse in a 320 Gbit/s data signal with an average power of 27 dBm is ∼2 W. In the HNLF used here, this peak power is sufficient for exciting high-order solitons (up to N∼11) due to the very weak dispersion at the signal wavelength. The HNLF samples are, however, significantly

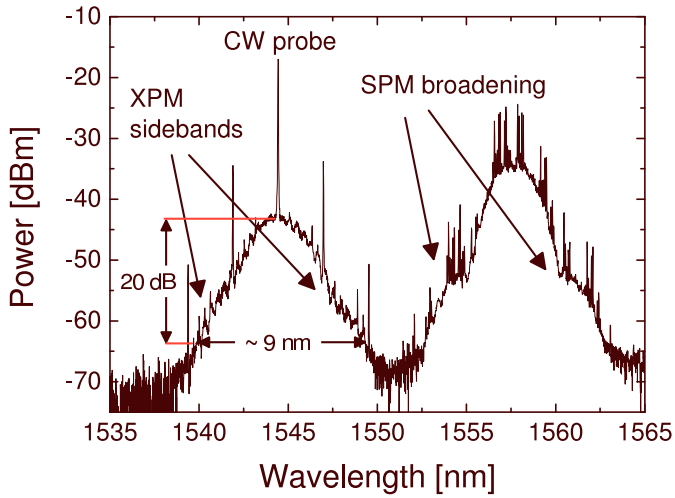

Figure 2.20: Spectrum at the output of the HNLF for 320 Gbit/s XPM wavelength conversion.

shorter than the soliton period, which is expected to reduce the effect of soliton evolution during wavelength conversion.

Figure 2.21 shows the spectra of the original data signal and the filtered XPM wavelength converted data signal. The 320 GHz spectral components from the pulsed nature of the signal are not clearly visible in the original data, as the multiplexed signal is not phase stabilised. The 320 GHz peaks are however clearly visible in the converted signal as this signal has adopted the phase of the CW probe as discussed previously. The spectrum of the filtered output has a 20 dB width of 6 nm, which is slightly broader than expected based on the 20 dB width of the XPM sidebands. However, shaping of the spectrum by strong filtering and strong amplification of the signal is believed to cause this change in the spectrum of the sideband after filtering.

Figure 2.22 (top) shows a cross-correlation between the 320 Gbit/s wavelength converted data signal and a 10 GHz sampling pulse train from an ERGO pulse source. The sampling pulses used for the cross-correlation are compressed using adiabatic soliton compression in a dispersion decreasing fibre (DDF) reducing the pulse width to ∼0.8 ps FWHM. The narrow sampling pulses ensure a temporal resolution sufficient for achieving a visible separation between all the pulses at 320 Gbit/s. Sampling at 10 GHz in the cross-correlator does not allow for the construction of eye diagrams. The resulting cross-correlation, thus, shows an average of the logical '1's and '0's in each bit-slot of the data signal. However, as each channel in the

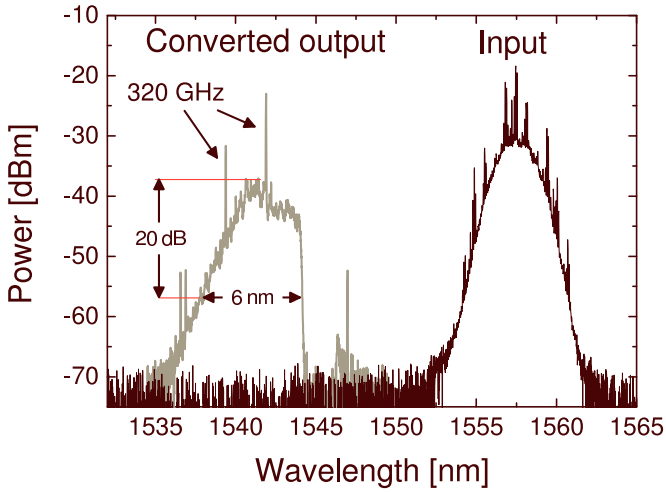

Figure 2.21: Optical spectrum of the input 320 Gbit/s signal and the wavelength converted output.

OTDM signal contain the same PRBS data, information about the channel equalisation in the multiplexed signal is directly visible. The peak pulse levels for the 32 channels in figure 2.22 are seen to be very even, both before and after conversion. This indicates similar performance of all the multiplexed channels both before and after wavelength conversion. Furthermore the pulse widths are virtually unchanged by the conversion, remaining at ~ 1.4 ps. The eye diagram in figure 2.23 shows the multiplexed 320 Gbit/s data signal on a 70 GHz electrical sampling oscilloscope with a 70 GHz photo-detector. Though it is not possible in this eye to resolve the individual pulses, it does however indicate well equalised channels.

The results of BER evaluations of the system performance are seen in figure 2.24. The figure contains the results for the two configurations of HNLF, (a): Using 500 m for conversion and 200 m for demultiplexing and (b): Using 200 m for conversion and 100 m for demultiplexing. In the case of configuration (a), which is identical to what was previously used for XPM conversion at 80 Gbit/s and 160 Gbit/s, a penalty of $\sim$4 dB in receiver sensitivity is observed compared to the non-converted demultiplexed 320 Gbit/s signal, which has a sensitivity at BER 10^{-9} of -35.5 dBm. No error floor is observed down to BER 10^{-9}. The penalty caused by wavelength conversion may have several sources. One may be slight pulse broadening due to walk-off in the HNLF between the original data signal and the CW probe. Another source of impairments may be pulse broad-

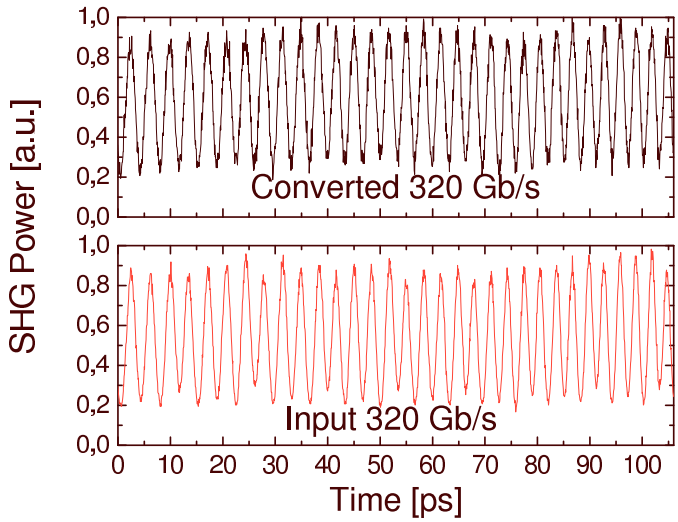

Figure 2.22: Cross-correlation for 320 Gbit/s XPM wavelength conversion in 200 m of HNLF.

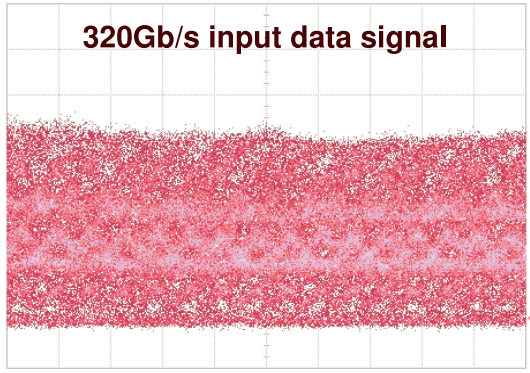

Figure 2.23: Eye diagram of the multiplexed 320 Gbit/s data signal, obtained on a 70 GHz electrical sampling oscilloscope, using a 70 GHz photo detector.

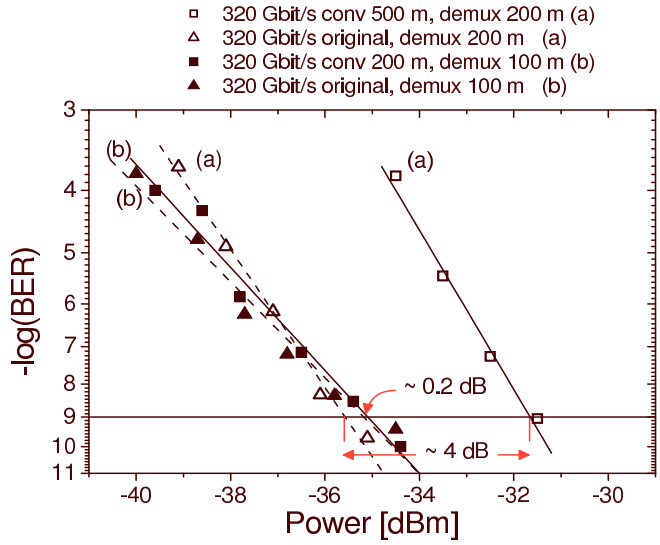

Figure 2.24: BER performance of the 320 Gbit/s XPM wavelength conversion for the two different configurations of HNLFs.

ening or pulse deformation caused by the filtering scheme used to isolate the wavelength converted signal. Finally, soliton effects exited by the original data signal in the HNLF may have affected the system performance. Receiver sensitivities at BER 10^{-9} for six consecutive demultiplexed channels in the converted signal can be seen in figure 2.25. In all cases, the eyes are clear and open however with a variation in receiver sensitivity of ~ 3 dB. This variation is partly due to weak pulse broadening during conversion, making the system increasingly sensitive to even small variations in the temporal alignment of the OTDM channels. This transforms small imperfections in the temporal alignment of the channels in the multiplexed signal, into cross-talk between neighboring channels. The three consecutive channels measured in the non-converted signal exhibit a more constant receiver sensitivity, being separated by only 0.6 dB. Reducing the HNLF length in the wavelength converter from 500 m to 200 m ($\sim 1\%$ of Z_0), reduces the penalty in receiver sensitivity significantly. The sensitivity is improved by 3.4 dB. Reducing the HNLF length in the demultiplexer to 100 m is, however, seen to cause a $\sim$0.4 dB penalty compared to using 200 m of HNLF for demultiplexing the non-converted 320 Gbit/s signal. By reducing the HNLF length to 200 m, the sensitivity penalty from doing the wavelength conversion is reduced to virtually penalty free (~ 0.2 dB)

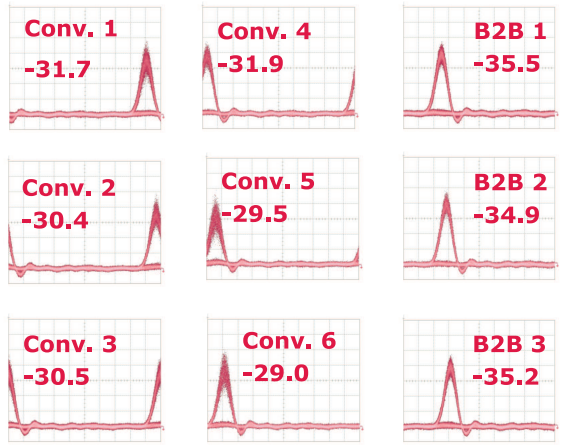

Figure 2.25: Receiver sensitivities and eye diagrams for 6 consecutive wavelength converted and demultiplexed channels, and for 3 unconverted reference channels.

performance compared with the demultiplexed non-converted signal. This is based on the assumption that the same penalty from the demultiplexer applies for both the converted and non-converted signal.

The XPM wavelength converter has been developed to operate virtually penalty free for conversion of a 320 Gbit/s data signal, by careful selection of fibre properties to reduce as much as possible the pulse broadening caused by the wavelength converting system. In this way even potential for 640 Gbit/s operation has been observed. Figure 2.26, shows an autocorrelation of a wavelength converted 640 Gbit/s signal obtained with the XPM conversion scheme. At the time of writing a complete characterisation of 640 Gbit/s XPM conversion has not yet been achieved, but the preliminary results seem very promising.

2.7 Principle and properties of SPM wavelength conversion

In the remaining part of this chapter, an approach to wavelength conversion based on self phase modulation in HNLF will be discussed. In this section the operating principle of this wavelength conversion scheme will be described.

Wavelength conversion and data reshaping by SPM was suggested in 1998 by P. Mamyshev [9]. It was demonstrated at 40 Gbit/s in a two-stage

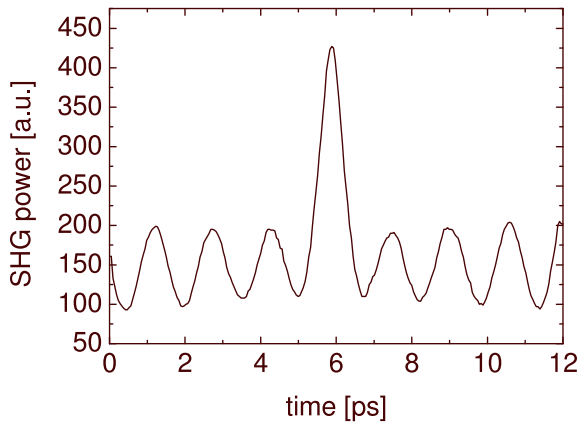

Figure 2.26: Autocorrelation of a 640 Gbit/s XPM wavelength converted signal.

regenerator for 1000000 km loop transmission in [16] and for signal reshaping after demultiplexing in a wavelength division multiplexing (WDM) receiver in [17]. Furthermore it has been used for wavelength conversion at 160 Gbit/s in a demonstration of optical 3R regeneration in [18]. In the following, the operating principle will be described, and a demonstration of wavelength conversion and noise suppression at 160 Gbit/s will be described and discussed.

Wavelength conversion by SPM in HNLF is somewhat similar to the previously described scheme relying on XPM. In both cases the wavelength conversion relies on the Kerr non-linearity in the HNLF to cause an intensity dependent non-linear phase shift of a signal passing through the fibre. In the case of XPM conversion, the non-linear phase shift caused by high power data pulses induces sidebands on a co-propagating CW probe. In the case of wavelength conversion by SPM, only the high power data pulses are present in the HNLF, and the spectral broadening of these pulses due to the non-linear phase shift induced in the fibre, is used to achieve wavelength conversion. This is done simply by introducing sufficient spectral broadening of the data pulses, to have their spectrum extend into the wavelength region, which is the target for wavelength conversion, and filter out these spectral components to form the converted signal.

$$\frac{\partial A}{\partial z} + \frac{i\beta_2}{2}\frac{\partial^2 A}{\partial t^2} + \frac{\alpha}{2}A = i\gamma|A|^2 A \tag{2.14}$$

Equation 2.14 describes the evolution of the slowly varying field enve-

lope, when a single field is propagating under the influence of loss, dispersion and SPM. In the absence of loss and dispersion, the equation reduces to 2.15.

$$\frac{\partial A}{\partial z} = i\gamma |A|^2 A \tag{2.15}$$

with the solution

$$A(z,T) = e^{i\phi(z,T)} A(0,T), \qquad \phi(z,T) = \gamma |A|^2 z \tag{2.16}$$

It is seen that the phase shift caused by SPM is basically the same as the one caused by XPM (equation 2.5) except for the factor 2, making XPM a more effective process.

As indicated previously, strong optical data pulses launched into the anomalous dispersion regime of a fibre with low dispersion can introduce soliton effects, which may be undesirable. High-order solitons may change their pulse shape during propagation and may split up into lower order solitons and non-solitonic radiation (soliton fission [19]). Thus, soliton processes may cause the generated spectrum to be highly sensitive to the peak power and shape of each data pulse launched into the fibre, resulting in unstable spectral broadening. More generally, modulation instability (the interplay between nonlinear effects and dispersion [10]) in the anomalous dispersion regime may deteriorate the quality of signals propagating in this dispersion regime.

Therefore, SPM (and possibly FWM) in the normal dispersion regime of an optical fibre is preferred for performing stable spectral broadening for wavelength conversion. In figure 2.27 the operating principle of the SPM wavelength converter is illustrated. Amplifying the data signal before injecting it into an HNLF, the strong optical pulses representing data marks in the data signal, will experience strong spectral broadening when passing through the fibre. The magnitude of the spectral broadening will define the range for possible wavelength conversion. Extraction of the wavelength converted signal is done by introducing an optical band pass filter at λ_2 within this range. In this way a wavelength converted copy of the data marks is extracted, while pulses with insufficient optical power to generate the required spectral broadening, are suppressed. Similar to the case of XPM conversion, this represents a regenerative property of the wavelength converter, as even quite significant noise in the data spaces will be suppressed in the converted output [9]. Amplitude variations in the input data

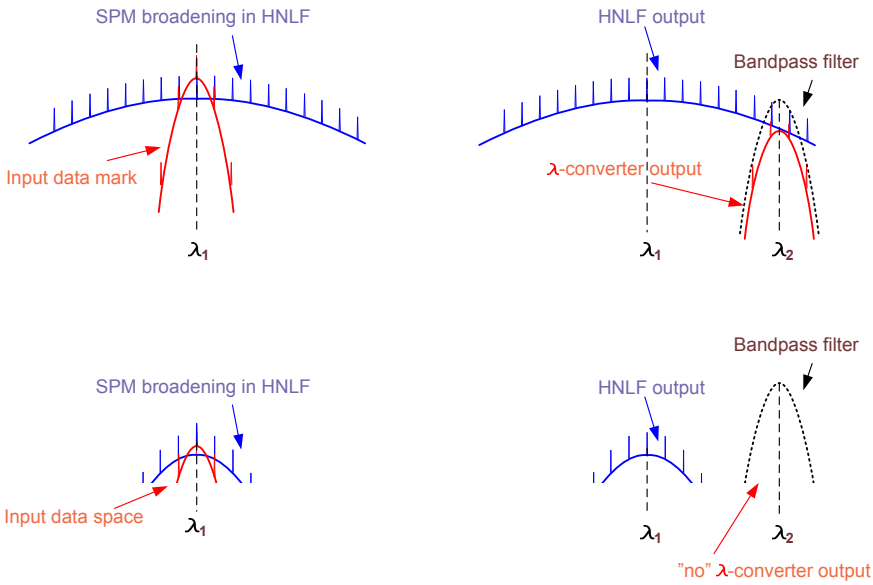

Figure 2.27: Principle of wavelength conversion by SPM in an HNLF. Strong pulses in the input signal, corresponding to data marks, have their spectrum broadened by SPM, which can be used for wavelength conversion. Data spaces, even ones containing small amounts of optical power, do not generate sufficient spectral broadening to do wavelength conversion.

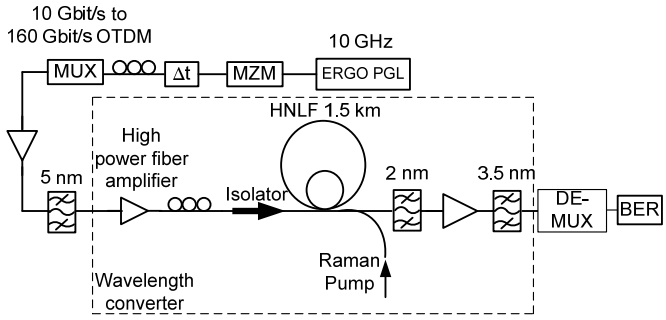

Figure 2.28: Experimental setup for the system investigation of the SPM wavelength converter.

pulses, will affect the width of the broadened spectrum corresponding to the power of each individual pulse, meaning that a wavelength converted data signal filtered out at one of the edges of the broadened spectrum, will be degraded by the initial signal variation.

2.8 160 Gbit/s SPM wavelength conversion and regeneration

In this section experimental investigations of 160 Gbit/s SPM wavelength conversion will be discussed. Noise suppression properties of the wavelength conversion are also demonstrated and discussed [20].

The experimental setup for 160 Gbit/s SPM wavelength conversion is shown in figure 2.28. The optical OTDM transmitter is very similar to what was used in the previous experiments. The data signal is formed by 2 ps pulses, data modulated at 10 Gbit/s and subsequently multiplexed to 160 Gbit/s. The 160 Gbit/s data signal is amplified by an EDFA to $\sim$ 30 dBm and injected into a 1.5 km span of HNLF in order to achieve strong SPM. The HNLF has $\gamma \sim 10$ $W^{-1}km^{-1}$, λ_0 $\sim$1552 nm and a flat dispersion profile (slope$\sim$0.017 ps/nm^{2}km). In the HNLF a counter-propagating Raman pump at 1450 nm and pump power of 200 mW enhances the SPM process, amplifying the signal throughout the length of the HNLF. The wavelength converted data signal is extracted by optical bandpass filtering of the generated *super-continuum* using a 2 nm Gaussian shaped bandpass filter centered at 1557 nm . The wavelength converted signal is subsequently demultiplexed to 10 Gbit/s in a NOLM using 2 ps control pulses and the same receiver configuration as in the experiments

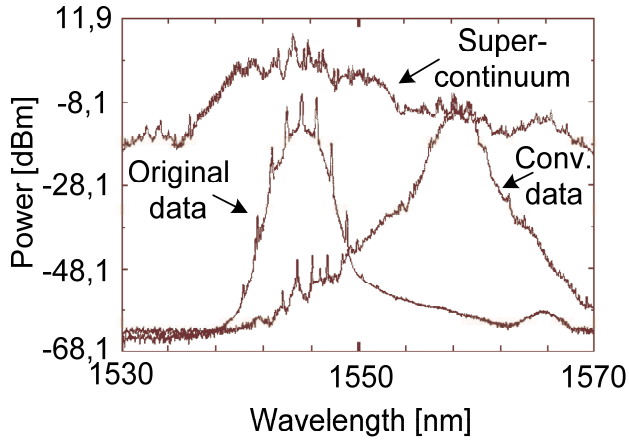

Figure 2.29: Spectra of the original data signal, the SPM broadened signal and the filtered wavelength converted signal.

described previously in this chapter.

In figure 2.29 the spectra obtained for SPM wavelength conversion are shown. The original data signal at 1546 nm has its spectrum broadened to cover the entire C-band, from passing through the HNLF at very high peak power. The data signal initially travels in the normal dispersion regime of the fibre, where the stability of the signal will not be degraded by excitation of solitons. However at the output of the HNLF the spectrum will have broadened far into the anomalous dispersion regime, where the target wavelength for the conversion is also located. Not only SPM contribute to broadening the spectrum of the pulses traveling through the HNLF. FWM between different parts of the spectrum will also contribute to broadening the spectrum, by introducing new spectral components in the signal [21], and stimulated Raman scattering (SRS) will broaden the spectrum by shifting power to higher wavelengths as the pulse propagates through the fibre. The filtered output spectrum is also seen in the figure. Some overlap with the original signal is recognised as the optical filtering is not sufficient to completely suppress the original data signal, and some modulation at 1546 nm is seen in the filtered output signal. The signal at 1546 nm is, however, suppressed > 40 dB in the output signal. Contrary to the XPM conversion there is no stable phase relationship between the pulses in the converted output. Thus the clear modulation peaks of the XPM converter output are not seen in the SPM converted output. The

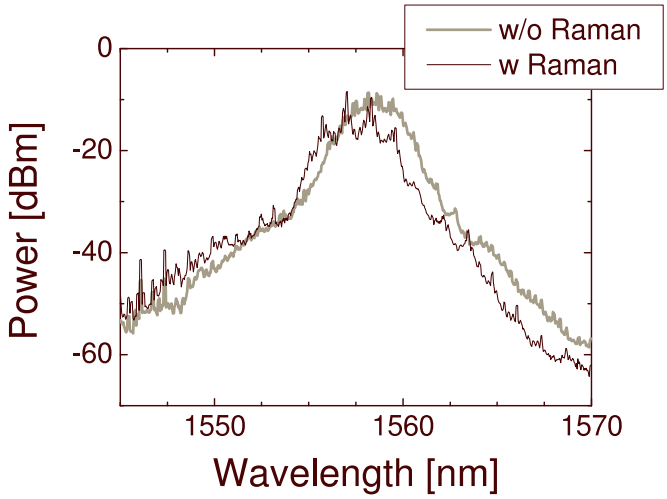

Figure 2.30: The effect on the converted signal spectrum from adding Raman gain to the conversion process.

converted pulses initially have the same phase relationship as the original signal, possibly with the addition of phase variations due to amplitude variations in the original signal.

In figure 2.30 the effect of using Raman gain to enhance the wavelength conversion is shown. The spectra are rather similar, however with slightly stronger modulation peaks in the Raman assisted case. Since the multiplexer used to generate the original signal is not phase stabilised, the modulation peaks will vary over time as the phase relation between pulses change. The stronger modulation peaks in the spectrum when applying Raman gain is however a fairly consistent feature which might indicate an improvement in the noise properties of the signal, causing the 160 GHz frequency content in the converted spectrum to be more visible.

Figure 2.31 shows the BER performance of the wavelength converter at 80 Gbit/s and at 160 Gbit/s. In both cases, error free operation is obtained. At 80 Gbit/s without Raman gain in the HNLF the optimum demultiplexed receiver sensitivity at BER 10^{-9} is -28.1 dBm, which is improved to -29.8 dBm when adding Raman gain, i.e. an improvement of 1.7 dB. Increasing the bit rate to 160 Gbit/s results in only marginal error free performance with a receiver sensitivity of a mere -23.8 dBm without Raman gain. This is strongly improved by the addition of Raman gain, to almost the same level as for 80 Gbit/s. The receiver sensitivity at 160 Gbit/s with Raman gain is -28.9 dB, corresponding to a 5.1 dB improvement over the

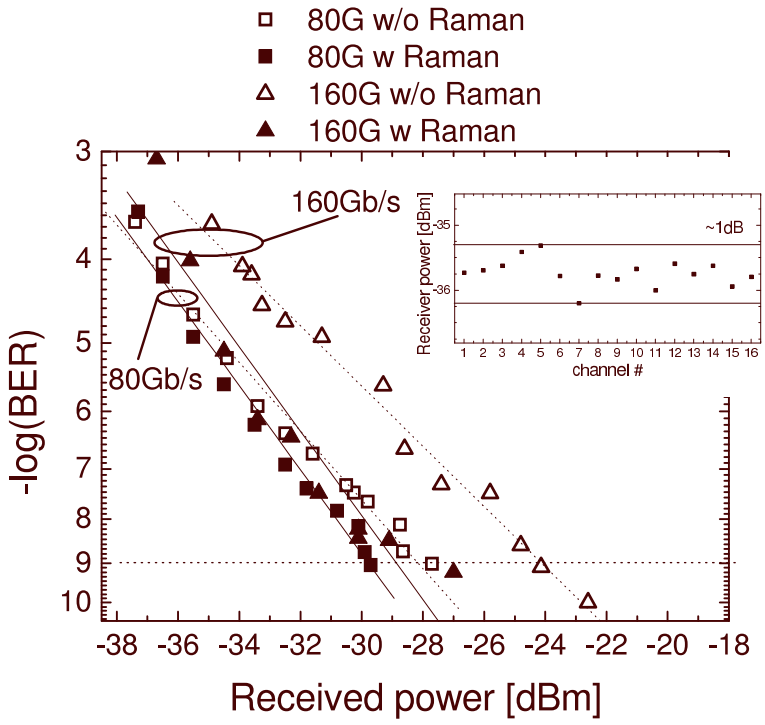

Figure 2.31: BER results of the 160 Gbit/s system investigation of the SPM wavelength converter.

case with no Raman gain in the HNLF. Furthermore, at 160 Gbit/s the required pump power of the data signal into the HNLF is relaxed from 30 dBm to 27 dBm when the Raman pump is used. This is parallel to what was observed for XPM conversion. The inset in figure 2.31 shows the receiver sensitivity for the 16 demultiplexed tributary channels in the original 160 Gbit/s data signal. They are seen to have very similar performance, with less than 1 dB variation in sensitivity. Comparing the average sensitivity of the original signal to the sensitivity of the wavelength converted signal, a penalty of ~ 7 dB for 160 Gbit/s wavelength conversion is recognised. There are several possible sources for this penalty. One contribution to the penalty may be instabilities in the converted signal caused by the formation of solitons at the target wavelength of the conversion, as well as effects of modulation instability. The longer HNLF length corresponds to $\sim 9\%$ of the soliton period, which may cause soliton evolution to be a limitation. A second source of noise in the converter may be instabilities caused by SBS from the narrow spectral components which may appear in

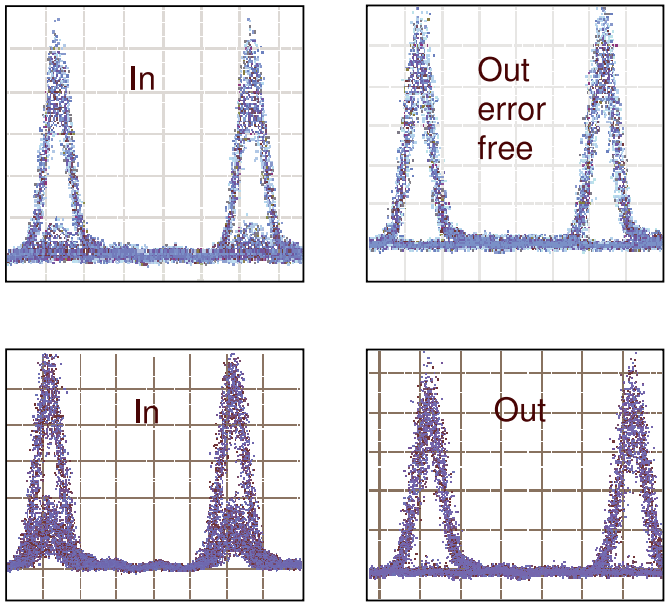

Figure 2.32: Eye diagrams of the original signal and the wavelength converted signal for two different amounts of noise induced in the 0-level.

the spectrum of the multiplexed 160 Gbit/s signal (see Appendix A). As no measures have been taken to ensure a minimum line width of the spectral components in the signal, small variations in the delays in the optical multiplexer will cause the spectral content of the data signal to vary. For certain states of the delays in the multiplexer, narrow spectral components in the spectrum may rise above the SBS threshold, causing the signal to become unstable [10].

The left column in figure 2.32 shows eye diagrams for the data modulated 10 Gbit/s pulses before multiplexing to 160 Gbit/s in the transmitter. In the two cases shown, different amounts of noise is imposed on the '0'-level in the data by detuning the bias for the MZM used for data modulation. This reduces the suppression of pulses, causing the noise which is observed in the '0'-level. The right column in figure 2.32 contains the eye diagrams recorded for the SPM converted and demultiplexed data signal, corresponding to the two different input signals. In both cases the eye diagrams for the converted signals show that noise in the '0'-level is strongly suppressed by the SPM conversion. However BER evaluation of the signals does not reflect this improvement. Figure 2.33 shows the BER results when introducing moderate '0'-level noise in the signal, corresponding to the upper eye

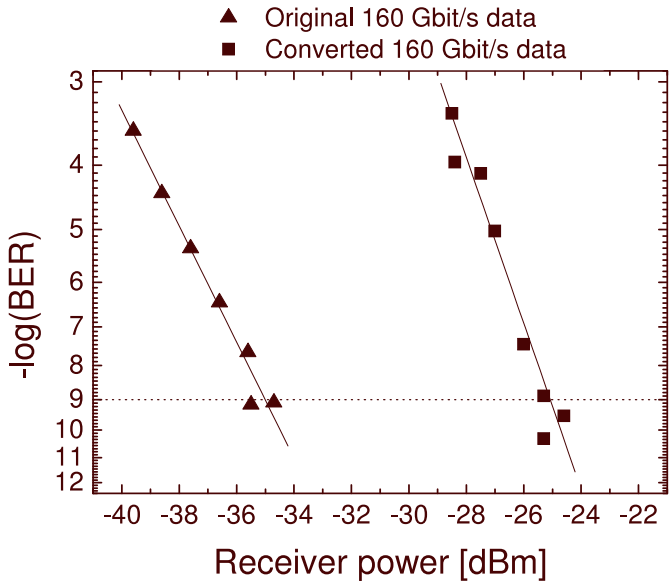

Figure 2.33: BER performance of a wavelength converted signal and the original signal for a degraded 0-level in the input signal.

diagrams in figure 2.32. For this configuration a penalty of ∼10 dB is caused by SPM conversion and demultiplexing. The source of this penalty is not completely understood. It may originate from interaction between solitons forming at the target wavelength in the conversion, and the unsuppressed pulses in the '0'-level of the input data signal. This may cause data pulses to propagate as solitons at the target wavelength of the conversion, while spectral broadening of the unsuppressed '0'-level pulses may not transfer sufficient power to this wavelength range to form solitons. In this way the output signal may consist of data marks formed by strong optical pulses propagating as solitons, and data spaces containing very weak pulses propagating as dispersive waves. Interactions between these two types of pulses in the output signal, may be the cause of the increase in penalty observed in the BER results. Introducing stronger '0'-level noise, corresponding to the bottom left eye diagram in figure 2.32, makes it impossible to achieve error free operation of the system, but the eye diagram after conversion and demultiplexing still shows strong suppression of the introduced noise - figure 2.32 bottom right.

In this implementation, wavelength conversion by spectral broadening and subsequent filtering is associated with a significant penalty, as dis-

cussed previously. The suppression of noise through wavelength conversion is clearly demonstrated by eye diagrams, while BER characterisations reveal additional penalty.

2.9 Summary

In this chapter two approaches to all-optical wavelength conversion of OOK modulated data signals are investigated experimentally and discussed. XPM conversion was seen to have the ability to reduce noise in the '0'-level of the original signal, to an extent where the BER performance was improved for an 80 Gbit/s data signal. Wavelength conversion with negligible penalty has so far been achieved up 320 Gbit/s. Contrary to this, wavelength conversion by spectral broadening, mainly through SPM, was seen to cause significant penalty to the performance of the signal. The two types of wavelength conversion were performed in HNLF samples of very similar properties, which may not be optimum for SPM. In this way the original and the wavelength converted signal wavelengths were placed on either side of the zero dispersion wavelength of the fibre, in order to minimise GVD induced walk-off between the two signals during conversion. In both cases, walk-off will result in pulse broadening of the data signal during conversion, making the optical pulses forming the output signal, broader than the pulses of the original data signal. For SPM wavelength conversion, broadening the spectrum into the anomalous dispersion regime may cause optical solitons to form, which may degrade the system performance, as described above. In the case of XPM conversion, no pulse energy is transferred to the target wavelength of the conversion. The original data signal is propagating in the anomalous dispersion regime, presumably as high-order solitons. XPM conversion could however be performed using only a few hundred meters of HNLF, which is believed to have significantly reduced the impact of the soliton effects. As a more suitable wavelength allocation for XPM conversion, it is suggested to convert from the normal- to the anomalous dispersion regime. In this way while traveling through the HNLF the intensity profile in the anomalous dispersion regime will remain that of the CW probe, although with localised phase and frequency variations, corresponding to the data pattern of the original signal. The constant intensity profile of the CW probe prevents the formation of optical SPM-based solitons in the wavelength converted output. However modulation instability and SBS would still affect the performance of the system, and the interplay between the XPM induced chirp and the dispersion at the target wavelength of the

converter, may cause soliton-like behavior. The realisation of this modification will require either an HNLF with the inverse dispersion slope compared to the ones used here, or a change in wavelength allocations of the input and output signals as well as FBGs for the appropriate wavelengths.

Based on the results of this chapter, XPM wavelength conversion far outperforms conversion by spectral broadening - SPM. This result is, however, affected by the choice of dispersion properties in the HNLF samples, which were more appropriate for XPM conversion. SPM conversion in other types of fibre has been demonstrated in systems with much lower penalty e.g. [18]. The ideal dispersion profile for an HNLF sample for SPM conversion is believed to be a constant and very low normal dispersion, which will minimise pulse broadening and eliminate soliton effects.

In the next chapter, wavelength conversion of phase modulated signals will be addressed. None of the conversion schemes demonstrated in this chapter are suitable for wavelength conversion of phase modulated data signals. In the case of XPM conversion, only the intensity profile of the original signal is reflected in the modulation of the CW probe, meaning that any phase information in the original signal is lost in the converted output. In the case of SPM conversion, amplitude variations in the original data signal will affect the phase of the converted signal. In this way, in order to perform phase preserving wavelength conversion, very stringent requirements will be imposed on the tolerable amount of amplitude variation in the original phase modulated data signal.

Chapter 3

Wavelength Conversion by FWM

3.1 Introduction

In recent years the appearance of new modulation formats for data transmission, where the phase of the optical signal is carrying the information have attracted much attention. These phase shift keying (PSK) modulation formats have several implementations. However differential phase shift keying (DPSK) is currently one of the most popular format for phase modulated data, as it eliminates the need for an absolute phase reference for demodulating the phase modulated signal [22]. Extending DPSK to the simplest multilevel modulation scheme gives rise to the differential quadrature phase shift keying (DQPSK) format, where four phase levels are used to carry data - effectively doubling the bit-rate carried by a given symbol-rate. The main advantages of these modulation formats are improved transmission properties compared to amplitude modulated signals due to e.g. improved resilience to intra-channel four wave mixing [23]. As both data marks and spaces contain optical power, balanced detection can be implemented to further improve system performance. Additionally the DPSK format has potential for multilevel modulation, increasing the data rates for a given symbol rate. As a consequence, systems for phase maintaining high-speed signal processing for future optical networks are being investigated by numerous groups around the world. To increase the transparency of potential future optical networks, all-optical signal processing is being investigated. As mentioned in the previous chapter, wavelength conversion is a key signal processing functionality, and wavelength conversion

of phase modulated optical data signals is the focus of this chapter.

So far a limited number of schemes for high speed all-optical wavelength conversion of phase modulated data signals have been proposed using different non-linear media. The main requirement met by all of these schemes, is preservation of the optical phase information during wavelength conversion. This requirement disqualifies many of the reported optical wavelength conversion schemes, including the cross-phase modulation (XPM) and self phase modulation (SPM) conversion schemes discussed in chapter 2. One scheme for such phase maintaining wavelength conversion is based on semiconductor optical amplifiers in a Mach-Zhender interferometer structure. This has been used in wavelength conversion of ∼40 Gbit/s DPSK data [24]. In a periodically poled lithium niobate (PPLN) waveguide a combination of second harmonic generation (SHG) and difference frequency generation (DFG) has been used for wavelength conversion of 42.8 Gbit/s DQPSK data signals in a wavelength division multiplexing (WDM) configuration [25]. This scheme was also demonstrated very recently for wavelength conversion of 160 Gbit/s DPSK and 320 Gbit/s DQPSK data signals [26]. A third scheme based on four-wave mixing (FWM) in highly non-linear fibre (HNLF) has previously been demonstrated for wavelength conversion of DPSK signals at 40 Gbit/s in a WDM configuration, as well as for a single wavelength 80 Gbit/s DQPSK signal [27, 28].
Four wave mixing in fibre has the advantage of having potential for very high speed operation due to the fast response of the non-linear Kerr effect. Furthermore, the very flat dispersion profile which is achievable in non-linear fibres is expected to allow for conversion with minimal walk-off between signals. This will reduce pulse broadening during conversion, confirming the potential for high bit-rate operation.

The experimental results in this chapter contain the first demonstration of single channel DPSK wavelength conversion at 160 Gbit/s as well as the first demonstration of DQPSK wavelength conversion at 320 Gbit/s [29]. As mentioned above these results have later been matched by experiments performed using a PPLN waveguide. The wavelength conversion presented in this chapter is performed using FWM in HNLF. Wavelength conversion of DPSK signals up to 160 Gbit/s is penalty free in terms of receiver sensitivity, while DQPSK conversion up to 320 Gbit/s is associated with a 4 dB penalty in receiver sensitivity at a bit error rate (BER) of 10^{-9}.

3.2 SBS suppression for FWM wavelength conversion

Wavelength conversion by FWM has been demonstrated numerous times in literature see e.g. [30,31]. The phase maintaining property of FWM makes it the most obvious candidate for wavelength conversion of phase modulated data signals in optical fibres. While preserving the phase relationship between pulses, FWM also has the property of inverting the temporal dependence of the optical spectrum during conversion i.e. changing the direction of any chirp the spectrum might contain. This has been used for dispersion compensation, as a special application of the FWM wavelength converter [32].
Common to most of the demonstrations of FWM-based wavelength conversion, is the use of a single continuous wave (CW) pump for inducing degenerate FWM between the CW and the data signal. One of the main advantages of using a CW pump, is that no synchronisation of the wavelength converter to the incoming signal is needed. This strongly reduces the complexity of the wavelength converter. However a severe limitation is imposed on the applicable pump power, due to the low stimulated brillouin scattering (SBS) threshold, which applies to a narrow line width CW pump (see equation A.1). Several techniques have been demonstrated to increase the SBS threshold, allowing higher pump powers to be applied for FWM in the fibre. These techniques include introduction of a temperature gradient in the fibre [33], applying stress to the fibre [34] and manufacturing special fibres with high SBS thresholds by varying the fibre parameters along the fibre length. In [35] a 7 dB increase in SBS threshold was achieved by altering dopant concentrations along the fibre length. All of these techniques rely on modifying fibre parameters relevant to SBS. A different approach to SBS suppression is to modify the optical signal in the fibre to avoid introducing SBS. As indicated in equation A.1 in appendix A, this can be done by increasing the spectral width of the pump signal. For signal processing applications like wavelength conversion, this is often done by applying phase modulation to the pump signal before injecting it into the fibre [36]. In this way the constant power in the pump is maintained, which is important from a system perspective. However a time dependent phase modulation of the pump will cause a corresponding chirping of the pump. Due to the nature of the FWM process this perturbation of the pump wavelength, will be transferred to the converted signal at twice the strength, as seen in figure 3.1. The figure shows the effect of changes in

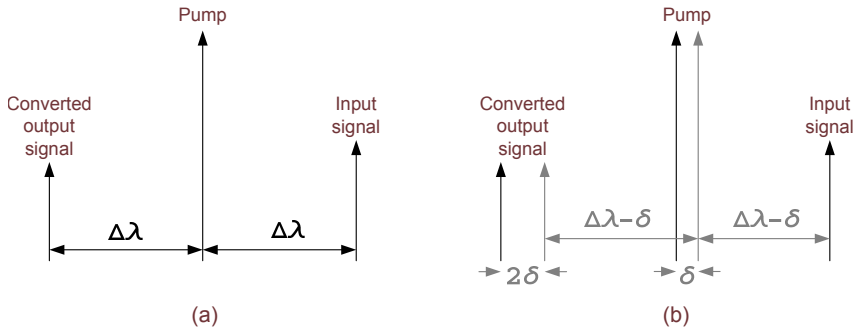

Figure 3.1: The effect on FWM wavelength conversion of a small perturbation in the pump wavelength caused by e.g. phase modulation of the pump. (a) shows a schematic of the wavelength allocations for degenerate FWM. (b) shows the effect of a small perturbation δ to the wavelength of the pump.

the pump wavelength, altering the wavelength spacing between the pump and the signal. The wavelength separation from the pump to the signal is the same as the separation between the pump and the FWM idler (the wavelength converted output). Thus any change in the pump wavelength will cause a change in the idler wavelength with twice the magnitude. Depending on the specific system, this may limit the application of phase modulation for SBS suppression.

In the present implementation, FWM is used for wavelength conversion of a phase modulated data signal (DPSK or DQPSK), which is demodulated into an on-off keying (OOK) signal in the receiver before it is detected. The demodulator is a Mach-Zehnder (MZ)-type fibre interferometer with a differential delay of 25 ps, corresponding to one symbol in a 40 Gbaud data signal. The operation of such a demodulator, will be affected by small variations in the wavelength of the phase modulated data signal, causing a reduction in eye-opening in the demodulated output. The effect is significantly stronger for DQPSK demodulation compared to demodulation of DPSK, as described in [37]. This effect becomes relevant for wavelength conversion by FWM, due to the impact of phase modulating the pump, which is described above. A 100 MHz sinusoidal phase modulation of the pump with a modulation depth of ~ 2.5 rad is estimated to induce a peak-peak frequency modulation of the pump of ~ 500 MHz. As indicated in figure 3.1, this perturbation is doubled in the wavelength converted output, resulting in a maximum frequency perturbation of ~ 1 GHz. For demodulation of a 40 Gbit/s DPSK data signal this corresponds to $\sim 2.5\%$ of the bit rate, while it corresponds to $\sim 1.25\%$ of the bit rate of an 80 Gbit/s DQPSK

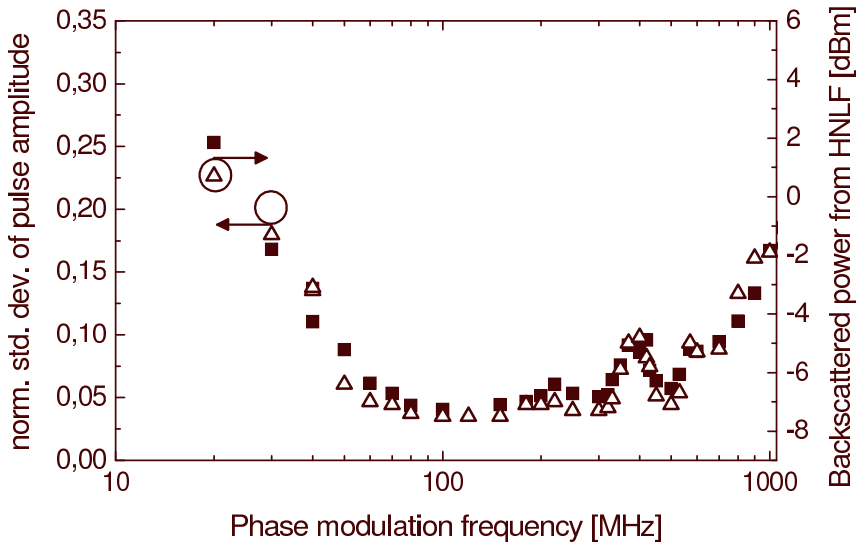

Figure 3.2: The figure shows the effect of varying the phase modulation frequency for SBS suppression in terms of amplitude noise in the wavelength converted demodulated pulses and in terms of backscattered pump power from the HNLF.

data signal. These are the two relevant bit rates for the experiments described in this chapter, as the optical time division multiplexing (OTDM) base rate for these investigations is 40 Gbaud. For DPSK a 2.5% frequency perturbation is expected to cause less than 0.3 dB penalty in receiver sensitivity at BER 10^{-10}, from [37]. This penalty, however, increases to more than 1.5 dB for a 1.25 % perturbation of the DQPSK signal. These values cannot be directly transferred to the present system configuration, as they apply to a 40 Gbaud ETDM system using 33% duty cycle RZ pulses, but they do however indicate a potential limitation to the application of phase modulating the FWM pump in order to reduce SBS. For wavelength conversion of multi-level phase modulated signals (DQPSK being the simplest example) even small frequency perturbations from the pump are thus expected to affect the system performance by deteriorating the result of delayed demodulation.

In order to determine the appropriate phase modulation frequency for the pump in the FWM converter, the backscattered pump power from the HNLF is measured along with the noise in the wavelength converted demodulated pulse amplitudes, for various modulation frequencies. The results are seen in figure 3.2. For this characterisation the delay line interferometer (DLI) is configured for DPSK demodulation and a 40 GHz

train of unmodulated pulses are wavelength converted and passed through the DLI. The pulses are analysed, at the DLI output port set for constructive interference, using a 50 GHz photo-detector and a 70 GHz electrical sampling oscilloscope. The standard deviation in the pulse peak power is measured and normalised by the mean peak power of the pulse, and the results are shown on the right-hand axis in figure 3.2. The backscattered pump power from the HNLF where FWM is performed, is shown on the left-hand axis in the figure. The measurements are made for a constant pump power of $\sim$ 23 dBm into the HNLF. It is seen that for an increase in modulation frequency up to around 100 MHz there is a significant reduction in the backscattered pump power, as well as in the amplitude noise of the converted and demodulated pulses. This is clearly due to an increase in the SBS threshold, which for 100 MHz modulation has risen above the applied pump power. For constant pump power, further increase in modulation frequency has negligible effect as expected. At $\sim$ 400 MHz a local increase in both backscattered power and pulse amplitude noise is observed. The SBS suppression for this modulation frequency is apparently less effective, however the origin of this local variation is not well known. A resonance in the employed phase modulator may cause a reduction in modulation depth at this frequency, or the 400 MHz modulation frequency is less appropriate for SBS suppression in the given configuration. The increase in backscattered power and amplitude noise starting around 600 MHz is caused by a decrease in the modulation depth in the phase modulator, as the cut-off frequency of the driving amplifier is reached. Based on this characterisation, the choice of 100 MHz phase modulation frequency for the system implementation of the FWM wavelength converter is made. A lower frequency will cause SBS to limit the performance of the wavelength converter, while a higher frequency will increase the wavelength perturbation of the converted signal, increasing the penalty caused by the demodulation, without improving the performance in terms of SBS suppression.

3.3 320 Gbit/s DQPSK wavelength conversion

In this section the results of system investigations of the performance of the FWM based wavelength converter will be presented.
Figure 3.3 shows the experimental set-up used for the system characterisation of the FWM based wavelength converter. The transmitter used in this setup is based on a semiconductor mode-locked laser generating a 10 GHz pulse train at 1550 nm with pulse width of 1.5 ps full width at half

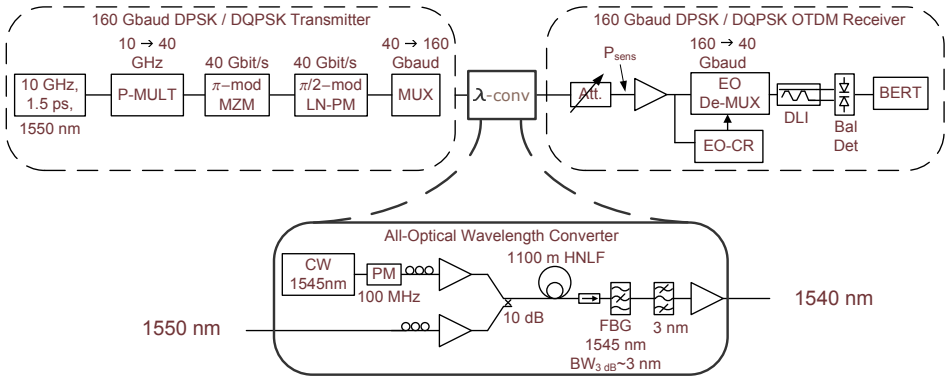

Figure 3.3: Setup for FWM wavelength conversion.

maximum (FWHM). The generated pulse train is multiplied to 40 GHz in a phase stabilised pulse multiplier (P-MULT), consisting of two half-bit delay fibre multiplexer stages with thermal regulation of the phase difference in each stage. In this way a constant phase relation between consecutive pulses can be ensured, which is essential for the subsequent differential phase modulation. Data modulation is performed using two concatenated modulators in order to create either a DPSK or a DQPSK data signal. A $LiNbO_3$ Mach-Zender type modulator driven by an electrical data signal (pseudo random bit sequence (PRBS) $2^7 - 1$) is used to encode the π phase shifts for DPSK. This DPSK modulation scheme has the advantage of ensuring the correct phase shift, despite imperfections in the electrical drive signal. These imperfections will instead cause amplitude variations in the phase modulated pulses. However, the amplitude variations are less critical on the system performance compared to the phase variations which would be induced if a simple phase modulator was used with the same drive signal [22]. For encoding the additional $\pi/2$ phase shift for DQPSK a conventional $LiNbO_3$ phase modulator (LN-PM) is used. In this case imperfections in the drive signal will lead to phase variations as described above. The driving data signal is delayed 48 bit, compared to the optical signal, between the two modulators. The modulated 40 Gbaud signal is then multiplexed in a fibre-delay multiplexer to generate signals up to 160 Gbaud as input to the wavelength converter.
In the wavelength converter the data signal is amplified and injected into 1100 m of HNLF with a non-linearity measured to be $\gamma \sim 10.3\ W^{-1}km^{-1}$.[1]

[1]The measured value is a factor two less than what is specified by the manufacturer. This is believed to be due to the use of different methods for determining γ

The HNLF has zero dispersion at $\lambda_0 = 1548$ nm and dispersion slope $S = 0.03$ ps/nm^2/km. The data signal is injected into the HNLF through the weak arm of a 10 dB coupler, giving a signal power into the HNLF of ∼3 dBm. The CW pump at 1545 nm is phase modulated at 100 MHz to suppress SBS in the HNLF as described above. The pump is subsequently amplified and coupled into the HNLF through the strong arm of the 10 dB coupler, resulting in a pump power of ∼22 dBm into the HNLF. Polarisation controllers are used to align the pump and signal to optimise the polarisation overlap in the HNLF.

At the output of the HNLF an optical isolator blocks the reflected power from an fibre bragg grating (FBG) which is used for spectral filtering. The FBG is used as a notch filter to suppress the 1545 nm pump power by ∼ 40 dB in the wavelength converter output. This significantly relaxes the requirements for the subsequent optical band pass filter used to isolate the wavelength converted output at 1540 nm. A combination of the notch filter and a single 3 nm bandwidth bandpass filter is sufficient to suppress the unwanted spectral components in the wavelength converter output.

The wavelength converted signal is then received in a pre-amplified 160 Gbaud OTDM receiver, which is synchronised to the incoming signal by extracting a 40 GHz clock using an electro-optical clock recovery (EO-CR). The data signal is demultiplexed to its 40 Gbaud tributary OTDM channels using an electro absorption modulator (EAM) based demultiplexer. After demultiplexing from 160 Gbaud to 40 Gbaud the signal is demodulated in a fibre based DLI with 25 ps differential delay. Both outputs from the DLI are detected in a balanced detection configuration, increasing the sensitivity of the receiver [22]. Finally the system performance is evaluated by BER measurements. As discussed previously the phase modulation of the CW pump causes a weak modulation of the carrier frequency of the wavelength converted signal. This reduces the maximum contrast between the two output arms of the DLI by 3 dB when demodulating the converted signal compared to demodulating the original data signal. The contrast is measured as the largest obtainable difference in power between the two DLI outputs, when injecting a pulse train with no data modulation into the DLI.

The process of FWM wavelength conversion in the HNLF is shown in figure 3.4 (a). The input data signal and the CW pump generate FWM when they are co-polarised in the fibre, and the wavelength converted data signal (the idler) is created. As seen in the spectrum the conversion efficiency is about -10 dB, which is mainly limited by the amount of power in

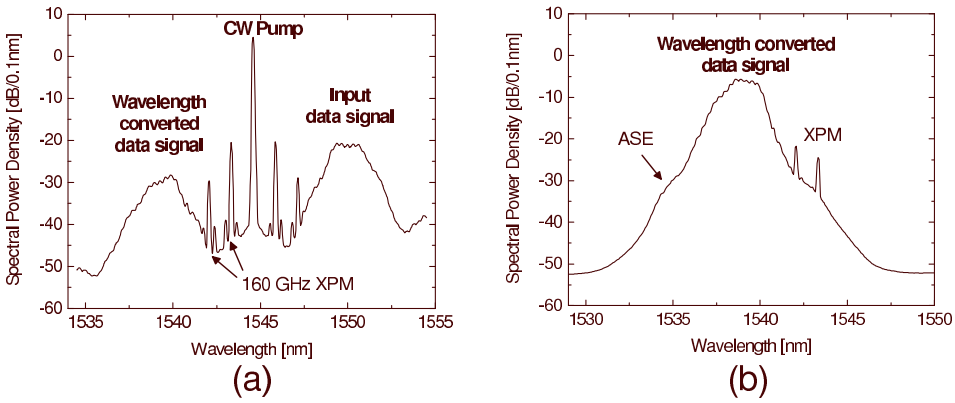

Figure 3.4: Optical spectra for FWM wavelength conversion. (a) shows the spectrum at the output of the HNLF before filtering. (b) shows the wavelength converted signal after filtering - i.e. the wavelength converter output.

the CW pump. The peaks on either side of the CW pump are generated through XPM between the pump and the input data signal. The peaks are spaced 160 GHz corresponding to the symbol rate of the data signal, and are clearly visible due to the phase matched nature of the sidebands as discussed in chapter 2. In figure 3.4 (b) the spectrum of the filtered and amplified wavelength converted data signal at the converter output is seen. Some indication of the peaks caused by XPM broadening of the CW pump is still observed and the indicated shoulders are due to a small amount of unsuppressed amplified spontaneous emission (ASE) after filtering. The optical signal to noise ratio is measured to be ∼37 dB in the converted signal. Figure 3.5 shows an autocorrelation trace of the wavelength converted data pulses. The pulse width is increased by ∼50 fs compared to the 1.5 ps pulses in the original data signal, and are thus still sufficiently narrow for 160 Gbaud operation. In figure 3.6, the eye diagrams from the balanced detector after demultiplexing and demodulation of the signal are shown for DPSK and for DQPSK at 40 Gbaud. For DPSK the eye is clear and open for both the original and for the wavelength converted signal. When using the DQPSK modulation format the eye opening after demodulation is somewhat smaller in the original signal due to the closer spacing of the data carrying phase levels. The increased amplitude noise in the DQPSK eyes is due to imperfect phase shifts generated in the phase modulator used to create the $\pi/2$ phase shifts. A small amount of additional noise is seen in the wavelength converted DQPSK eye compared to the eye for the non-converted signal. This is ascribed to the effect of the

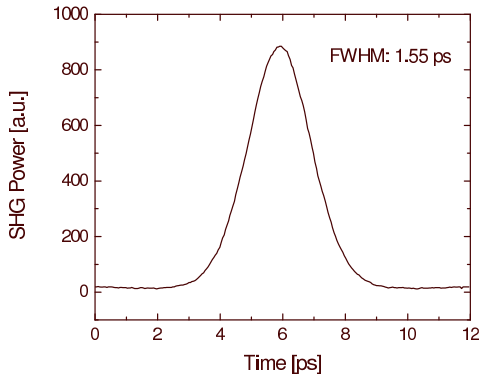

Figure 3.5: Autocorrelation of the wavelength converter output pulses.

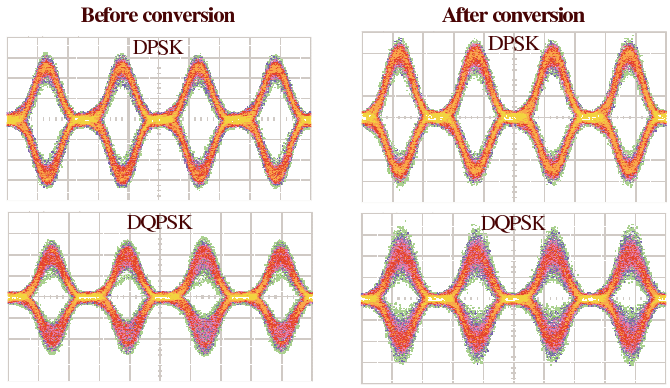

Figure 3.6: Eye diagrams for wavelength converter input and output signals.

SBS suppression scheme, as mentioned previously. This reduction in eye opening is expected to be associated with a penalty in system performance, which is also seen in the BER characterisations. In figures 3.7 and 3.8, BER measurements before and after the wavelength converter are shown as a function of the average power at the input to the 160 Gbaud receiver. The performance for conversion of DPSK data is shown in figure 3.7 for conversion of data signals at 40, 80 and 160 Gbit/s. The wavelength conversion is seen to cause only negligible penalty in receiver sensitivity, with a penalty of less than 0.3 dB at a BER of 10^{-9}. In determining the BER all tributary channels are measured and a variation in receiver sensitivity of $\sim$0.5 dB is found. For DQPSK the BER measurements for conversion of 80, 160 and 320 Gbit/s data are shown in figure 3.8. Error free operation is achieved at a $\sim$4 dB penalty for all bit rates, which clearly shows that the

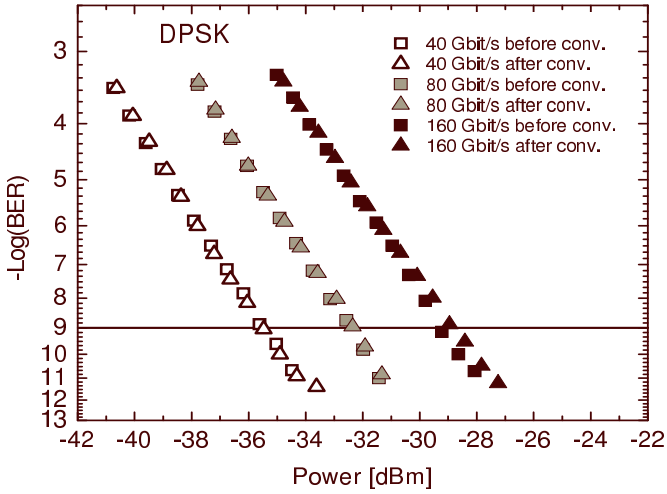

Figure 3.7: BER results for FWM conversion of 40, 80 and 160 Gbit/s DPSK data signals.

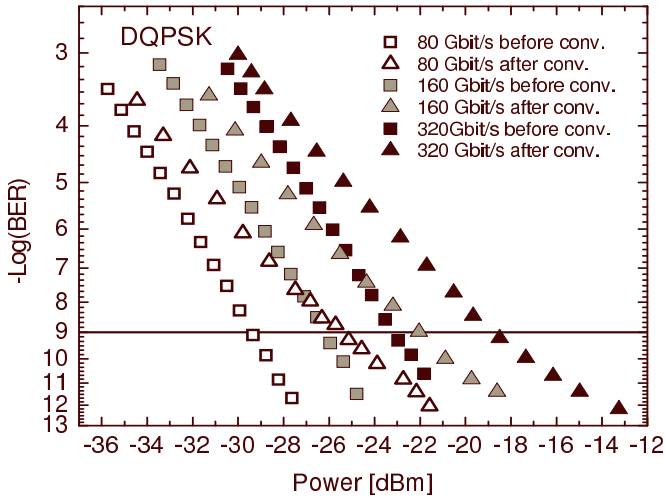

Figure 3.8: BER results for FWM conversion of 80, 160 and 320 Gbit/s DQPSK data signals.

performance of the converter is not limited by the bit rate. The penalty for the converted DQPSK signals is consistent with the expected effect of using phase modulation of the FWM pump for SBS suppression, as discussed previously. The BER measurements confirm that the DQPSK signal is significantly more sensitive to the frequency perturbations induced during wavelength conversion, compared with the DPSK signal. The penalty of 4 dB is somewhat larger than predicted based on [37]. This difference is attributed to imperfections in the DLI as well as additional phase modulation of the pump due to e.g. non-linear effects in the HNLF, mainly XPM from the original data signal as seen in figure 3.4. This signal degradation due to the phase modulation of the CW pump could potentially be reduced by applying a different scheme for SBS suppression, such as heating or stressing the fibre [33, 34].

3.4 Summary

Phase maintaining wavelength conversion based on FWM in HNLF is investigated for conversion of high-speed DPSK and DQPSK data signals. Error free and penalty free wavelength conversion of DPSK data signals up to 160 Gbit/s is achieved. SBS suppression is implemented in the form of a simple phase modulation scheme for broadening the line-width of the CW FWM pump. This scheme is seen to introduce only negligible penalty for the conversion of DPSK data signals, while DQPSK conversion suffers 4 dB penalty in receiver sensitivity. However error free wavelength conversion of DQPSK data signals up to 320 Gbit/s is demonstrated. The conversion efficiency of $\sim$ -10 dB is mainly limited by the applicable pump power, which in turn is limited by the SBS suppression scheme. Improvements in the SBS suppression could potentially allow for much higher conversion efficiencies through the introduction of parametric gain in the converter.
Based on the results of this chapter it is clear that one of the main issues to be solved in the implementation of FWM based wavelength converters for phase modulated data signals, is the identification of an appropriate SBS suppression scheme. The two main requirements of such a scheme is on one hand the ability to efficiently suppress SBS, while on the other hand not introducing additional impairments in the converted signal through FWM mediated frequency perturbations.
Despite these challenges results in this chapter indicate a significant potential of FWM in HNLF for high-speed wavelength conversion of phase modulated data signals in future all-optical networks.

Chapter 4

Data Format Conversion

4.1 Introduction

Having addressed the issue of wavelength conversion in the two previous chapters, the attention is now turned to another potentially useful system functionality. Novel modulation formats for data transmission like D(X)PSK have been demonstrated to provide increased robustness as well as the potential for increasing data capacity through multi-level modulation. However, future high speed optical networks may comprise several coexisting modulation formats in order to accommodate different requirements like robustness, bandwidth, simplicity or spectral efficiency in different regions of the network. In such high-speed photonic networks, it may be desirable to have those domains with different modulation formats transparently connected. This would require all-optical signal processing to perform e.g. data format conversion.
Some previous work has been done in this area, including the conversion of a 160 Gbit/s differential phase shift keying (DPSK) signal to on-off keying (OOK) in [38]. Conversion from OOK to DPSK has been performed at 10 Gbit/s using semiconductor optical amplifiers (SOAs) [39].

In this chapter a scheme for all-optical OOK to DPSK format conversion based on cross-phase modulation (XPM) in an highly non-linear fibre (HNLF) is presented and demonstrated. The converter is demonstrated in a transmission experiment for converting a 160 Gbit/s OOK signal to a 160 Gbit/s DPSK signal midway in a 320 km fiber link [40]. Furthermore the same format conversion scheme is demonstrated for the novel application of all-optically combining two separate data signals of

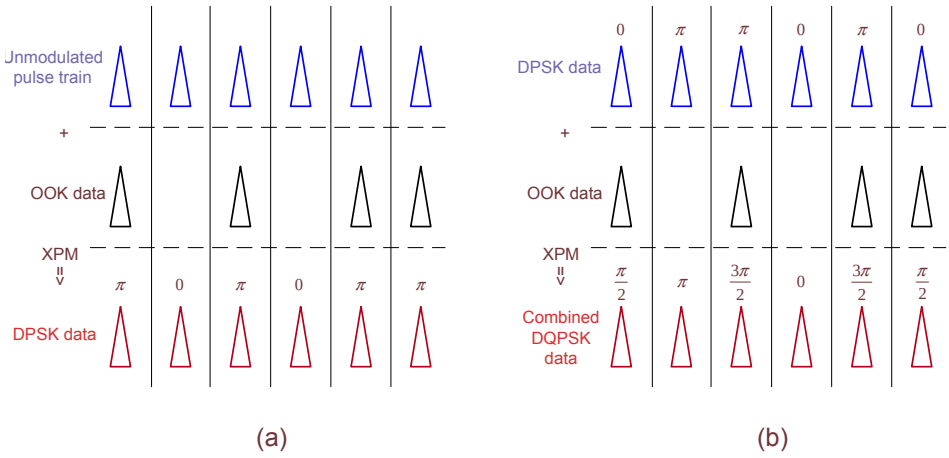

Figure 4.1: Principle behind format conversion by XPM.

different modulation formats into one signal, using a multilevel modulation format (differential quadrature phase shift keying (DQPSK)). In this chapter the combination of a DPSK signal and an OOK signal into a single DQPSK signal is demonstrated. The symbol-rate of the two tributary signals is maintained in the combined output signal, which carries the data of both signals. The spectral efficiency of the output signal is thus doubled compared to either of the input signals [41]. The all-optical combiner is demonstrated by combining an 80 Gbit/s incoming DPSK data signal with a locally generated 80 Gbit/s OOK data signal to a 160 Gbit/s DQPSK data signal half-way in a 320 km fibre link.

4.2 Principle of format conversion by XPM

In this section the principle of format conversion by XPM is described. The idea is basically to use XPM, here performed in an HNLF, to add phase modulation to a probe signal. The phase modulation represents a data content as in e.g. DPSK signals and follows the amplitude profile of the signal inducing the XPM. The probe signal can be either an unmodulated carrier or pulse train, or it can be a previously modulated signal, where XPM adds additional data in a multi level modulation scheme e.g. DQPSK. In figure 4.1 the principle of format conversion by XPM is illustrated. The figure describes the two configurations, which will be investigated in this chapter. In the first case (a) an OOK modulated data signal is used to

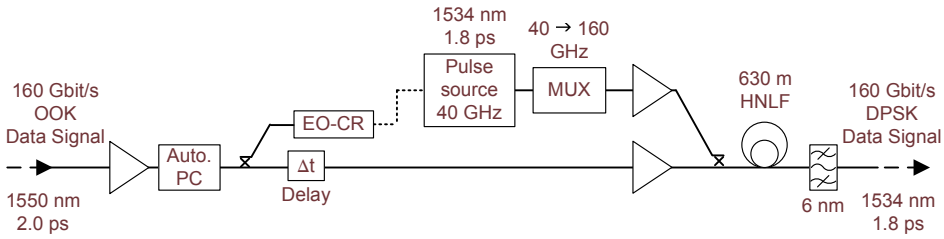

Figure 4.2: The figure shows the experimental setup for format conversion from OOK to DPSK by XPM.

phase modulate an unmodulated pulse train through XPM. This means that whenever an unmodulated pulse co-propagates with an OOK data mark, the pulse is ideally subjected to a π phase shift. In this way the data that was contained in the amplitude modulation of the OOK signal, will be contained in the phase of the pulse train at the output of the converter. In the second case (b) the unmodulated pulse train is substituted by a DPSK modulated data signal. By reducing the pulse powers the OOK data pulses are now used to introduce $\pi/2$ phase shifts in addition to the existing phase shifts of the DPSK data signal. In this way the data content of both the original DPSK signal and the added OOK signal will be contained in the resulting DQPSK signal.
Using XPM for data modulation may be associated with a limitation due to the shape of the pulse used for inducing XPM. As discussed in chapter 2, XPM induced by an optical pulse will follow the pulse shape. This means that e.g. a Gaussian shaped optical pulse will cause a Gaussian shaped phase modulation through XPM. This is not optimum for phase modulating data signals, as one would ideally apply a constant phase shift to the entire pulse in order to maximise the achievable contrast when demodulating the signal. The impact of this non-constant phase shift may be reduced by allowing a small amount of group-velocity dispersion (GVD) induced walk-off between the two signals, during the XPM induced phase modulation. This principle has been used previously to create flat-top switching windows using Gaussian pulses (M. Jinno in [42]).

4.3 OOK to DPSK format conversion

The experimental setup used to implement the all-optical format converter is shown in figure 4.2. The key component of the format converter is 630 m of HNLF with zero-dispersion λ_0=1560.5 nm and dispersion slope

S=0.03 ps/nm^2/km. The non-linearity is specified by the manufacturer to be γ=20 W^{-1}km^{-1}. An unmodulated 160 GHz pulse train is generated in the format converter at a wavelength of 1534 nm and pulse widths of 1.8 ps full width at half maximum (FWHM). The pulse train is generated by a 10 GHz erbium glass oscillator (ERGO) pulse source and multiplied to 40 GHz in a phase stabilised pulse multiplier (P-MULT). This allows for demodulation and detection of the DPSK data signal at 40 Gbit/s, since the 40 GHz tributaries to the multiplexed pulse train has a stable phase relationship. The pulse train was then multiplied from 40 GHz to 160 GHz in a standard optical time division multiplexing (OTDM) multiplexer. The pulse train was coupled into the HNLF together with the original OOK data signal via a 3 dB coupler. The OOK signal to be converted was at 1550 nm containing 2 ps pulses. An automatic polarisation controller [1] was used to set and maintain the optimum polarisation of the OOK data signal, compensating for variations in the input signal to ensure stable operation of the converter. The 160 GHz pulse train was synchronized to the incoming OOK signal by a PLL-based electro-optical clock-recovery (EO-CR) and the signals were aligned for temporal overlap in the HNLF by an optical delay line. The input powers into the HNLF were ∼20 dBm and ∼7 dBm for the 160 Gbit/s OOK signal and the 160 GHz pulse train, respectively. Figure 4.3 shows the optical spectrum recorded at the output of the HNLF. A 6 nm bandpass filter was used to select the DPSK data signal at the output of the format converter, suppressing the original OOK signal.

To test its performance, the format converter was introduced in a 160 Gbit/s transmission system as seen in figure 4.4. The 160 Gbit/s OOK data signal (PRBS $2^7 - 1$) was generated in an OTDM transmitter based on an ERGO pulse source and data modulated at 10 Gbit/s. It was subsequently multiplexed up to 160 Gbit/s. The OOK data signal was transmitted over a 160 km fiber link comprising 2 80 km fiber spans, each consisting of super large area fibre (SLA) and inverse dispersion fibre (IDF), before it was fed into the format converter. After the format converter, the 160 Gbit/s DPSK data signal, which was now at 1534 nm, was further transmitted over a second 160 km SLA-IDF fiber link. The signal was finally received in a 160 Gbit/s DPSK receiver. The receiver was synchronised to the signal by a second PLL-based EO-CR and the signal was demultiplexed to 40 Gbit/s using an electro absorption modulator (EAM). Demodulation

[1] The automatic polarisation controller consisted of a motorised polarisation controller and a polariser in a feedback loop maintaining constant (minimum) power through the polariser.

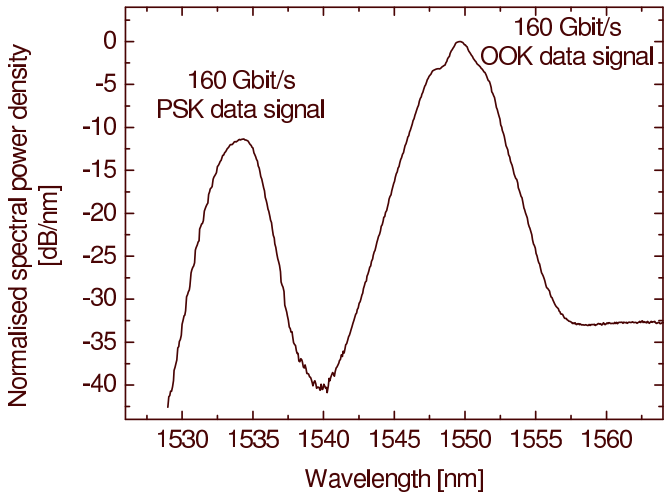

Figure 4.3: Optical spectrum for XPM format conversion at the output of the HNLF before filtering is performed.

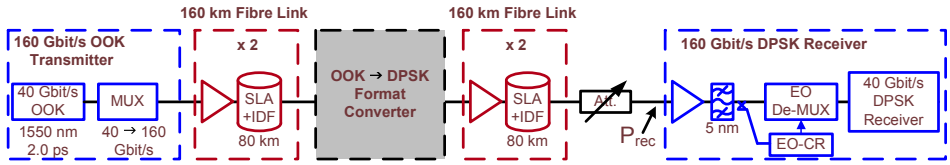

Figure 4.4: Transmission setup used for evaluation of the format converter inline in a transmission system.

was performed in a delay line interferometer (DLI) with 25 ps differential delay.

In figure 4.5, the results of bit error rate (BER) characterisations of the system performance can be seen. The system was characterised at 40 Gbit/s as well as at 160 Gbit/s. In both cases a conventional DPSK signal at 1534 nm generated by a Mach-Zehnder modulator (MZM) was used as reference. In a back-to-back configuration without any transmission, the format converter was seen to introduce ∼2 dB penalty in the receiver sensitivity for both 40 and 160 Gbit/s operation. This penalty is mainly attributed to a non-constant phase shift generated by XPM in the format converter due to the Gaussian pulse shape, as discussed previously. The non-constant phase shift caused a reduction in the achievable contrast in the DLI, which in turn led to a penalty in receiver sensitivity. The 160 Gbit/s measurements are all shifted ∼6 dB down in receiver sensitiv-

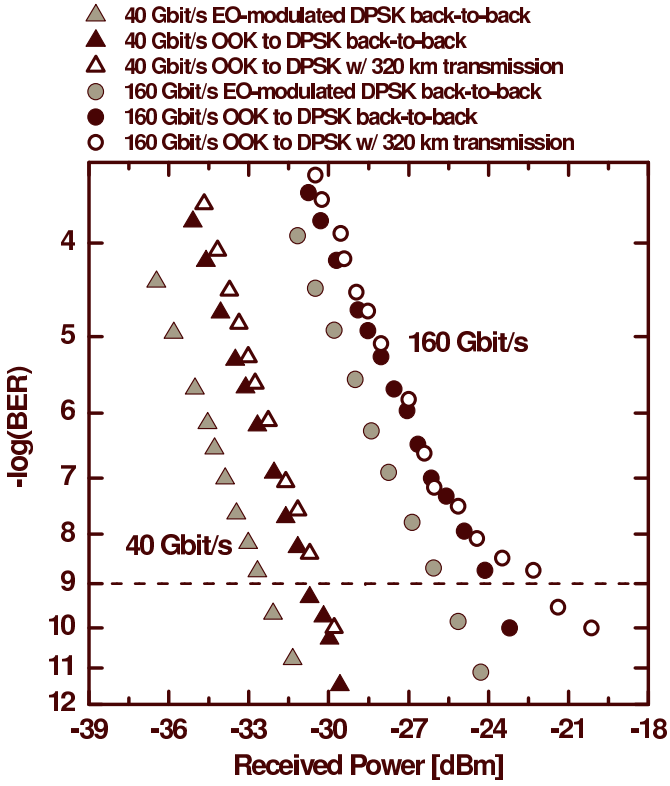

Figure 4.5: BER performance of the format converter with and without transmission compared with the performance of a conventional EO modulated DPSK signal.

ity. This shift is caused by the configuration of the BER measurements, where the received power was measured before demultiplexing the OTDM signal to extract one tributary channel. This means that a 6 dB difference is expected when increasing the bit rate from 40 to 160 Gbit/s and thus only ∼0.5 dB excess penalty from multiplexing and demultiplexing was observed.
Operating the format converter at 40 Gbit/s in the middle of the 320 km transmission line was seen to cause negligible penalty (< 0.5 dB at BER 10^{-9}) compared to the back-to-back performance. However at 160 Gbit/s some indication of an error floor was observed, which caused the penalty in receiver sensitivity to increase to ∼ 1.5 dB. This error floor is caused by suboptimum performance in the converter's clock recovery, affecting the synchronisation of the two signals in the format converter. A malfunction in the clock recovery causes instabilities and excess phase noise in the recovered clock signal. The conversion process is not expected to contribute to the observed error floor.

4.4 OOK and DPSK to DQPSK format combination

The format converter's potential for adding additional modulation levels to a previously modulated signal, is tested by introducing minor changes to the setup described above.
The layout of the format converter is largely maintained. The main difference is the designation of the signals in the converter. Previously the OOK signal was the sole source of data, which was transferred to the pulse train generated in the format converter. In this implementation the OOK data signal is generated in the converter and used to modulate a DPSK signal, which is received from an external source. The resulting DQPSK data signal contains the data of both the OOK signal and the DPSK signal, and the process is thus *format combination* [41] rather than *format conversion*.
The setup for the all-optical DPSK/OOK to DQPSK format combiner is seen in figure 4.6. The input powers into the HNLF in the format combiner are modified compared to the previous implementation, in order to achieve the correct XPM phase shift. An 80 Gbit/s OOK data signal is injected with ∼15 dBm, while the 80 Gbit/s DPSK signal is injected with ∼3 dBm. In both cases the reduction in power is slightly larger than the 3 dB caused by the reduction in bit rate from 160 Gbit/s to 80 Gbit/s. The power of the OOK signal is reduced in order to reduce the XPM phase shift from

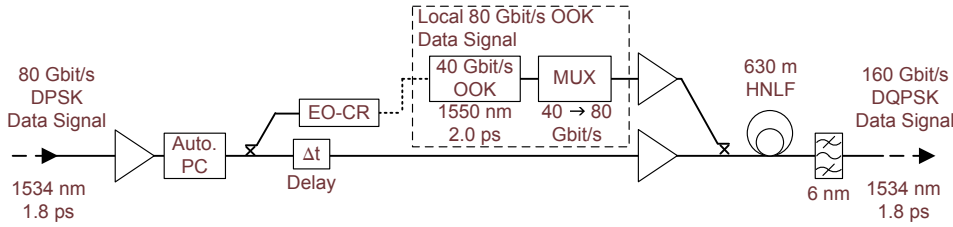

Figure 4.6: The setup for all-optical combination of an OOK data signal and a DPSK signal into a DQPSK signal.

π to $\pi/2$. The power of the DPSK signal is reduced in order to minimise the amount of excess phase noise caused by self phase modulation (SPM) in the HNLF. Even small variations in pulse shape and pulse powers in the multiplexed DPSK signal, can translate into phase distortions through SPM in the HNLF.

The transmission setup is identical to the one used previously, however in this case the DPSK signal is traveling through the first half of the link. The signal is generated by data modulating a phase stable 40 GHz pulse train in a MZM and subsequently multiplexing it up to 80 Gbit/s. After transmission the signal is modulated in the format combiner, becoming a DQPSK signal, which is transmitted trough the last part of the link. In this way the wavelength of the transmitted signal (1534 nm) is maintained throughout the system. In the receiver the DQPSK signal is demultiplexed in and EAM and demodulated using a DLI. BER measurements are performed using a programmable error detector, which replaces a dedicated post-processing circuit to recover the original data logic. The delay-line interferometer is alternately adjusted to measure both phase components of the DQPSK data signal.

The results of the BER measurements for the combined DQPSK data signal are shown in figure 4.7. Error-free performance is achieved for back-to-back operation and when including transmission over the complete 320 km fibre link. For the OTDM channel shown in figure 4.7, the penalty from introducing transmission is ~ 2 dB. The eye diagram in figure 4.7, shows the combined DQPSK signal after demultiplexing and demodulation. Some noise is observed in the eye diagrams, indicating imperfections in the DQPSK signal.

Figure 4.8 shows the receiver sensitivity at BER 10^{-9} for all channels in the combined DQPSK signal, in back-to-back configuration and in the transmission system. Both phase components for each OTDM tributary channel

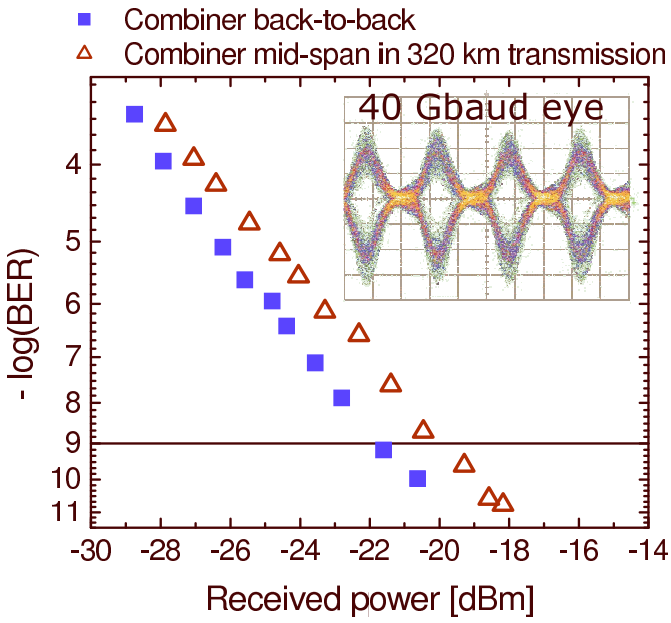

Figure 4.7: BER results for the format combiner in back-to-back configuration and inline in the transmission span.

are measured. The variations in receiver sensitivities are comparable for the two configurations and are expected to be caused by amplitude variations in the multiplexed DPSK and OOK data signals. For all the measured channels a penalty is associated with implementing the converter in the transmission span. This penalty is expected to be mainly caused by the last sections of the transmission span, where the combined DQPSK signal is transmitted 160 km. Imperfections in the modulation of the DQPSK signal, may cause it to be increasingly sensitive to transmission impairments, resulting in the observed penalties.

4.5 Discussion and summary

XPM in HNLF has successfully been demonstrated as a way of encoding phase modulated data signals. This has been shown by encoding π phase shifts onto an unmodulated pulse train, forming a DPSK data signal, and by encoding $\pi/2$ phase shifts onto a DPSK data signal, forming a DQPSK data signal. In both cases it was possible to implement the functionality in a transmission system.

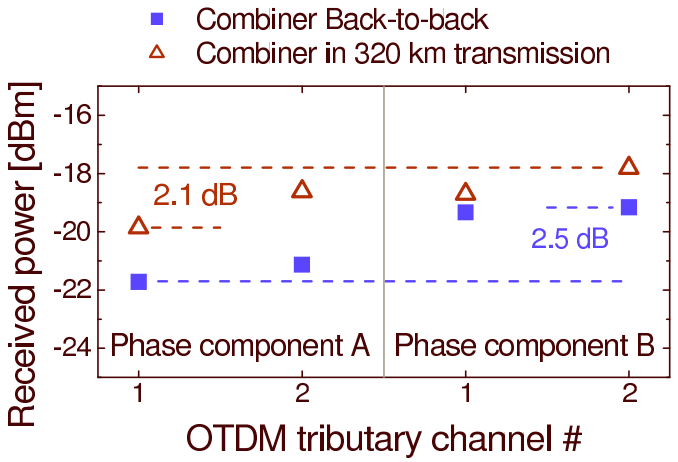

Figure 4.8: Channel sensitivities for the format combiner. Both OTDM channels and both phase states are measured.

The format conversion from OOK to DPSK is associated with a wavelength conversion, which is inherent to the conversion scheme. In the present implementation of the format converter, the combination of dispersion profile in the HNLF and the wavelength allocation of the two signals is used to reduce the effect of the non-constant XPM induced phase shift, otherwise determined by the pulse shape. The GVD induced walk-off between the two signals is introduced to cause a significantly more constant phase shift across the pulses that will form the DPSK output signal. In practice this means that too little walk-off between the signals will cause an inconstant phase shift across a data pulse, while a large walk-off will result in inter-symbol interference (ISI) between neighboring pulses. Thus a severe limitation is imposes on the tunability of the wavelength conversion as this affects the walk-off in the HNLF. In the current configuration it is not expected that a large tuning range for the wavelength conversion can be achieved, while maintaining the same performance of the format converter.

Depending on the application of the converter, the issue may arise that the data in the phase modulated output signal is not encoded as differential phase shifts, but rather as phase shifts with respect to the original phase of the signal. The same applies to most other means of generating phase shift keying (PSK) or DPSK data signals, and this is the reason why DPSK data needs to be pre-coded before modulation is performed. In these characterisations the issue has not been acute due to the features of the pseudo random bit sequence (PRBS) pattern eliminating the need for pre-coding

or post-processing the signals in order to recover the original data. The term 'DPSK' for the converted output was chosen based on the applied demodulation scheme, although the logic of the OOK signal is not directly reflected by differential phase shifts in the signal. In order to implement the format converter as suggested here, some processing of the demodulated data is necessary to recover the logic of the OOK data signal.

The issue of recovering the original data becomes more acute when implementing the system as a format combiner. Here the situation resembled that of using two concatenated modulators to create a DQPSK signal. The demodulated data for each setting of a DLI demodulator will contain information encoded by both modulators, and thus no DLI configuration will grant access to the data originating from one modulator. In the implementation of the optical format combiner suggested here, pre-coding the data to overcome this problem, is not considered as a useful approach as the two tributary signals have different points of origin. In order for the DLI outputs to reflect the original data logic the two inputs to the format combiner will need to have the same origin, where pre-coding can be performed. Thus a post-processing scheme implemented after demodulation will be preferable for recovering the logic of the original data.

Chapter 5

XPM Based Clock Recovery and Channel ID

One of the main issues to be addressed in order for optical time division multiplexing (OTDM) to become a feasible network technology is the ability to unambiguously identify the individual tributary channels. This ability will be essential for implementing any network functionality based on OTDM technology. A few schemes have been proposed to address the issue of channel identification. One of these is the pilot tone modulation, where amplitude modulation is used to mark one OTDM channel before multiplexing the signal. This modulation can subsequently be recognised after demultiplexing, which will supply a reference for labeling the remaining channels [43]. A second proposed scheme for channel identification relies on aligning the phase of the OTDM channels in the multiplexer in a way which allows for the extraction of a base rate clock in the receiver [44]. The idea is that the extracted base rate clock will have a stable phase relationship with the OTDM signal, and can serve as a reference for channel identification.
This issue of channel identification originates from the lack of a global clock reference throughout a transmission system. This also leads to a second important issue to be addressed in high-speed communication systems, namely that of clock recovery. There have been two main approaches to this issue. One is based on locking an electro-optical phase-locked loop (PLL) to the OTDM signal, and thus synchronising a base rate clock to the received signal [45]. The second approach is based on injection locking of an optical pulse source. This forces an optical pulse train to be formed, which is synchronised to the high speed signal. This can be at a reduced repetition

rate, in which case the generated pulse train corresponds to a subharmonic clock signal for the OTDM data signal e.g. [46].
In this chapter, a scheme for combining channel identification and clock recovery (CR) is proposed. Similar to [44], this scheme relies on phase modulation of the OTDM data signal. In the proposed scheme one channel in the multiplexed signal, is phase modulated through cross-phase modulation (XPM) with an optical pulse train at the base rate. This phase modulation is subsequently detected in the receiver by sideband filtering, and is used for both clock recovery and channel identification. The system has been demonstrated in a transmission experiment at 320 Gbit/s, and characterised in more detail at 160 Gbit/s [47].

5.1 Principle of the clock recovery and channel ID

The principle behind the proposed scheme for clock recovery and channel identification is shown in figure 5.1. After the generation of a conventional

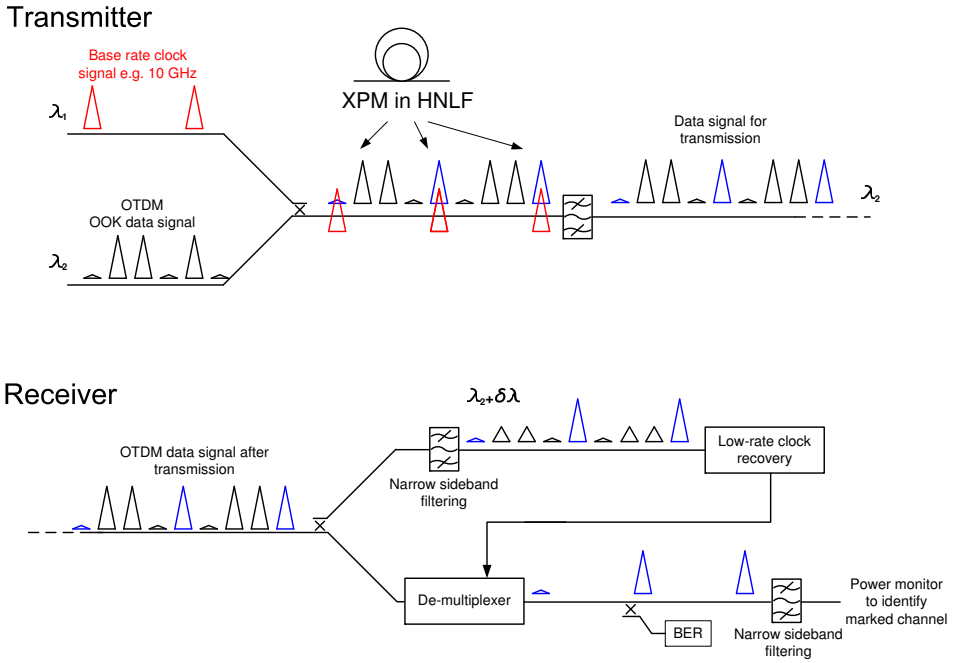

Figure 5.1: The principle of CR and channel ID by XPM in the transmitter and sideband filtering in the receiver.

OTDM on-off keying (OOK) data signal, XPM between the data signal and a pulse train at the channel base rate is performed. The pulse train is synchronised with the OTDM signal and is temporally aligned to modulate only one of the OTDM channels. This imposes a chirp on the pulses of that particular channel, slightly altering their optical spectrum.
In the receiver, after transmission of the signal, the spectral components generated by XPM in the transmitter, are filtered out. This filtered sideband from the labeled channel corresponds to a low-contrast demultiplexing of that particular channel. A similar scheme with stronger XPM has been characterised as a data demultiplexer in by L. Jie in [48]. In this implementation the demultiplexed signal is only made strong enough to allow a CR circuit at the base rate to lock to it. This strongly reduces the necessary amount of XPM induced chirp, making the signal more suitable for transmission. The clock supplied by the base rate CR is then used to synchronise the demultiplexer, and the receiver electronics. After demultiplexing, a similar sideband filtering is performed, and the filtered power is detected as a means of detecting the XPM-labeled channel. In this way, a specific channel can be identified simply by enumerating with respect to the labeled channel.
In this way a clock recovery scheme with inherent channel identification can be realised using only base rate electronics. This means that the scheme may have potential for operating at even higher bit rates, than the currently achieved 320 Gbit/s.

5.2 320 Gbit/s transmission with clock recovery and channel ID

The experimental setup for the demonstration of XPM based CR and channel identification is shown in figure 5.2. A high-speed optical signal is generated in a standard OTDM transmitter comprising a 10 GHz erbium glass oscillator (ERGO) pulse source generating 1.3 ps pulses at 1557 nm, which are data modulated in a Mach-Zender modulator ($2^7 - 1$ pseudo random bit sequence (PRBS)) and multiplexed to 160 or 320 Gbit/s. The high-speed data signal is injected into 100 m of highly non-linear fibre (HNLF) along with a 10 GHz pulse train at 1544 nm from a second ERGO pulse source. The two signals are temporally aligned for overlap between one of the 10 Gbit/s tributary channels in the high-speed signal and the 10 GHz pulse train, in order to induce XPM between the two signals. At the output of the HNLF the pulses at 1544 nm are suppressed by a band pass

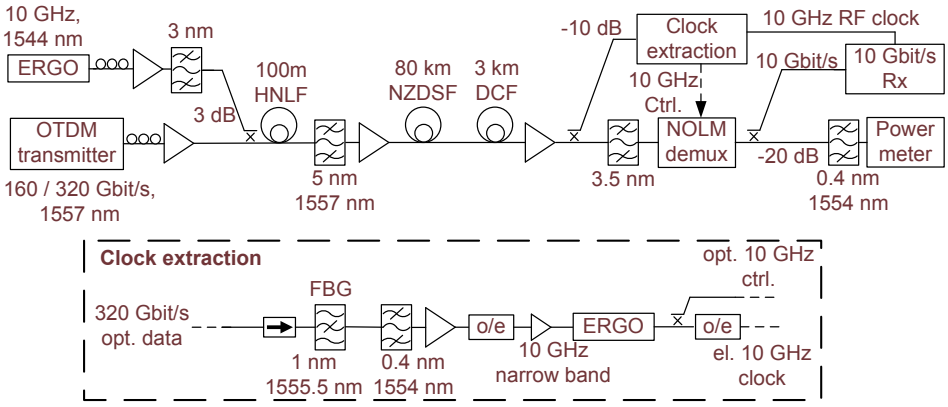

Figure 5.2: XPM modulation and transmission setup.

filter and the 320 Gbit/s data signal is transmitted through 80 km of non-zero dispersion shifted fibre (NZDSF) compensated with 3 km of dispersion compensating fibre (DCF). After transmission, the signal is split in a 10 dB coupler. The weak output is used for clock extraction while the strong output is injected into a non-linear optical loop mirror (NOLM) for demultiplexing. Clock extraction is performed by filtering on the low wavelength edge of the data spectrum, using a combination of a fibre bragg grating (FBG) notch filter and a 0.4 nm Gaussian shaped band pass filter to isolate the sideband created on the marked data channel by XPM in the transmitter. The filtered sideband is then detected in a photo-detector and the electrical signal is filtered to enhance the 10 GHz component. An ERGO optical pulse source at 1543 nm is synchronised to the 10 GHz component in the detected RF clock signal using its internal PLL. In this way the base rate clock is extracted to synchronise the demultiplexer and the receiver electronics. The optical output of the pulse source then represents a 10 GHz clock signal which is synchronised to one specific channel in the input data signal. Clock extraction is achieved for PRBS lengths up to $2^{15} - 1^1$, limited by the particular PLL used in the ERGO. The optical pulses from the ERGO in the receiver, are then split into two arms. One is used as control pulses for the demultiplexer and the other is o/e converted to generate a 10 GHz RF clock to synchronise the base rate receiver. The 320 Gbit/s data signal is demultiplexed in a NOLM comprising 50 m of HNLF (dispersion slope $\sim$0.018 ps/nm^{2}km, zero dispersion at 1554 nm

[1]This is the PRBS sequence encoded on the 10 Gbit/s tributary channels. The multiplexed signal is only a PRBS for $2^7 - 1$.

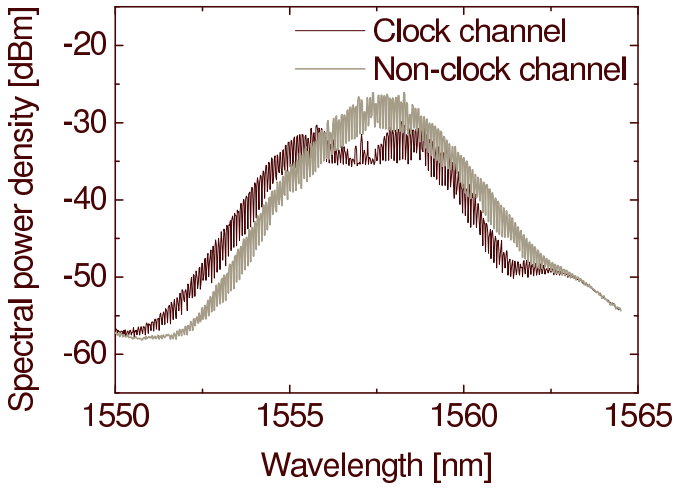

Figure 5.3: Spectrum of demultiplexed data signal for the clock channel and for one other channel.

and γ ~10.5 $W^{-1}km^{-1}$). A 20 dB coupler is used to tap the demultiplexed signal for channel identification. A narrow filter at the edge of the signal spectrum is used to identify the channel carrying the clock mark, similar to what is done for clock extraction. The power through the filter is measured using a sensitive low bandwidth power meter. The strong output from the demultiplexer is used for bit error rate (BER) measurements.

As discussed previously, the label used for CR and channel identification, is applied as a phase modulation to one OTDM channel by XPM in the HNLF before transmission. This generates spectral sidebands on the optical spectrum of that particular data channel slightly broadening its spectrum. In figure 5.3 the spectrum of the labeled channel is shown after demultiplexing along with the spectrum of one of the unmarked channels. In the CR scheme the sidebands are detected by filtering at the edge of the spectrum (~1554 nm). The difference detected in this filtered sideband power, between the labeled clock channel and the remaining channels after demultiplexing can be seen in figure 5.4. A 6 dB power contrast between the clock channel and the remaining channels is achieved in this way, as seen in figure 5.4, yielding a clear channel identification. The slight spectral broadening associated with the chirp induced in the labeled channel, is expected to make this channel slightly more susceptible to dispersion in the transmission span. However, this is easily overcome by standard passive dispersion compensation in the demonstration. Figure 5.5 shows

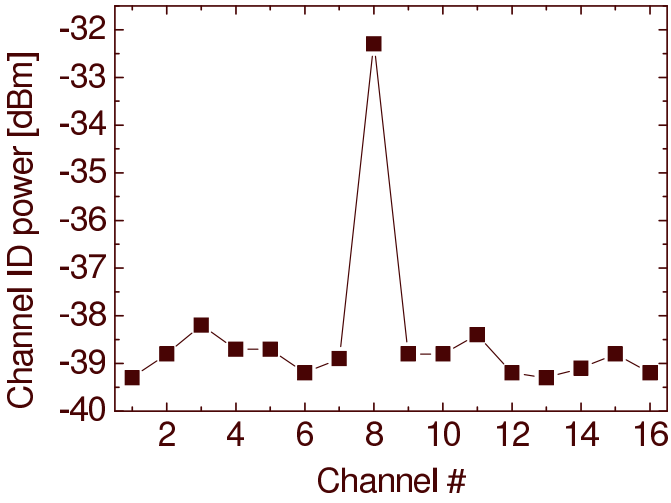

Figure 5.4: Measured power for identifying the clock channel in the receiver.

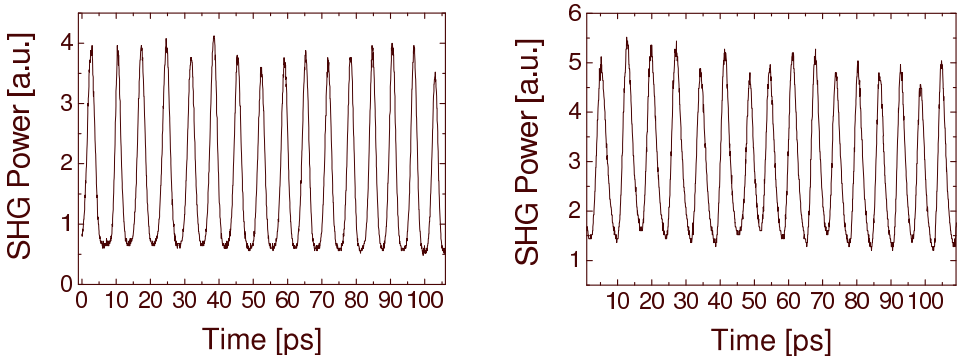

Figure 5.5: 160 Gbit/s data with phase modulated clock before transmission (left) and after 80 km transmission (right).

the cross correlations of a 160 Gbit/s data signal with phase modulated clock channel before transmission (left) and after transmission (right). In both cases no discernible pulse width difference among the 16 channels is observed indicating sufficient dispersion compensation in the transmission line.

Figure 5.6 shows BER measurements for the 320 Gbit/s data signal transmitted 80 km with a clock-labeled data channel. BER curves for the clock modulated channel and for one other channel are shown. Both are error free with no error floor. The clock channel has a penalty in receiver sensitivity of only 1.2 dB, demonstrating that this scheme is applicable for

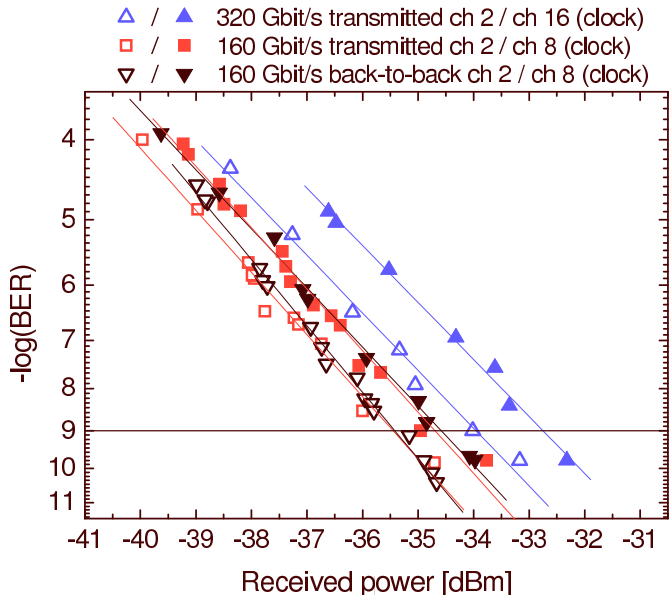

Figure 5.6: BER: 160 / 320 Gbit/s (PRBS 2^7-1) 80 km transmission and back-to-back with phase modulated clock.

OTDM signals up to at least 320 Gbit/s. For a 160 Gbit/s data signal, BER curves are shown with and without transmission for the clock channel and for one other channel. In all cases error free operation is achieved. The clock channel has a penalty in receiver sensitivity of less than 0.8 dB compared with the unmarked channel in back-to-back operation. It is seen that the 80 km transmission has almost no effect on the performance of the signal, indicating that the clock is effectively recovered in the receiver. In figure 5.7, the receiver sensitivities for 160 Gbit/s transmission with the phase modulated clock are shown, along with the sensitivities for 160 Gbit/s back-to-back using the electrical clock from the transmitter to synchronise the receiver. In both cases all channels achieve error free operation. For the transmitted signal the receiver sensitivities at BER 10^{-9}, vary within 1.3 dB with an average sensitivity of -35.4 dBm. This shows that the performance of the marked channel lies within the overall sensitivity variation of the signal, rendering it virtually penalty-free. In the back-to-back case without XPM labeling the variation is 0.7 dB and the average sensitivity is -35.7 dBm. The increase in channel variation after transmission is expected to be due to imperfect multiplexing of the data signal resulting in slightly varying impact of the transmission impairments, in particular the

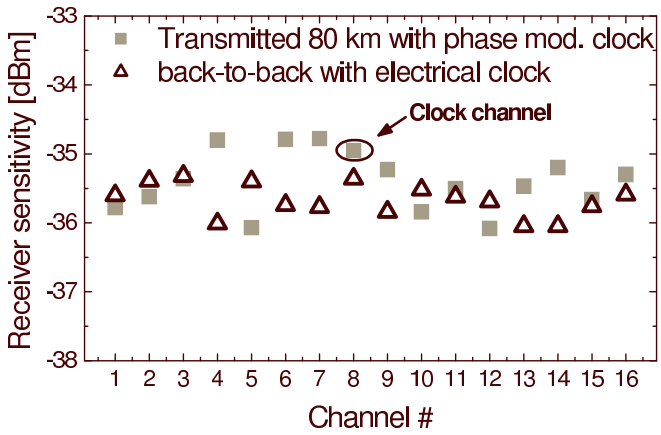

Figure 5.7: Receiver sensitivities for 160 Gbit/s (PRBS $2^7 - 1$) data signal transmitted 80 km with phase modulated clock and back-to-back with electrical clock (i.e. without XPM labeling).

non-linear effects affecting the signal during transmission.

5.3 Discussion and summary

As opposed to most previously proposed schemes for channel identification by labeling specific OTDM channels, this scheme introduces the label on the channel after the high speed signal has been generated. This introduces some potential for networking, since a label can be added to a signal originating from a separate source (e.g. a different network node). One desirable extra functionality is the ability to erase the label on a channel without loosing the information carried by that channel. One solution to this can be the XPM-based wavelength conversion described in chapter 2, which is insensitive to the chirp of the labeled channel. With the described scheme it is believed that a network node can be implemented, which is capable of receiving a data signal with a labeled channel and synchronise to this signal as described. Add and drop operations can then be performed, which may generate an OTDM signal with several labeled channels or no labeled channels. All labels on channels are finally erased by e.g. XPM wavelength conversion of the signal and a new label is modulated onto a designated channel, before the signal is transmitted further into the network.

In this chapter, a scheme for combined clock recovery and channel identification is proposed and demonstrated. A 320 Gbit/s data signal with an

XPM labeled channel is transmitted 80 km. The clock is successfully extracted from the signal by sideband filtering and reliable channel identification is obtained. Error free performance with low penalty is demonstrated for the transmitted signal using the recovered phase modulated clock.

Chapter 6

Increased Timing Tolerance using Flat-top Pulses

One of the key issues faced when implementing optical switches for processing of high-speed serial data signals is the pronounced sensitivity to timing jitter and temporal mismatch, which is usually inherent in such systems. Therefore it can be very advantageous to have a switch with a high tolerance to timing inaccuracies. One way of reducing the sensitivity to timing jitter is to establish a rectangular temporal switching window [42, 49]. This provides increased resilience to timing jitter-induced errors, and also reduces the required absolute accuracy for temporal bit alignment. For high-speed signal processing (>100 Gbit/s serial data rates) optical switching i.e. a switch controlled by an optical gating pulse, is currently the only option. A switch gated by an optical signal will in most configurations have a switching window which is highly dependent on the shape of the optical pulse used to control the switch. One approach to the issue of constructing timing jitter tolerant optical switches is therefor the implementation of optical pulse shaping. An alternate approach is the construction of a switch which reduces the dependence of the switching window on the control pulse shape. In [42] group-velocity dispersion (GVD)-induced walk-off between control pulse and data signal in a non-linear optical loop mirror (NOLM) demultiplexer causes a Gaussian control pulse to generate a flat-top switching window. This approach is very useful for laboratory characterisations etc. However it is believed that a scheme based on shaped control pulses, where the switch can be designed to be mainly dependent on the pulse shape, is potentially much more versatile in terms of e.g. transparency to signal wavelength and switching window shape and duration.

Previously, a highly bi-refringent fibre has been used to generate a pulse with a flat top, which was implemented in a 160 Gbit/s regenerator [18].

In this chapter three different approaches to generating rectangular optical pulses for switching will be discussed and validated by experimental results. The first approach is a novel application of the optical fourier transform (OFT) technique described in [50]. In this approach the optical spectrum is shaped by filtering and subsequently the shape is transferred to the time domain by the OFT process. This technique is verified in a 160 Gbit/s demultiplexing experiment [51, 52]. A significant increase in timing tolerance is observed when using the rectangular shaped pulses as control for the demultiplexer compared to using Gaussian shaped control pulses.

The second pulse shaping scheme to be addressed in this chapter is the application of a sinc-shaped optical filter corresponding to a rectangular shaped pulse in the time domain. This has previously been demonstrated in an 80 Gbit/s demultiplexing experiment [53]. This scheme is highly dependent on the ability to manufacture the appropriate sinc-shaped filter. In the present implementation the filter is realised as a super-structured fibre bragg grating (SSFBG). In this chapter a 160 Gbit/s optical re-timer is demonstrated, which is based on rectangular pulses generated using such a SSFBG. The re-timer provided a reduction in RMS timing jitter from 410 fs to 250 fs and a significant improvement in bit error rate (BER) performance as error free operation could only be achieved after re-timing of the noisy input data signal [54, 55].

The third pulse shaping scheme demonstrated in this chapter is based on a novel linear signal processing scheme [56] that exploits an optical differentiator [57] based on a specially tailored long period grating (LPG) to generate a pulse with a 400 fs flat-top region. This pulse is subsequently used to gate a NOLM demultiplexer, resulting in a significant increase in the timing tolerance of the switch. This is verified in a 640 Gbit/s demultiplexing experiment. Flat-top switching pulses enabled error free demultiplexing of a data signal with the high integrated timing jitter of 230 fs. Using Gaussian switching pulses the timing jitter prevented error free demultiplexing [58]. The timing tolerance was estimated by demultiplexing a 640 Gbit/s data signal with only $\sim$100 fs timing jitter, and a timing tolerance of 350 fs was found for the demultiplexer, when using flat-top control pulses [59]. For the low-noise data signal an improvement in receiver sensitivity of 14 dB was also observed when using flat-top control pulses for demultiplexing in stead of Gaussian ones.

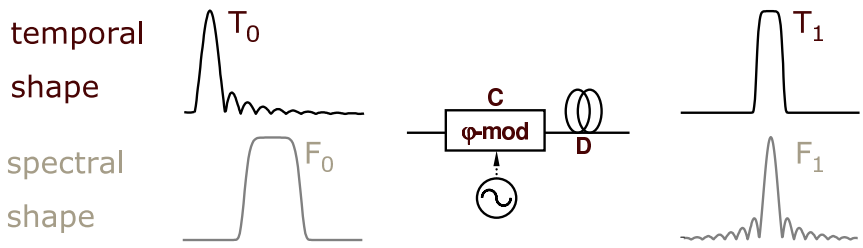

Figure 6.1: The figure shows the principle behind the optical fourier transform, where the spectral shape and the time domain shape of a signal are swapped.

6.1 Pulse shaping by the OFT method

The principle of pulse shaping by the OFT method, is illustrated in figure 6.1. The basic idea is to let a Fourier transform pair swap domains by a linear transformation. This is achieved by adding a linear chirp to the input pulse and subsequently transmitting it through a dispersive medium [50] (see Appendix B for the theoretical derivation of OFT by linear chirp and dispersion). In order to achieve appropriate pulse shaping, the spectrum of the original Gaussian shaped pulse, is filtered to obtain a spectral shape corresponding to the desired time-domain shape after OFT. A temporally narrow, and hence spectrally wide, pulse is injected into a filter with a square-like filter function. The output of the filter will thus be spectrally square, with the temporal shape of a sinc-function. Using a sinusoidal phase modulation to modulate the pulse, a linear chirp is approximated. By carefully balancing the added chirp and the dispersion of a length of fibre, the transform pairs will swap their domain shapes. In the present configuration a rectangular shaped spectrum is transformed into a rectangular shaped pulse in the time domain.

6.1.1 Generation of rectangular pulses by OFT

The motivation for generating flat-top or rectangular shaped pulses, is the generation of corresponding flat-top or rectangular switching windows. This is desirable in order to reduce the impact of relative timing jitter and timing mismatch between an incoming data signal, and an optical switch. To this end, a rectangular shaped pulse is generated and used as control pulse in an ultra-fast fibre-based switch in this case a NOLM. The switching window of the NOLM is largely determined by the shape of the control pulse, with possible modifications for pulse walk-off in the NOLM. The

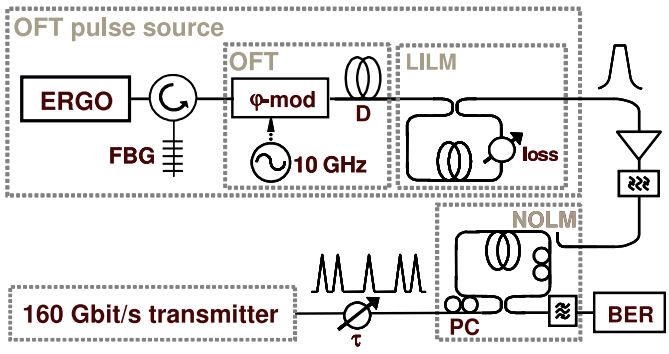

Figure 6.2: Setup for rectangular pulse shaping using OFT to generate control pulses for a 160 Gbit/s NOLM demultiplexer.

experimental setup for OFT pulse shaping is shown in figure 6.2. A 2 ps optical pulse with a spectral full width at half maximum (FWHM) of 3.5 nm centred at 1545 nm is generated by an erbium glass oscillator (ERGO) pulse source. The pulses are filtered using a fibre bragg grating (FBG) in reflection configuration with an optical circulator resulting in a rectangular shaped bandpass filtering with a 3-dB bandwidth of 2 nm. This rectangular shaped spectrum is injected into a chirp-dispersion unit, where it is phase modulated (φ-mod) at 10 GHz. By matching the induced chirp to the total dispersion (D) of a dispersive medium (here 4.5 km single mode fibre (SMF) is found experimentally to be appropriate), the transformation from the spectral domain to the temporal domain is performed, and rectangular pulses are obtained. The rectangular pulses generated in this way are degraded by the presence of pedestals, which are suppressed by passing them through a loss-imbalanced loop mirror (LILM). The LILM contains an attenuator placed asymmetrically in the loop which is formed by 500 m highly non-linear fibre (HNLF). This construction causes a difference in self phase modulation (SPM) induced accumulated phase shift of the signals propagating in opposite directions in the loop. In this way an intensity dependent filtering is achieved, suppressing the weak pulse components, where the difference in accumulated phase shift from passing through the loop is smallest. The rectangular pulses are subsequently amplified and used to gate a NOLM demultiplexer, which demultiplexes a 160 Gbit/s, $2^7 - 1$ pseudo random bit sequence (PRBS), single-polarisation optical time division multiplexing (OTDM) data signal down to 10 Gbit/s for subsequent BER measurements. The temporal displacement between data and control pulses is controlled using an optical time delay (τ).

Figure 6.3 shows pairs of spectra and temporal cross-correlations at different points in the OFT pulse shaping process. The cross-correlations are performed using 1.7 ps sampling pulses, which limits the temporal resolution. At the output of the FBG the original 3.5 nm Gaussian spectrum is shaped into a ∼2 nm wide rectangular spectrum. In the time domain this spectral shaping is seen to produce significant trailing pulses, which is expected as a perfectly rectangular spectrum will be associated with a time domain *sinc* shaped pulse. The 'tail' of trailing pulses covers ∼40 ps from the main pulse.

Figure 6.3 (centre) shows the output of the chirp-dispersion unit where OFT is performed. The 10 GHz phase modulation induces a sinusoidal phase shift with a modulation depth of 1.5π peak-to-peak. At the output of the dispersive medium, the induced chirp has been matched so that the rectangular spectral shape has now been transferred to the time domain, yielding a rectangular pulse (figure 6.3 (centre, bottom)) with a 4 ps flat top and an 11 ps FWHM. Some residual trailing pulses are observed after OFT, as seen in the cross-correlation. These are expected to be partly due to imperfect compensation of the dispersion of the FBG-based rectangular filter. A second contribution may be the approximation of a parabolic phase modulation by a sinusoidal modulation. Finally, the filtered spectrum from the FBG also exhibits some side lobes, which may have been transformed into the time domain along with the rectangular shape. As the full time domain shape of the pulses after filtering stretches across ∼40 ps, a 10 GHz sine shaped modulation will deviate substantially from a parabolic shape for some parts of the pulses. These residual trailing pulses are the main reason why the LILM is included in the pulse shaper. The intensity dependent transfer function of the LILM servs to suppress the trailing pulses, as well as steepen the edges of the main pulse - approximating a rectangular shape even better. The output of the LILM is shown in figure 6.3 (right). It is seen that the trailing pulses are significantly suppressed resulting in an improvement of the pulse tail extinction ratio (PTER) from 6 dB to 18 dB by passing the signal through the LILM. The pulse has a 3 ps wide flat top and its FWHM is ∼6.5 ps.

Figure 6.4 shows a comparison between the theoretically expected behavior of the OFT and the experimental results (see Appendix B for further details).

The experimental spectrum at the input to the OFT (figure 6.4 left) is fitted by a 3'rd order supergaussian shape with 0.75 nm 1/e spectral width. Transforming this yields a supergaussian OFT output in the time

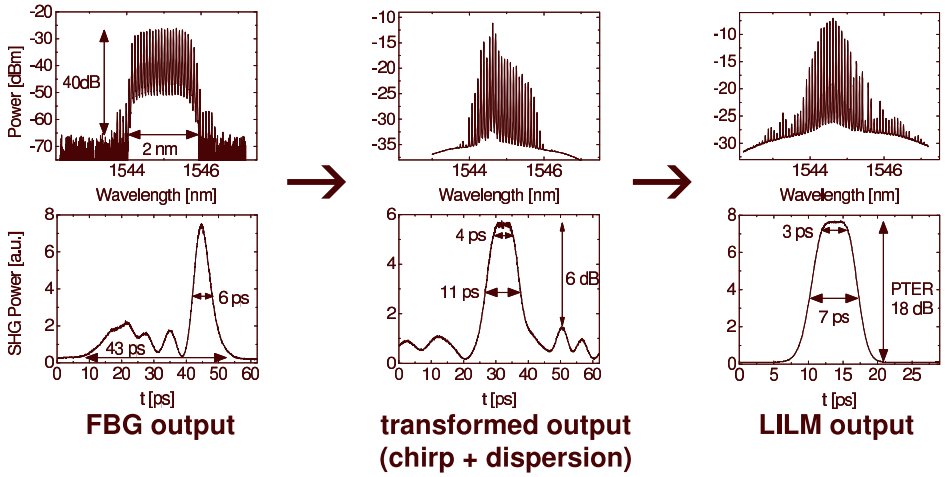

Figure 6.3: The figure shows spectra and temporal shapes of the signal at different key points in the OFT pulse shaper.

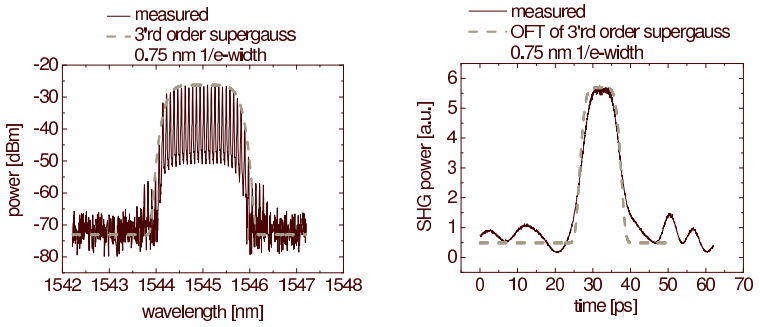

Figure 6.4: Comparison of theory with experiments.

domain with a 5.7 ps 1/e width, matching the experimental value. The theoretically required length of SMF for achieving a pulse width matching the experimental value was $\sim 1/10$ of what was used in the experiment. However, in practice the SMF applied after the phase modulator compensates both the dispersion of the FBG and the induced chirp. Without any dispersion in the FBG the temporal shape of the filter output is expected to be somewhat narrower, based on the width of the filtered spectrum. A main pulse of ∼4 ps FWHM and a total length of the temporal sinc profile of ∼20 ps corresponds to the 2 nm wide spectrum. Thus, some dispersion compensation (here by SMF) is needed to counteract the dispersion from the FBG. Figure 6.4 (right) shows the comparison between the measured cross-correlation and theoretically predicted OFT. The flat-top region of the actual pulse may be reduced in the cross-correlation output due to the broad sampling pulse. Similarly the FWHM of the cross-correlation will be larger than the actual pulse width. Thus, perfect agreement between the experimental and theoretical results is not expected, but a clear confirmation of the pulse shaping principle is however achieved.

6.1.2 160 Gbit/s demultiplexing verification

In order to demonstrate the use of the generated rectangular pulses (after the LILM) in a system, they are applied as control pulses in an OTDM NOLM-demultiplexer. The OTDM data is generated by the use of a second ERGO pulse source running at 10 GHz, data modulated with a 2^7-1 PRBS sequence in a Mach-Zehnder modulator (MZM) before being multiplexed to 160 Gbit/s. The data signal is at 1557 nm and both the NOLM and the LILM comprise 500 m HNLF with zero dispersion at 1551 nm and a dispersion slope of 0.017 ps/nm^2/km. The walk-off between control and data signals in the demultiplexer is minimised in this way in order to ensure that the switching window shape is determined by the control pulse shape.

In figure 6.5 (left) receiver sensitivities for achieving BER 10^{-9} is shown for all 16 OTDM channels demultiplexed using the OFT shaped rectangular pulses. Despite the relatively wide control pulses (3 ps flat top and 6.5 ps FWHM in the cross-correlations) no indication of inter-symbol interference (ISI) from neighboring channels is observed, and error free operation is archived for all channels with an average receiver sensitivity of -34.5 dBm. To the right in figure 6.5 eye diagrams for all the demultiplexed channels are shown. Also here no sign of ISI is observed.

Figure 6.6 shows the timing tolerance between data and control signal for the 160 Gbit/s demultiplexer by demultiplexing channel 10 using the

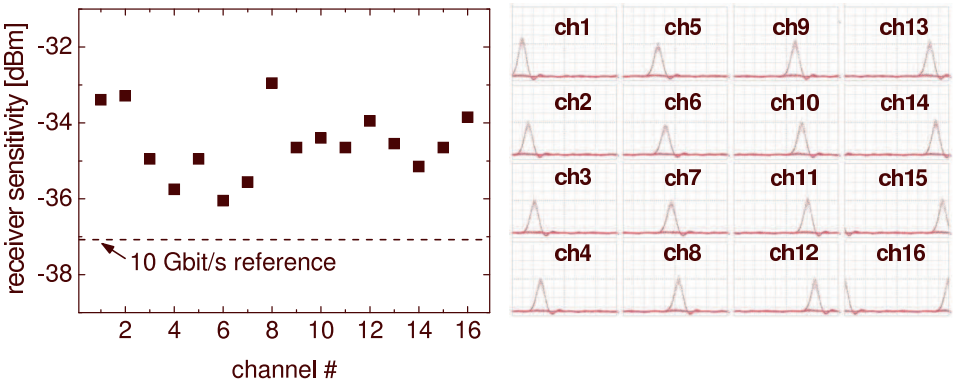

Figure 6.5: Receiver sensitivities and eye diagrams for demultiplexing the 16 OTDM channels, using rectangular control pulses for switching in the demultiplexer.

rectangular shaped control pulse. For comparison, the demultiplexing is also performed with a 2 ps FWHM Gaussian pulse. In order to evaluate the effect of the rectangular shaped control pulse, the relative delay between control and data is altered in steps and for each step, the BER is evaluated. The receiver power is set to 5 dB above the receiver sensitivity for both pulse types to allow for some margin. This measurement is used to characterise how big a time displacement between data and control can be tolerated. It can also be considered as a static measure of the amount of timing jitter which can be tolerated by the switch configuration. The rectangular pulse is seen to maintain error-free performance with a 2.6 ps tolerance to temporal displacement. The Gaussian pulse on the other hand, only ensures error-free operation within a 1 ps tolerance. As seen in the eye diagrams inset in figure 6.6 interference from neighboring channels is limiting the BER for large displacements of the signals, when demultiplexing with the rectangular pulse. This is caused by the FWHM of the rectangular pulse being slightly too large for the 160 Gbit/s bit-rate. This results in neighboring channels being switched through the demultiplexer sooner than desired, when a time displacement is introduced, leading to ISI. This also contributes to the steeper BER curves in figure 6.6 when the rectangular pulses are used. This indicates that an increase in displacement tolerance can be expected if the FWHM of the rectangular pulses is further reduced. In this case a larger part of the flat-top region of the pulse can be utilised without causing ISI - increasing the displacement tolerance.

6.2 Pulse shaping by SSFBG

The pulse shaping scheme to be addressed in this section is based on spectral shaping of a signal in a specially designed filter to generate a spectrum corresponding to the desired temporal shape. In this section such a pulse shaper is used to generate rectangular shaped pulses, which are used in a demonstration of all-optical re-timing of a 160 Gbit/s data signal. The re-timing is performed by reshaping the RZ data pulses into longer rectangular (flat-top) pulses and then switching them in a non-linear Kerr switch using a synchronous optical clock signal [18,60]. The required pulse shaping is performed using a SSFBG filter, which allows for accurate pulse shaping by tailoring the spectral response of the filter [61]. To obtain rectangular pulses in the time domain the SSFBG is required to transform the spectrum of the input signal (close to Gaussian) into a sinc-shaped output. In this implementation the Kerr switch was wavelength maintaining. This is considered to be advantageous for system implementation, as re-timing can be performed without altering the wavelength of the signal.

6.2.1 Experimental setup for 160 Gbit/s re-timing

The experimental setup of the re-timer and the system demonstration is shown in figure 6.7. A 10 GHz semiconductor tunable mode-locked laser (TMLL) generating ∼1.8 ps Gaussian pulses, forms the basis of an OTDM transmitter. The operating wavelength of the laser is 1557 nm and the the generated pulse train has an inherent RMS timing jitter of 410 fs. These pulses are data modulated ($2^7 - 1$ PRBS) and subsequently multiplexed to 160 Gbit/s. The data is then fed to the pulse shaping SSFBG, which converts the 1.8 ps Gaussian pulses into ∼5 ps FWHM rectangular pulses. These are then aligned in polarisation so as to be blocked by the polariser in the Kerr switch (20 dB suppression). A short clock pulse then rotates the polarisation of the rectangular data pulse where the two are overlapping in time when propagating through the HNLF. In this way the part of the rectangular data signal overlapping with the re-timing control signal is switched through the polariser, while the rest of the data pulse is blocked. That is to say, the re-timed data pulses are carved out by the short clock pulses, which have low timing jitter. Thus, the re-timed data pulses adopt the low jitter and temporal position of the clock pulses, while maintaining the original wavelength (1557 nm). The clock pulse being narrower than the flat-topped signal generated by the SSFBG ensures that the switching is tolerant to timing jitter and timing variations in the data signal.

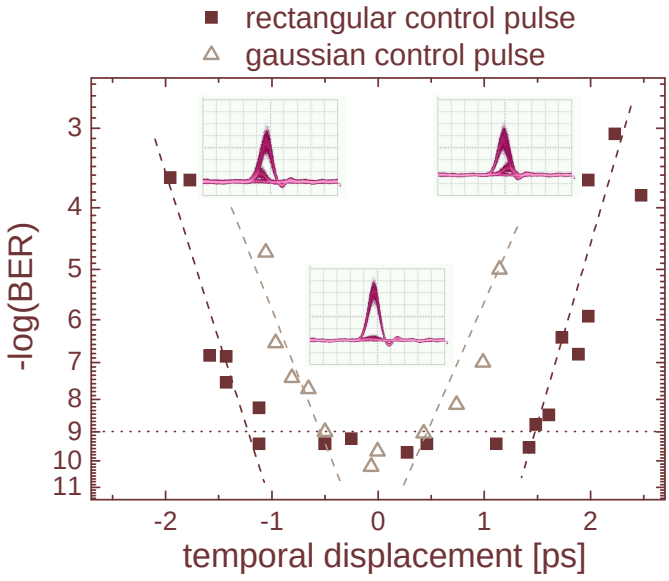

Figure 6.6: Effect of temporal displacement between 160 Gbit/s data signal and demultiplexer control pulses for flat-top and Gaussian shaped control pulses.

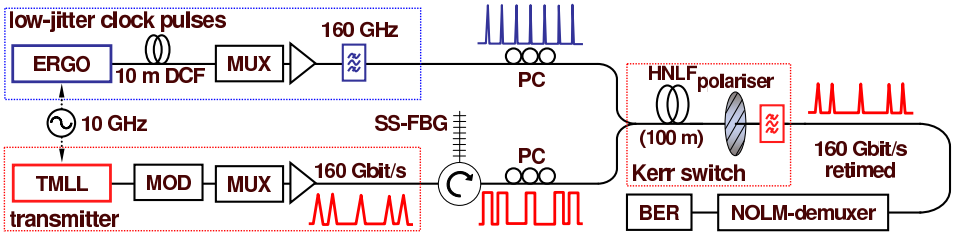

Figure 6.7: The figure shows the experimental setup for 160 Gbit/s all-optical re-timing using a SSFBG for pulse shaping.

The clock pulses are generated by a 10 GHz ERGO pulse source with low RMS timing jitter (∼210 fs). The wavelength is 1544 nm and the pulses are 1.3 ps FWHM when linearly compressed in dispersion compensating fibre (DCF) to compensate the inherent chirp of the pulse source. The pulses are synchronised to the data pulses via the same RF synthesiser in this back-to-back demonstration, and are multiplexed to 160 GHz. The 160 GHz re-timing pulse train is amplified and filtered and its state of polarisation is aligned at 45° to the axis of the Kerr switch polariser. In this way a cross-phase modulation (XPM) induced polarisation rotation of 90° is achieved, which is the basis of the Kerr switch [10]. The Kerr switch contains a 100 m HNLF with dispersion slope ∼0.017 ps/nm^{2}km, zero dispersion at 1551 nm, and non-linear coefficient γ ∼10.5 W^{-1}km^{-1}. These fibre properties ensure negligible GVD induced signal walk-off and pulse broadening. The 160 Gbit/s re-timed data pulses at the output of the Kerr switch have largely adopted the properties of the clock pulses (FWHM ∼ 1.2 ps and RMS timing jitter ∼250 fs). For BER characterisations, the re-timed data signal is demultiplexed to 10 Gbit/s in a NOLM demultiplexer containing 50 m HNLF (slope 0.018 ps/nm^{2}km, zero dispersion wavelength at 1554 nm, $\gamma \sim 10.5$ W^{-1}km^{-1}).

6.2.2 SSFBG pulse shaping results

Figure 6.8 (a) compares the spectra of the 10 GHz TMLL pulses before and after filtering in the SSFBG. The input spectrum has ∼2 nm FWHM, and the output spectrum has clear sinc-function features corresponding to a rectangular shape in the time domain. The SSFBG filter is seen to extend beyond the width of the input spectrum indicating that the input is not sufficiently wide to sample all the features of the sinc-shape. The outermost lobes in the filtered sinc spectrum are thus formed by filtered amplified spontaneous emission (ASE) and are not contributing to the signal spectrum. It is expected that a broader input spectrum would generate a more rectangular output pulse than is the case here. The slight spectral asymmetry observed results from asymmetry in the SSFBG spectral response.

Figure 6.8 (b) shows the corresponding temporal profile of the filtered output from the SSFBG, measured as a cross-correlation with a ∼600 fs sampling pulse. The limited width of the input spectrum causes the flanks of the generated rectangular pulse to be less steep than expected. The FWHM of the measured temporal pulse is 5.7 ps and the flat-top region of the pulse extends over ∼2 ps. This is sufficient to strongly reduce the

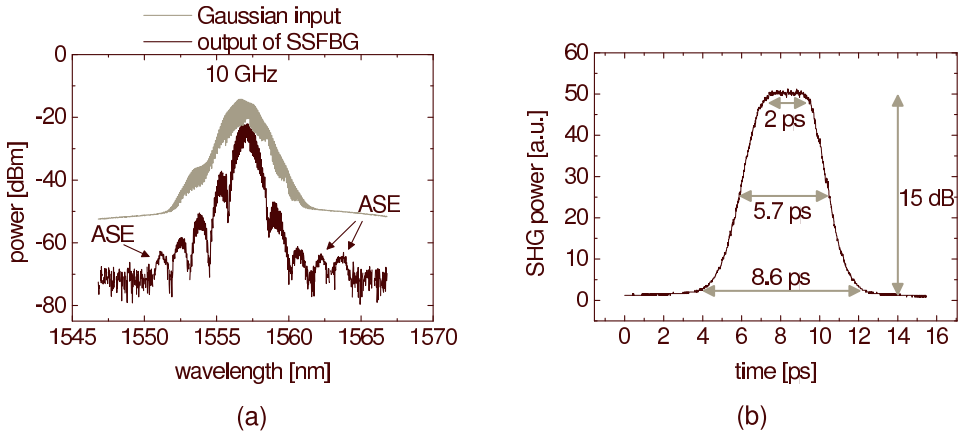

Figure 6.8: (a) Signal spectra before and after the SSFBG. (b) Temporal profile of flat-top output pulse shape with 5.7 ps FWHM.

transfer of timing jitter into amplitude noise in the re-timing switch, for the 410 fs RMS timing jitter of the incident data pulses.

6.2.3 Results of 160 Gbit/s re-timing

Figure 6.9 shows results before and after the optical re-timing system at 160 Gbit/s. The input to the Kerr switch is 1.3 ps clock pulses and 5.7 ps rectangular data pulses. In the top right plot cross-correlations of the two signals are seen together, illustrating the timing tolerance of the switch. In the spectrum the 160 GHz tones can be seen on the sinc-like filtered spectrum from the SSFBG (top left). The clock pulses are aligned to the nominal centre of the data time slot in the 160 Gbit/s data signal. In this way they sample the part of the flat-top waveform occupying the centre of the 160 Gbit/s time slot. As only a part of the data pulse corresponding to the clock pulse width is sampled, the re-timed data pulses are 1.2 ps wide, and the RMS timing jitter is drastically reduced to ∼250 fs (measured on a 70 GHz digital sampling oscilloscope at 40 Gbit/s). The output spectrum from the Kerr switch is slightly broader than the original signal due to the reduction in pulse width by the switching - figure 6.9 (bottom left). The 160 Gbit/s eye diagram after the re-timer shows some amplitude noise, but has clear and open eyes.

The results in table 6.1 clearly show that the timing jitter of the switched pulses is drastically reduced from ∼410 fs to ∼250 fs (close to the clock pulse jitter). A slight increase in the amplitude noise is noted for the pulses at

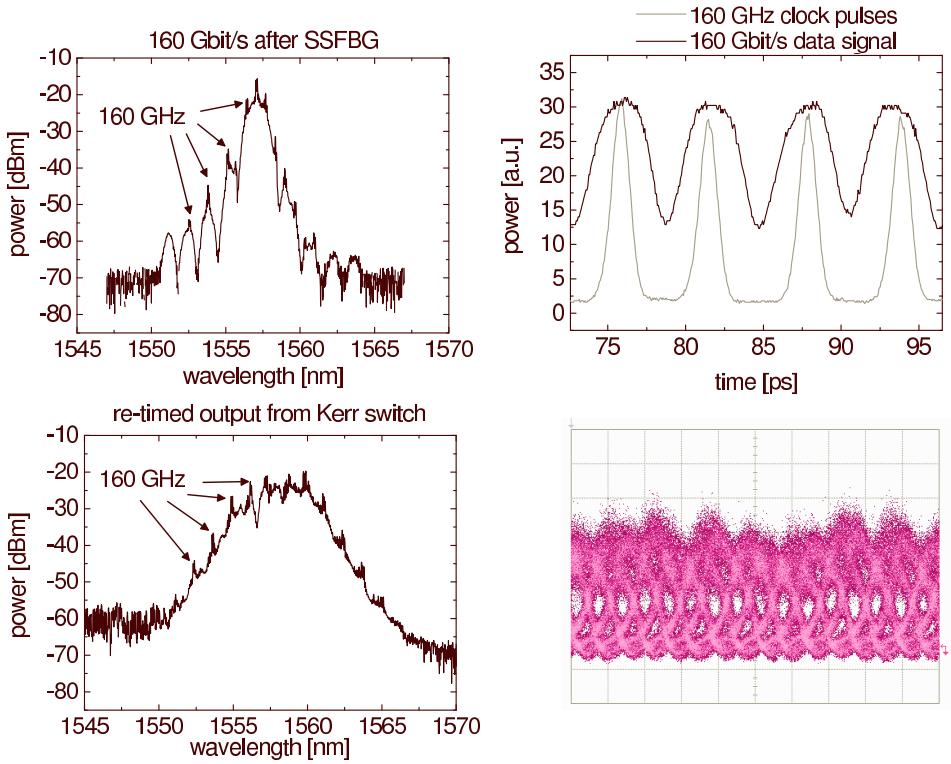

Figure 6.9: Switching results. Top: Input to Kerr switch sinc'ed data pulses with 5.7 ps FWHM and 2 ps flat-top, and clock pulses with 1.3 ps FWHM. Bottom: Output of Kerr switch, i.e. retimed data FWHM 1.2 ps, and timing jitter 250 fs

Table 6.1: Timing and amplitude jitter values at different points of the system. The measurements were taken at 40 Gbit/s.

	Original pulse	Clock pulse	Re-timed pulse
$\tau_{rms}[fs]$	410	210	250
$\sigma_{a.j.}[\%]$	3.6	2.4	7.1

the output of the switch. Indeed in table 6.1 the amplitude noise standard deviation values for the marks normalised to their corresponding mean values ($\sigma_{a.j.}$) are listed at different points in the system. The increase in the switched pulse amplitude noise is possibly linked to non-uniformity of the flat-top region of the shaped data pulses. Additionally slight distortions of the rectangular data pulses may be caused by SPM in the HNLF.

In order to confirm the benefit of using the optical re-timer BER mea-

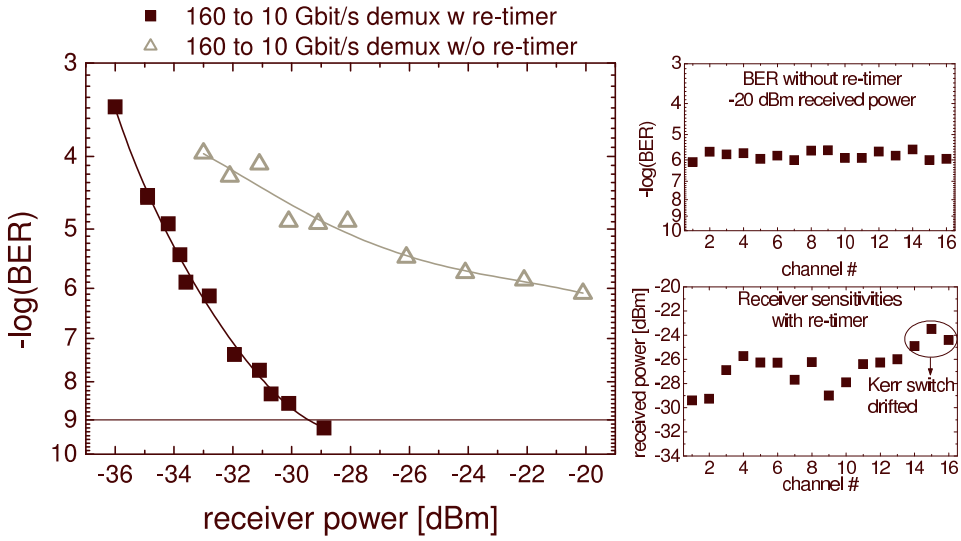

Figure 6.10: The figure shows BER results for 160 Gbit/s demultiplexing with and without the re-timer. For the case without the re-timer, the achievable BER for a received power of -20 dBm is shown for all the OTDM channels. For the case with the re-timer, the receiver sensitivity is shown for all channels.

surements are performed with and without the use of re-timing. Figure 6.10 shows the results of the BER characterisation. All 16 channels in the OTDM signal are successfully re-timed and error free operation is achieved for all of them (figure 6.10 lower right). This is in sharp contrast to the case when re-timing is not applied. In that case, the 410 fs RMS timing jitter creates a severe error floor for all channels, and at the maximum obtainable receiver power of -20 dBm no BER better than 10^{-6} is achieved (figure 6.10 upper right). This clearly demonstrates the benefit of the re-timer. Among the re-timed channels with an average sensitivity of -27 dBm, there is a 5 dB variation in sensitivity. This is due to imperfect multiplexing of the pulses in the data and clock arms and polarisation drifts in the used Kerr switch. Full BER curves are also shown with and without re-timing confirming the severe error floor encountered when demultiplexing the signal without preceding re-timing. Even though the performance is improved dramatically with the re-timer, there is still some curvature of the BER curve indicating an error floor below BER 10^{-9}. This is expected to be caused by the increase in amplitude noise caused by the re-timer. Despite this amplitude noise in the re-timed signal, the effect of the re-timer is clear.

6.3 Pulse shaping by LPG filtering

In the remaining part of this chapter, pulse shaping using a specially designed LPG will be discussed and applied in a 640 Gbit/s demultiplexing experiment. The LPG is designed to introduce a coupling between the core mode of a fibre and certain cladding modes. A signal coupled into the fibre containing the LPG will thus experience coupling into a cladding mode of that fibre for a specific frequency ω_0 given by the structure of the LPG. If ω_0 is identical to the centre frequency (carrier frequency) of the incoming signal, the filtering performed by the LPG will simply correspond to a differentiation of the time domain shape of the incoming optical pulse [57]. In the spectral domain the LPG filtering creates a dip at the centre of the spectrum (when the carrier frequency is equal to ω_0) and introduces a π phase shift between the two sides of the filtered spectrum. In figure 6.11 (a) the process of optical differentiation of a Gaussian input pulse is illustrated. Figure 6.11 (b) shows the effect of increasing the spectral offset $\Delta\omega$ between ω_0 and the carrier frequency of the input signal. For $\Delta\omega \neq 0$ the output of the LPG becomes a superposition of the input signal and its time derivative. By carefully selecting the detuning $\Delta\omega$ and thus the ratio of the two contributions to the superposition, it is possible to realise a pulse shape with a pronounced flat-top feature [56]. In practice $\Delta\omega$ is adjusted either by tuning the LPG filter by stretching the fibre containing the grating or by changing the wavelength of the input signal.
One essential advantage of this pulse shaping technique is its versatility in terms of pulse widths. The width of the flat-top output pulse is determined by the described superposition which means that it depends solely on the width of the input pulse, as long as the filtering can accommodate the spectral width of the input signal. A given LPG filter has a limited bandwidth in which the requirements for optical differentiation are satisfied. In the following the flexibility of the LPG pulse shaper in terms of pulse widths will be utilised to generate very narrow flat-top pulses suitable for demultiplexing 640 Gbit/s serial data signals.

6.4 640 Gbit/s demultiplexing

In figure 6.12 the experimental setup for the LPG based pulse shaper implemented in a 640 Gbit/s demultiplexer is shown [58, 59].

A 2 ps pulse with a 3.5 nm spectral FWHM centred at 1543 nm from an ERGO pulse source is soliton compressed by injecting it at high peak

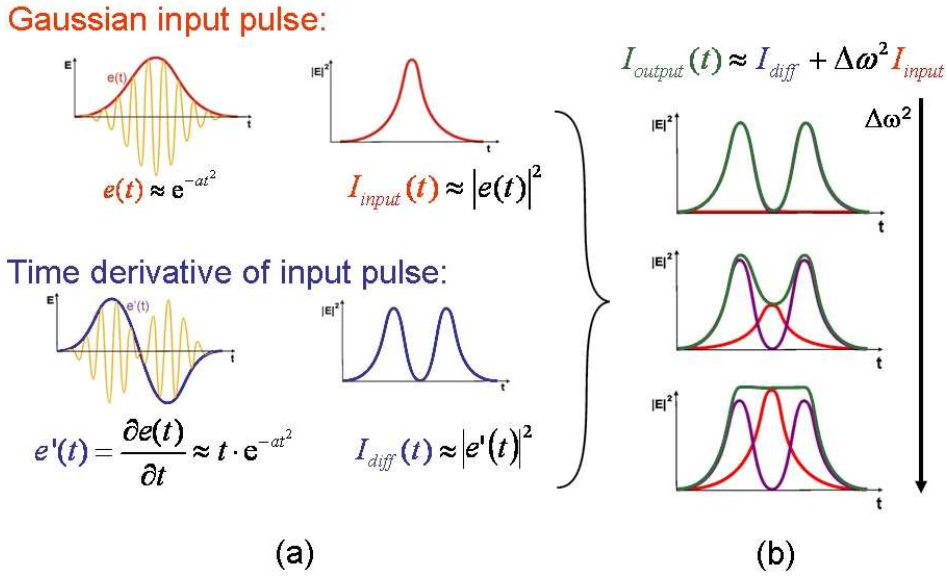

Figure 6.11: The principle of pulse shaping using the LPG-based filter. (a) shows the temporal profile of the input signal and filtered differentiated output signal assuming a Gaussian input pulse. (b) shows superposition of the input signal and the differentiated signal and the dependence on the filter detuning $\Delta\omega$. Figure from presentation of [56] at ECOC 2006

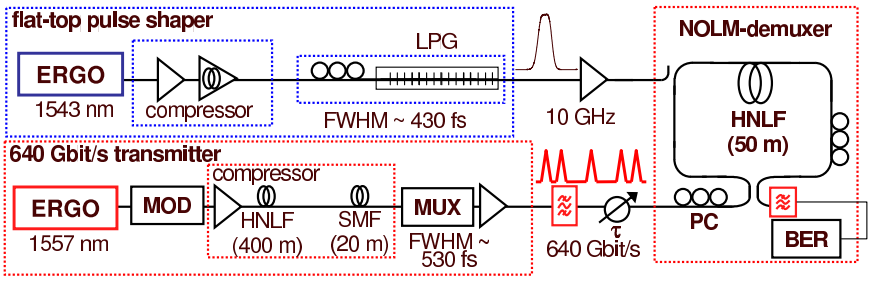

Figure 6.12: Setup for LPG pulse shaper to generate flat-top pulses as control for 640 Gbit/s demultiplexer.

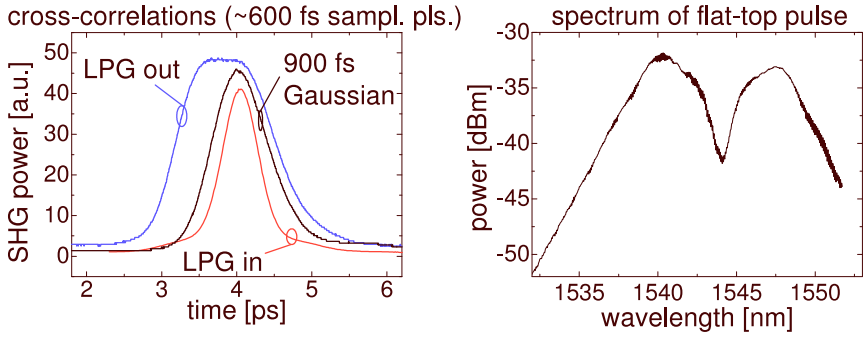

Figure 6.13: left - cross-correlation of the input and output pulse for the LPG pulse shaper, and a 900 fs Gaussian reference control pulse. right - optical spectrum after filtering in the LPG.

power into a fibre with high gain (an erbium doped fibre amplifier (EDFA)). In order for the generated soliton to maintain the balance between chirp and dispersion described in equation 2.12, for increasing pulse peak power, the soliton pulse width is reduced as the peak power increases through the EDFA fibre. An output pulse width of 430 fs is achieved in this way. The pulse is sent through the LPG filter and shaped as a flat-top pulse as described above. A flat-top pulse with FWHM of 1.4 ps and a flat region extending over ∼400 fs is achieved in this way. Figure 6.13 shows the the filtered spectrum with the characteristic dip of the LPG pulse shaper (right) and the time domain profile of the input and output pulses (left). For the mentioned pulse width, the detuning of the LPG from the central carrier wavelength of the pulse is ∼2 nm. The flat-top pulse is subsequently used as control in a NOLM demultiplexer containing 50 m of HNLF (dispersion slope ∼0.018 ps/nm^{2}km, zero dispersion at 1554 nm, and γ ∼10.5 W^{-1}km^{-1}).

A second ERGO pulse source at 1557 nm is used in a 640 Gbit/s OTDM transmitter producing a $2^7 - 1$ PRBS serial data signal in a single polarisation. The ERGO output is data modulated and multiplexed to 40 Gbit/s before pulse compression. This is done in order to reduce the impact of dispersion in the fibre based multiplexer, where the pulses travel through different lengths of fibre in order to provide the appropriate time delays. The initial stages of the multiplexer contain the longest delays in order to maintain the PRBS logic of the signal. It is thus advantageous to maintain a narrow spectral profile of the pulses when multiplexing up to 40 Gbit/s. The 40 Gbit/s data pulses are compressed by a combination of chirp by

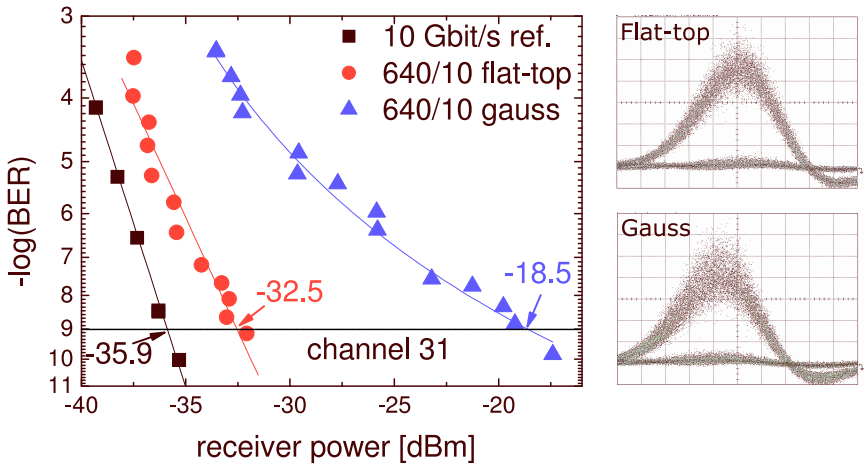

Figure 6.14: BER performance for demultiplexing 640 Gbit/s data signal using flat-top and Gaussian control pulses. The eye diagrams show the signal after demultiplexing using the two different control pulses.

SPM in an HNLF and subsequent dispersion in SMF to linearly compress the chirped pulses. Before the dispersive fibre, the broadened spectrum of the pulses is filtered using a 9 nm wide Gaussian filter centred at 1560 nm. This filtering serves to reduce amplitude noise and pulse pedestals in the compressed pulses significantly compared to filtering at the centre wavelength of the input signal - essentially taking advantage of the SPM reshaping described by P. Mamyshev in [9]. The obtained data pulses are 530 fs FWHM (7.5 nm spectral FWHM corresponding to ∼1.14 times transform limit). The 640 Gbit/s data signal is demultiplexed down to 10 Gbit/s in the NOLM for subsequent BER characterisation. In order to minimise the timing jitter in the optical signals a free running ERGO laser is used as a low-noise clock reference to synchronise the other pulse source as well as the system electronics. In terms of phase noise the free running ERGO pulse source far outperforms the available electrical synthesiser, and the timing jitter of the data and control signals are both measured to be ∼100 fs.

Figure 6.14 shows the BER results for 640 to 10 Gbit/s demultiplexing with the use of the LPG-shaped flat-top control pulses and using a 900 fs Gaussian control pulse as reference. Error-free performance is obtained for demultiplexing with both types of control pulses. However, the receiver sensitivity is improved by as much as 14 dB when using the flat-top control pulses compared to the Gaussian ones. The same OTDM channel is demultiplexed in both cases. The best performing channel is chosen for

the comparison in order to achieve error free operation with the Gaussian control pulse. Also shown in figure 6.14 is the demultiplexed eye diagrams obtained using the two different control pulses. It is seen that the flat-top control pulse introduces less amplitude noise in the demultiplexed signal. This indicates that less timing jitter is converted into amplitude noise in the demultiplexing process. The 10 Gbit/s reference signal has a sensitivity of -35.8 dBm and the demultiplexed channel from the 640 Gbit/s signal (channel number 31) has a receiver sensitivity of -32.5 dBm, when demultiplexed with the flat-top control pulse. There is thus a 3.3 dB penalty from pulse compression, multiplexing and demultiplexing of the signal. When demultiplexing the channel using a Gaussian control pulse the receiver sensitivity is -18.5 dBm.

To characterise the flat-top feature of the control pulse, the data signal is displaced in time relative to the position of the switching window of the demultiplexer. Figure 6.15 shows the results of this characterisation. The characterisation is performed at a received power 5 dB above the receiver sensitivity to allow for some measurement margin. The BER is measured for at number of relative temporal displacements between the signal and the demultiplexer switching window. The flat-top control pulse is seen to maintain error-free (BER $< 10^{-9}$) performance of the demultiplexing with a 350 fs tolerance to temporal displacement, which almost corresponds to the flat part of the pulse top (as measured on a cross-correlator). The BER increases rapidly once the data pulse has moved beyond the flat-top part of the control pulse. This rapid increase is caused by crosstalk from neighboring channels. Also shown in figure 6.15, are the receiver sensitivities at BER 10^{-9} when demultiplexing the 64 tributary channels in the OTDM signal using the flat-top pulses. All 64 channels can be isolated in the demultiplexer using the flat-top pulses, however there is a large spread in the measured sensitivities, caused by suboptimum multiplexing. 54 of the channels achieve error free operation. The 10 remaining channels are partly overlapping with a neighbor, causing the non error-free channels to appear in pairs. Despite this imperfection in the multiplexing of the data signal, the benefit of using flat-top pulses for demultiplexing is clear, and the LPG pulse shaping scheme is successfully used to provide appropriate flat-top control pulses for demultiplexing from 640 Gbit/s.

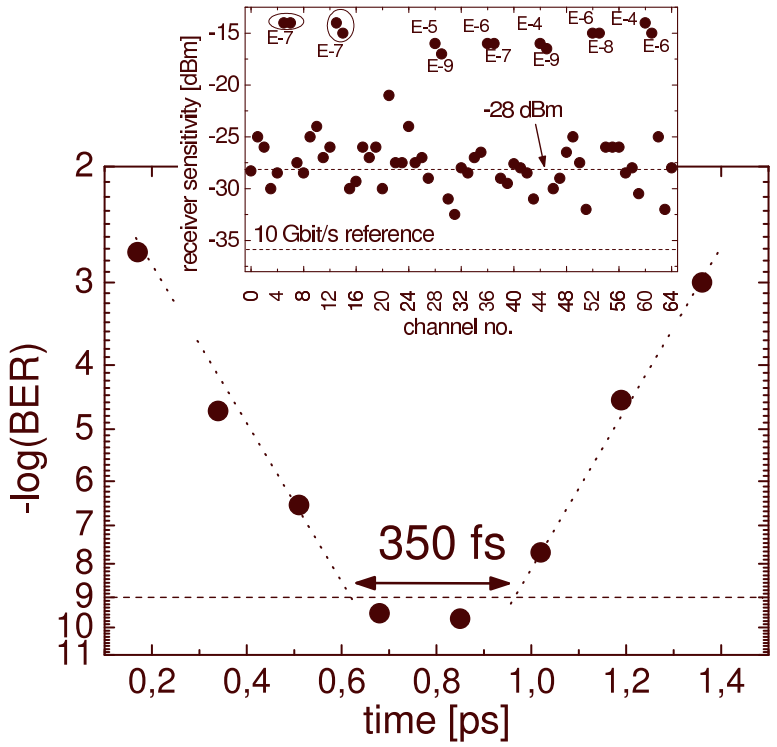

Figure 6.15: BER performance measured for various temporal displacements between the 640 Gbit/s data signal and the switching window in the demultiplexer. The inset shows the receiver sensitivity of all the OTDM channels. The average sensitivity for the error free channels was -28 dBm.

6.5 Discussion and summary

In this chapter three different schemes for increasing timing tolerance in optical switches using optical pulse shaping, have been presented and demonstrated. Pulse shaping by OFT to transform a shaped optical spectrum into a corresponding pulse shape is demonstrated for 160 Gbit/s demultiplexing. A rectangular shaped spectrum is transformed into a rectangular shaped pulse. This is used to demultiplex from 80 and 160 to 10 Gbit/s with increased jitter tolerance from 1 to 3 and 2.6 ps, respectively. However, due to the flexibility of the OFT pulse shaping scheme, it is expected that this scheme could be extended to significantly higher bit-rates. In the practical implementation it is mainly limited by the amount of chirp, which can be applied to the signal.

The two remaining schemes for pulse shaping both rely on optical fil-

tering of the input pulse to generate a flat-top output pulse. This has the advantage of reducing the complexity of the pulse shaper, as it is simply a filter. On the other hand it seriously reduces the flexibility of the pulse shapers. Once the filter is fabricated only minor adjustments can be made to e.g. the wavelength at which it operates. Of the two filtering schemes the LPG pulse shaper is considered to be the most versatile. The same filter can be used to generate a large range of output pulse widths as this mainly depends on the input pulse width. For this reason it is possible to use it for demultiplexing at a bit-rate as high as 640 Gbit/s, where a 14 dB sensitivity improvement is achieved by using flat-top control pulses. A 350 fs timing tolerance is recorded, confirming the benefit of using flat-top control pulses in the demultiplexer. The results on LPG pulse shaping includes the first demonstration of flat-top pulses used for 640 Gbit/s switching.

The FBG based pulse shaper has virtually no flexibility as the output pulse width and the wavelength are given once the filter is designed. From a practical point of view it is, however, by far the simplest and most stable of the pulse shapers addressed in this chapter. It is also the only polarisation insensitive pulse shaper of the three. This makes it an appropriate choice for the more complex setup associated with an all-optical re-timer. The all-optical pulse re-timing system is successfully demonstrated. The timing jitter of a 160 Gbit/s data signal is reduced from 410 fs to 250 fs. This improves the BER performance from a maximin obtainable BER of $\sim 10^{-6}$ to better than 10^{-9}.

Chapter 7

Conclusion

Throughout the chapters in this thesis several optical signal processing schemes and functionalities have been characterised and demonstrated in OTDM systems.

Wavelength conversion by XPM and SPM

The two approaches to all-optical wavelength conversion of on-off keying (OOK) modulated data signals were characterised and demonstrated experimentally.

XPM-based wavelength conversion of OTDM data signals from 80 Gbit/s to 320 Gbit/s using a novel filtering scheme for extracting the converted signal was demonstrated in this work. The effect of combining cross-phase modulation (XPM) with Raman gain during conversion was characterised. Regenerating properties of the XPM wavelength converter were demonstrated at 80 Gbit/s with a sensitivity improvement up to ∼4.5 dB. Inline XPM conversion in a 130 km transmission line was demonstrated at 160 Gbit/s, indicating the potential for using the XPM based conversion scheme in a wavelength converting network node. Finally, XPM conversion of a 320 Gbit/s data signal was demonstrated with a record-low penalty of ∼0.2 dB. This penalty was ∼10 dB lower than the only other reported demonstration of wavelength conversion at 320 Gbaud [8]. Preliminary results for 640 Gbit/s wavelength conversion were also obtained.

SPM-based wavelength conversion was demonstrated at 160 Gbit/s, and regenerative properties of the conversion were observed in the form of '0'-level noise suppression seen in data eye diagrams. However, in the investigated implementation wavelength conversion by spectral broadening was

seen to cause significant penalty to the performance of the signal compared with the XPM scheme.

Wavelength conversion by FWM

Phase maintaining wavelength conversion based on FWM was investigated for conversion of high-speed DPSK and DQPSK data signals. Error free and penalty free wavelength conversion of DPSK data signals up to 160 Gbit/s was achieved. SBS suppression was implemented in the form of a simple phase modulation scheme for broadening the line-width of the CW FWM pump. This scheme was seen to introduce only negligible penalty for the conversion of DPSK data signals, while DQPSK conversion suffered 4 dB penalty in receiver sensitivity. However error free wavelength conversion of DQPSK data signals up to 320 Gbit/s was demonstrated for the first time. The conversion efficiency of $\sim$ -10 dB was mainly limited by the applicable pump power, which in turn was limited by the SBS suppression scheme. Improvements in the SBS suppression could potentially allow for much higher conversion efficiencies through the introduction of parametric gain in the converter. Based on the obtained results it was concluded that the main limitation for this wavelength conversion scheme was the SBS suppression technique. Despite limitations due to SBS suppression the achieved results indicate a significant potential of FWM in HNLF for high-speed wavelength conversion of phase modulated data signals.

Data format conversion

A scheme for all-optical OOK to DPSK format conversion based on XPM in an HNLF was presented and demonstrated. The converter was demonstrated in a transmission experiment for converting a 160 Gbit/s OOK signal to a 160 Gbit/s DPSK signal midway in a 320 km fiber link. Furthermore the same format conversion scheme was demonstrated for the novel application of all-optically combining two separate data signals of different modulation formats into one signal, using a multilevel modulation format (DQPSK). The combination of a DPSK signal and an OOK signal into a single DQPSK signal was demonstrated. The symbol-rate of the two tributary signals was maintained in the combined output signal, which carried the data of both signals. The spectral efficiency of the output signal was thus doubled compared to either of the input signals. The all-optical combiner was demonstrated by combining an 80 Gbit/s incoming DPSK data signal with a locally generated 80 Gbit/s OOK data signal to

a 160 Gbit/s DQPSK data signal half-way in a 320 km fibre link.
In both implementations, the XPM scheme for encoding phase data was successful, and it is expected that even more phase states could be added with this technique to generate more complex modulation e.g. D8PSK.

Clock recovery and channel identification

A scheme for combined clock recovery and channel identification was proposed and demonstrated. In the proposed scheme one channel in the multiplexed signal, was phase modulated through XPM with an optical pulse train at the base rate. This phase modulation was subsequently detected in the receiver by sideband filtering, and was used for both clock recovery and channel identification. A 320 Gbit/s data signal with an XPM labeled channel was transmitted 80 km. The clock was successfully extracted from the signal by sideband filtering and reliable channel identification was obtained with a 6 dB power contrast in the filtered sideband identifying the labeled channel. Error free performance with low penalty was demonstrated for the transmitted signal using the recovered phase modulated clock.
This scheme is believed to have significant potential for clock recovery and channel identification in OTDM systems. Compared to most other clock recovery schemes, it is fairly simple and relies only on base-rate electronics. Furthermore it has the inherent benefit of channel identification. However, due to the addition of chirp to one data channel the sensitivity to dispersion will be increased.

Increased timing tolerance using flat-top pulses

Three different approaches to generating flat-top optical pulses for switching were experimentally demonstrated and characterised.

In the OFT scheme the optical spectrum of a pulse was shaped by filtering and subsequently the shape was transferred to the time domain by the OFT process. This technique was verified by demultiplexing from 80 and 160 to 10 Gbit/s. In these experiments the timing jitter tolerance was seen to increase from 1 to 3 and 2.6 ps, respectively. This was compared to using Gaussian shaped control pulses.
Due to the flexibility of the OFT pulse shaping scheme, it is expected that this scheme could be extended to significantly higher bit-rates. In the practical implementation it is mainly limited by the amount of chirp, which can be applied to the signal. One possible solution could be the use of XPM to chirp the pulses for OFT.

The second pulse shaping scheme to be addressed was the application of a SSFBG-based optical sinc filter. The spectral sinc shape corresponds to a rectangular shaped pulse in the time domain. These shaped pulses were used in a 160 Gbit/s optical re-timer. The re-timer provided a reduction in RMS timing jitter from 410 fs to 250 fs and a significant improvement in BER performance. Without the re-timer the best obtainable BER was $\sim 10^{-6}$ due to the large amount of timing jitter in the signal. After the re-timer a BER better than 10^{-9} was achieved.
From a practical point of view this pulse shaper was the simplest and most stable of the investigated pulse shapers, partly due to its insensitivity to polarisation. This made it an appropriate choice for the more complex setup associated with an all-optical re-timer. It did, however, lack the flexibility of the other pulse shaping schemes in terms of pulse width.

The third pulse shaping scheme demonstrated was based on an optical differentiator implemented in a specially tailored LPG. This was used to generate a pulse with a 400 fs flat-top region. This pulse was subsequently used to gate a NOLM demultiplexer, resulting in a significant increase in the timing tolerance of the switch. This was verified in a 640 Gbit/s demultiplexing experiment. Flat-top switching pulses enabled error free demultiplexing of a data signal with the high integrated timing jitter of 230 fs. Using Gaussian switching pulses the timing jitter prevented error free demultiplexing. The timing tolerance was estimated by demultiplexing a 640 Gbit/s data signal with only $\sim$100 fs timing jitter, and a timing tolerance of 350 fs was found for the demultiplexer, when using flat-top control pulses. For the low-noise data signal an improvement in receiver sensitivity of 14 dB was also observed when using flat-top control pulses for demultiplexing in stead of Gaussian ones. This was the first demonstration of flat-top pulses used for 640 Gbit/s switching.
Of the two filtering schemes the LPG pulse shaper is considered to be the most versatile. The same filter can be used to generate a large range of output pulse widths as this mainly depends on the input pulse width.

Summary

In this thesis several signal processing functionalities have been investigated and demonstrated. New functionalities are believed to have been proposed e.g. the optical format combiner and in part the clock recovery and channel identification scheme. Furthermore, novel applications of known techniques have been proposed e.g. the OFT pulse shaper and notch-filter assisted XPM. All of the addressed signal processing schemes have been charac-

terised and demonstrated in high-speed systems up to 640 Gbit/s, and it is believed that some contribution has been made towards promoting the development of optical signal processing for high-speed systems.

Appendices

Appendix A

SBS

In this appendix, two different issues regarding stimulated brillouin scattering (SBS) in systems for non-linear signal processing will be addressed. The first is the effect of cross-phase modulation (XPM) during signal processing to reduce the impact of SBS. The second issue is the generation of SBS by narrow spectral components in high-speed data signals.

A.1 SBS suppression by XPM

A high power continuous wave (CW) pump which is launched into a non-linear fibre will generate SBS through the excitation of acoustic phonons in the fibre. The threshold power at which the pump initiates SBS is estimated by the relation [10, 62]:

$$P_{thr} = \frac{21\ A_{eff}}{g_B\ L_{eff}}(1 + \frac{\Delta v_P}{\Delta v_B}) \tag{A.1}$$

where A_{eff} is the effective area of the fibre, g_b is the Brillouin gain coefficient $\sim 5 * 10^{-11}$ m/W, L_{eff} is the effective length, Δv_P is the spectral width of the pump assuming a Lorentzian spectral shape and Δv_B is the Brillouin gain bandwidth ~ 20 MHz.
In figure A.1 the backscattered power from a CW pump launched into 500 m of highly non-linear fibre (HNLF) is measured for increasing pump powers. The SBS threshold is seen to be ~ 11 dBm for this configuration. In equation A.1 the dependence of the SBS threshold on the spectral width of the CW pump is described for a Lorentzian shaped pump spectrum. In chapter 3 the effect of applying a sinusoidal phase modulation to the pump in order to broaden its spectrum, is estimated. A second source of spectral

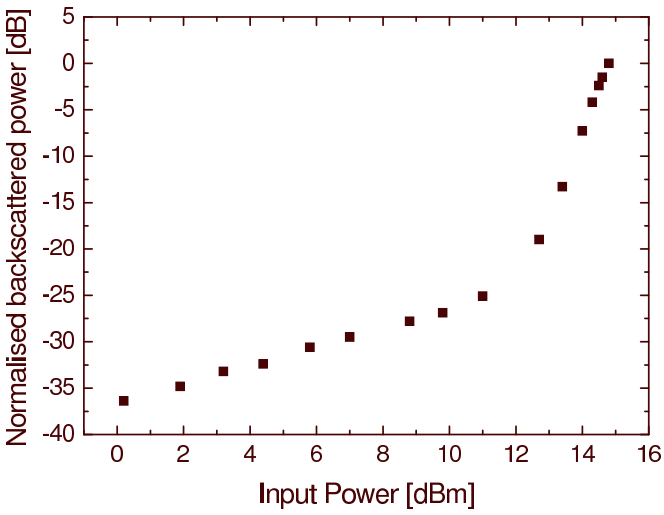

Figure A.1: SBS backscattered power from CW pump launched into 500 m of HNLF with $\gamma \sim 10\ W^{-1}km^{-1}$.

broadening of the CW pump is XPM between the pump and a data signal which might co-propagate with the pump in the HNLF. This XPM broadening of the CW pump is the basis for the wavelength conversion described in chapter 2 and is also observed for four-wave mixing (FWM) conversion in chapter 3. In figure A.2 the SBS backscattered power is measured for increasing XPM broadening of a CW pump in an HNLF. A CW pump is launched into 500 m of HNLF at 15 dBm along with a 160 Gbit/s data signal of varying power. The SBS backscatter from the CW pump is measured. Initially the 15 dBm CW power is well above the SBS threshold determined above. Increasing the XPM broadening of the pump is seen to significantly reduce the amount of backscattered power. In this characterisation a reduction up to 5.5 dB is achieved. This only corresponds to ~ 1 dB increase of the SBS threshold, but does however clearly demonstrate the effect of XPM on the SBS threshold.

A.2 SBS in high speed data signals

As discussed in chapter 2, a high-speed data signal or pulse train, where consecutive optical pulses are in phase, will demonstrate an optical spectrum with distinct modulation peaks spaced by the repetition rate of the pulses.

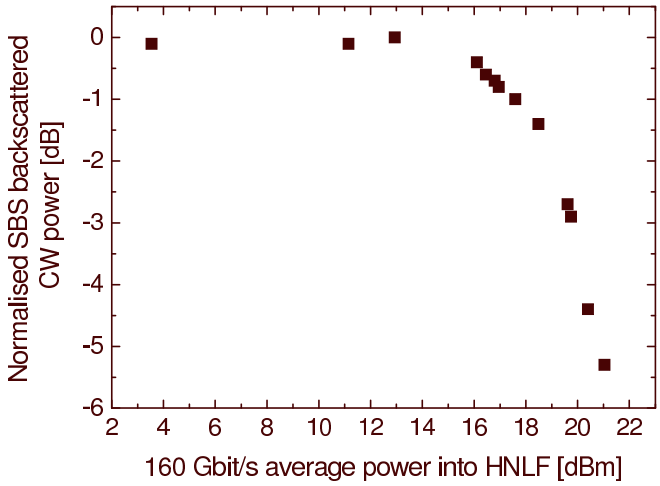

Figure A.2: Reduction in SBS backscattered power from CW pump launched into 500 m of HNLF with increasing power of co-propagating 160 Gbit/s signal.

Figure A.3 shows an optical spectrum for such a data signal with a bit rate of 160 Gbit/s. The narrow spectral components in such a signal may cause SBS in a non-linear fibre, similar to the narrow spectrum of a CW, if they acquire sufficient power. For high bit-rate data signals the limited number of spectral peaks contained within the data spectrum, may hold sufficient power to induce SBS in a fibre. To characterise this effect, the 160 Gbit/s signal shown in figure A.3 was launched into the same HNLF as above, at different average powers. The backscattered power was measured and is shown in figure A.4. The signal is clearly seen to have an SBS threshold, where the backscattered power increases rapidly, at $\sim$ 17 dBm average signal power. In a second measurement, phase modulation at 100 MHz was applied to the signal before launching it into the HNLF. This is seen to increase the SBS threshold $\sim$ 3 dB.

Adding phase modulation to the high-speed data signal, affects the coherence of the signal in a similar way as for a CW pump, and thus increases the SBS threshold by reducing the overall coherence of the signal. This corresponds to broadening the line width of the modulation peaks in the same way as phase modulation is used to broaden the line width of a CW pump in chapter 3.

In practice, the issue of SBS in high speed optical time division multiplexing (OTDM) data signals is rarely a limitation due to the construction of most

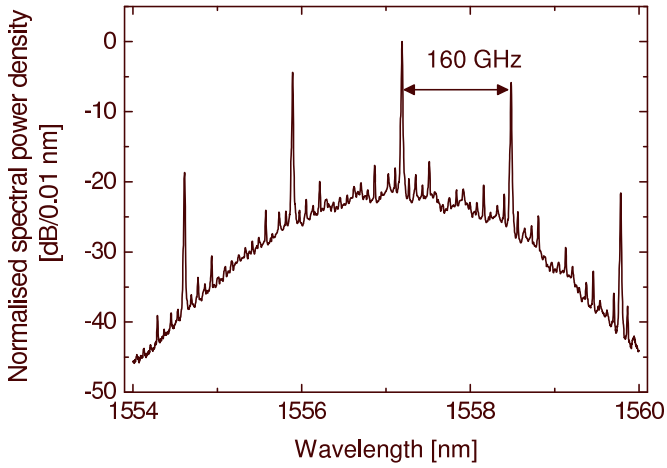

Figure A.3: Optical spectrum for 160 Gbit/s data signal with phase matched pulses after multiplexing.

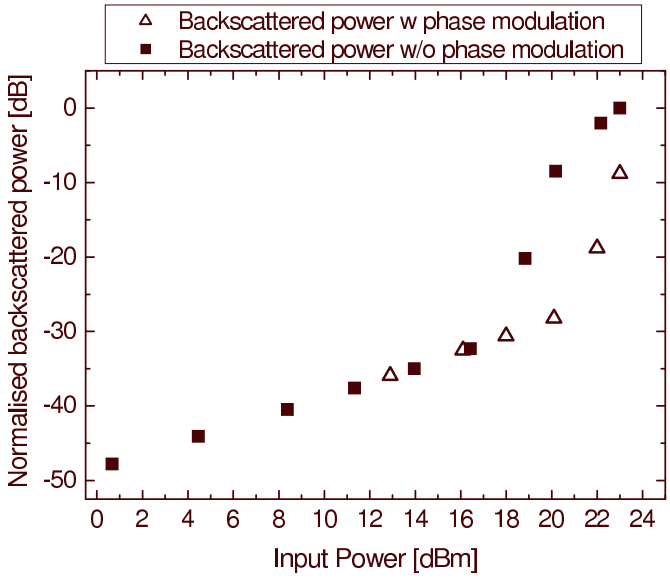

Figure A.4: Measured backscattered power from 160 Gbit/s signal launched into 500 m HNLF.

OTDM multiplexers, which are based on fibre couplers and delays. Unless very careful regulation of each stage is implemented to counter thermal and mechanical variations, there will not be a stable phase relationship between consecutive pulses in the multiplexed signal. In such a signal the narrow spectral components corresponding to the bit rate of the signal, as seen in figure A.3, will be strongly reduced. Depending on the exact phase relationship between pulses in each stage of the multiplexer, the strength of the lines in the spectrum corresponding to the base rate of the OTDM signal will vary. In the specific setup addressed here, the base rate is 10 Gbit/s, which means that the power of each peak in the spectrum in figure A.3 is distributed more or less unevenly over 16 lines with 10 GHz spacing, depending on the acquired phase of each pulse traveling through the multiplexer. For such a system, the power of one line in the spectrum will rarely reach the SBS threshold. However, as one of the steps towards introducing long-term stability in an OTDM system, the effect of variations in the multiplexed spectrum in terms of SBS should be addressed. Phase modulation of the multiplexed signal has been demonstrated as one means of increasing the SBS threshold.

Appendix B

OFT

In this appendix the principle of optical fourier transform (OFT)-based signal processing and pulse shaping will be covered in some detail. The work is based on the OFT approach described in [50] and focuses on the application to optical pulse shaping.

B.1 The optical Fourier transform

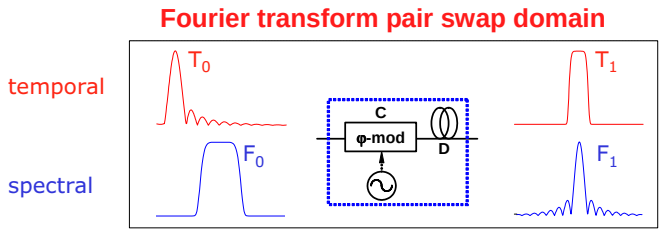

Figure B.1: The basic setup for OFT.

In figure B.1, the input and output powers in the spectral and temporal domains are shown. They relate to the electric field amplitudes as

$$T_j(t) = |t_j(t)|^2 \tag{B.1}$$

$$F_j(\omega) = |f_j(\omega)|^2 \tag{B.2}$$

Figure B.2 shows how the electric fields evolve through the different parts of the set-up. In the phase modulator, a linear chirp, C, is added to

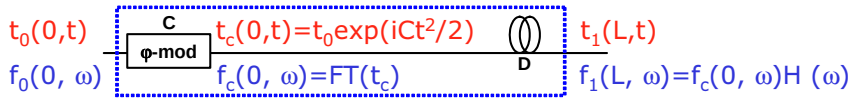

Figure B.2: The evolution of electric fields in the time and frequency domain during OFT.

the electric field yielding an electric field waveform of

$$t_c(0,t) = t_0(0,t)e^{\frac{i}{2}Ct^2} \tag{B.3}$$

Note, that in order to obtain a linear chirp, it is necessary to add a parabolic phase modulation, as the chirp is the time derivative of the phase. The chirped spectrum is the Fourier transform of the chirped waveform, i.e.

$$f_c(0,\omega) = FT(t_c) \tag{B.4}$$

The chirped waveform is now propagated through a length of dispersive medium, such as a fibre with accumulated dispersion $D = \beta_2 L$, where β_2 is the GVD parameter of the fibre and L is the total length of the fibre. The linear transfer function for such a fibre is $H(\omega) = e^{\frac{i}{2}\beta_2\omega^2 L}$, see e.g. [63]. Thus, the spectral output of the dispersive element becomes

$$f_1(L,\omega) = f_c(0,\omega) \cdot H(\omega) = f_c(0,\omega) \cdot e^{\frac{i}{2}\beta_2\omega^2 L} \tag{B.5}$$

and the output temporal shape is just the inverse Fourier transform of this, i.e.

$$\begin{aligned} t_1(L,t) &= FT^{-1}(f_1(L,\omega)) = FT^{-1}(f_c(0,\omega) \cdot e^{\frac{i}{2}\beta_2\omega^2 L}) \\ &= \int_{-\infty}^{\infty} t_c(t')h(t-t')dt \end{aligned} \tag{B.6}$$

where

$$h(t) = FT^{-1}(H) = \frac{1}{2\pi}\int e^{\frac{i}{2}\beta_2\omega^2 L}e^{-i\omega t}d\omega = \sqrt{\frac{i}{2\pi D}} \cdot e^{\frac{-i}{2D}t^2} \tag{B.7}$$

i.e. the output temporal shape is the convolution of the chirped input pulse to the dispersive element with the fibre response function $h(t)$. Now, assuming that the accumulated dispersion is matched to the chirp added to

the pulse ($D = 1/C$), and using the transformation $t/D = \omega$, and inserting into equation B.6, the output waveform becomes

$$\begin{aligned} t_1(L,t) &= \int_{-\infty}^{\infty} t_c(t')h(t-t')dt' \\ &= \sqrt{\frac{i}{2\pi D}} \int_{-\infty}^{\infty} t_0(t') \cdot e^{\frac{i}{2}Ct'^2} \cdot e^{\frac{-i}{2D}(t-t')^2} dt' \\ &= \sqrt{\frac{i}{2\pi D}} \cdot e^{\frac{-i}{2D}t^2} \int_{-\infty}^{\infty} t_0(t') \cdot e^{i\frac{t}{D}t'} dt' \\ &= \sqrt{\frac{i}{2\pi D}} \cdot e^{\frac{-i}{2D}t^2} \int_{-\infty}^{\infty} t_0(t') \cdot e^{i\omega t'} dt' \\ &= \sqrt{\frac{i}{2\pi D}} \cdot e^{\frac{-i}{2D}t^2} \cdot f_0(0,\omega) \end{aligned} \tag{B.8}$$

Finally, the intensity at the output of the OFT becomes

$$T_1 = |t_1|^2 = \frac{1}{2\pi D} \cdot |f_0|^2 = \frac{1}{2\pi D} \cdot F_0 \tag{B.9}$$

i.e. the output waveform is exactly given by the input spectral shape. This means that F_0 can be measured and T_1 can subsequently be determined, assuming ideal phase modulation.

B.2 OFT of supergaussian spectrum

The spectrum which was obtained experimentally by filtering can be approximated by a supergaussian shape (see figure 6.4). Thus F_0 is assumed to be supergaussian, i.e.

$$F_0 = A \cdot e^{-(\omega/\Delta\omega)^{2m}} \tag{B.10}$$

Setting $A = 1$, using the above transformation $t/D = \omega$ and equation B.9, the temporal output pulse shape is found to be

$$T_1 = \frac{1}{2\pi D} \cdot e^{-(t/D\Delta\omega)^{2m}} \tag{B.11}$$

i.e. exactly the same shape as the input spectrum, with a $1/e$ width given by

$$\Delta t_{1/e} = D\Delta\omega \tag{B.12}$$

The width of the output pulse is thus determined by the amount of dispersion D - as long as the requirement $D = 1/C$ is satisfied. In this way the OFT process can be applied as a pulse shaping scheme by transforming a signal with a desired spectral shape (in this case supergaussian) into an optical pulse with that particular shape in the time domain.

List of Acronyms

ASE	amplified spontaneous emission
BER	bit error rate
CR	clock recovery
CW	continuous wave
DCF	dispersion compensating fibre
DDF	dispersion decreasing fibre
DFG	difference frequency generation
DLI	delay line interferometer
DPSK	differential phase shift keying
DQPSK	differential quadrature phase shift keying
EAM	electro absorption modulator
EDFA	erbium doped fibre amplifier
ERGO	erbium glass oscillator
ETDM	electrical time division multiplexing
FBG	fibre bragg grating
FWHM	full width at half maximum
FWM	four-wave mixing
GVD	group-velocity dispersion

HNLF	highly non-linear fibre
ID	identification
IDF	inverse dispersion fibre
ISI	inter-symbol interference
LILM	loss-imbalanced loop mirror
LPG	long period grating
MUX	multiplexer
MZ	Mach-Zehnder
MZM	Mach-Zehnder modulator
NOLM	non-linear optical loop mirror
NZDSF	non-zero dispersion shifted fibre
OFT	optical fourier transform
OOK	on-off keying
OTDM	optical time division multiplexing
OSNR	optical signal to noise ratio
PBS	polarisation beam splitter
PLL	phase-locked loop
PMD	polarisation mode dispersion
PPLN	periodically poled lithium niobate
PRBS	pseudo random bit sequence
PSK	phase shift keying
PTER	pulse tail extinction ratio
SBS	stimulated brillouin scattering
SHG	second harmonic generation

SLA	super large area fibre
SMF	single mode fibre
SOA	semiconductor optical amplifier
SPM	self phase modulation
SRS	stimulated Raman scattering
SSFBG	super-structured fibre bragg grating
TMLL	tunable mode-locked laser
WDM	wavelength division multiplexing
XPM	cross-phase modulation

Bibliography

[1] P. J. Winzer, G. Raybon, and M. Duelk. "107-Gb/s optical ETDM transmitter for 100G Ethernet transport", in *Proceedings of the European Conference on Optical Communication, ECOC'05,* Glasgow, Scotland, Paper Th4.1.1, September 2005.

[2] M. Nakazawa, E. Yoshida, T. Yamamoto, E. Yamada, and A. Sahara. "TDM single channel 640 Gbit/s transmission experiment over 60 km using 400 fs pulse train and walk-off free, dispersion flattened nonlinear optical loop mirror", *Electronics Letters*, vol. 34, no. 9, pp. 907–908, April 1998.

[3] M. Nakazawa, T. Yamamoto, and K. R. Tamura. "1.28 Tbit/s-70 km OTDM transmission using third- and fourth-order simultaneous dispersion compensation with a phase modulator", *Electronics Letters*, vol. 36, no. 24, pp. 2027–2029, November 2000.

[4] H. G. Weber, C. Schubert, S. Ferber, M. Kroh, C. Schmidt Langhorst, R. Ludwig, V. Marembert, C. Boerner, F. Futami, and S. Watanabe. "Single channel 1.28 Tbit/s and 2.56 Tbit/s DQPSK transmission", in *Proceedings of the European Conference on Optical Communication, ECOC'05,* Glasgow, Scotland, Paper Th4.1.2, September 2005.

[5] B. Olsson, P. Öhlén, L. Rau, and D. J. Blumenthal. "A Simple and Robust 40-Gb/s Wavelength Converter Using Fiber Cross-Phase Modulation and Optical Filtering", *IEEE Photonics Technology Letters*, vol. 12, no. 7, pp. 846–848, July 2000.

[6] L. Rau, W. Wang, S. Camatel, H. Poulsen, and D. J. Blumenthal. "All-optical 160-Gb/s phase reconstructing wavelength conversion using cross-phase modulation (XPM) in dispersion-shifted fiber", *IEEE Photonics Technology Letters*, vol. 16, no. 11, pp. 2520–2522, November 2004.

[7] W. Wang, H. Poulsen, L. Rau, H. Chou, J. E. Bowers, and D. J. Blumenthal. "Raman-enhanced regenerative ultrafast all-optical fiber XPM wavelength converter", *Journal of Lightwave Technology*, vol. 23, no. 3, pp. 1105–1115, March 2005.

[8] Y. Liu, E. Tangdiongga, Z. Li, H. de Waardt, A. M. J. Koonen, G. D. Khoe, H. J. S. Dorren, X. Shu, and I. Bennion. "Error-Free 320 Gb/s SOA-Based Wavelength Conversion Using Optical Filtering", in *Technical Digest of the Optical Fiber Communication Conference, OFC'06,* Anaheim, California, U.S.A., Paper PDP28, March 2006.

[9] P. V. Mamyshev. "All-optical data regeneration based on self-phase modulation effect", in *Proceedings of the European Conference on Optical Communication, ECOC'98,* Madrid, Spain, pp. 475–476, September 1998.

[10] G. P. Agrawal. *Nonlinear Fiber Optics.* Academic Press, Third edition, 2001. ISBN 0-12-045143-3.

[11] M. Galili, L. K. Oxenløwe, D. Zibar, A. Clausen, and P. Jeppesen. "Characterisation of Systems for Raman-Assisted High-Speed Wavelength Conversion", in *Technical Digest of the Conference on Lasers and Electro-Optics, CLEO'05,* Baltimore, Maryland, U.S.A., pp. 288–290, Paper CMQ2, May 2005.

[12] M. Galili, L. K. Oxenløwe, D. Zibar, A. T. Clausen, H.-J. Deyerl, N. Plougmann, M. Kristensen, and P. Jeppesen. "160 Gb/s notch-filtered Raman-assisted XPM wavelength converter", in *Proceedings of the European Conference on Optical Communication, ECOC'05,* Glasgow, Scotland, pp. 113–114, Paper Mo4.5.3, September 2005.

[13] M. Galili, L. K. Oxenløwe, H. C. H. Mulvad, D. Zibar, A. T. Clausen, and P. Jeppesen. "160 Gb/s Raman-assisted notch-filtered XPM wavelength conversion and transmission", in *Technical Digest of the Optical Fiber Communication Conference, OFC'06,* Anaheim, California, U.S.A., Paper OWW2, March 2006.

[14] R. J. Essiambre, B. Mikkelsen, and G. Raybon. "Intra-channel cross-phase modulation and four-wave mixing in high-speed TDM systems", *Electronics Letters*, vol. 35, no. 18, pp. 1576–1578, September 1999.

[15] M. Galili, L. K. Oxenløwe, H. C. H. Mulvad, A. T. Clausen, and P. Jeppesen. "Raman-assisted XPM wavelength conversion at

320 Gb/s", in *Proceedings of the European Conference on Optical Communication, ECOC'06,* Cannes, France, pp. 333–334, Paper We3.P.106, September 2006.

[16] G. Raybon, Y. Su, J. Leuthold, R. J. Essiambre, T. Her, C. Joergensen, P. Steinvurzel, and K. D. K. Feder. "40 Gbit/s pseudo-linear transmission over one million kilometers", in *Technical Digest of the Optical Fiber Communication Conference, OFC'02,* Anaheim, California, U.S.A., Paper FD10, March 2002.

[17] N. Yoshikane, I. Morita, T. Tsuritani, A. Agata, N. Edagawa, and S. Akiba. "Benefit of SPM-based all-optical reshaper in receiver for long-haul DWDM transmission systems", *IEEE Journal of Selected Topics in Quantum Electronics*, vol. 10, no. 2, pp. 412–420, March 2004.

[18] S. Watanabe, F. Futami, R. Okabe, Y. Takita, S. Ferber, R. Ludwig, C. Schubert, C. Schmidt, and H. G. Weber. "160 Gbit/s optical 3R-regenerator in a fiber transmission experiment", in *Technical Digest of the Optical Fiber Communication Conference, OFC'03,* Atlanta, Georgia, U.S.A., Paper PD16, March 2003.

[19] J. Herrmann, U. Griebner, N. Zhavoronkov, A. Husakou, D. Nickel, J. C. Knight, W. J. Wadsworth, P. S. J. Russell, and G. Korn. "Experimental Evidence for Supercontinuum Generation by Fission of Higher-Order Solitons in Photonic Fibers", *Physical Review Letters*, vol. 88, no. 17, pp. 173901–1–173901–1, April 2002.

[20] M. Galili, L. K. Oxenløwe, D. Zibar, A. T. Clausen, and P. Jeppesen. "160 Gb/s Raman-assisted SPM wavelength converter", in *Proceedings of the European Conference on Optical Communication, ECOC'04,* Stockholm, Sweden, pp. 28–29, Paper Th4.3.1, September 2004.

[21] M. J. Dudley, L. Provino, N. Grossard, H. Maillotte, R. S. Windeler, B. J. Eggleton, and S. Coen. "Supercontinuum generation in air-silica microstructured fibers with nanosecond and femtosecond pulse pumping", *Journal of the Optical Society of America B*, vol. 19, no. 4, pp. 765–771, April 2002.

[22] A. H. Gnauck and P. J. Winzer. "Optical Phase-Shift-Keyed Transmission", *Journal of Lightwave Technology*, vol. 23, no. 1, pp. 115–130, January 2005.

[23] A. H. Gnauck, X. Liu, X. Wei, D. M. Gill, and E. C. Burrows. "Comparison of modulation formats for 42.7-gb/s single-channel transmission through 1980 km of SSMF", *IEEE Photonics Technology Letters*, vol. 16, no. 3, pp. 909–911, March 2004.

[24] B. Sartorius, J. Leuthold, C. Bornholdt, J. Slovak, M. Schlak, C. Schmidt, A. Marculescu, P. Vorreau, S. Tsadka, and W. Freude. "All-optical DPSK wavelength converter based on MZI with integrated SOAs and phase shifters", in *Technical Digest of the Optical Fiber Communication Conference, OFC'06,* Anaheim, California, U.S.A., Paper OWS6, March 2006.

[25] S. L. Jansen, D. van der Borne, A. Schopflin, E. Gottwald, P. M. Krummrich, G. D. Khoe, and H. de Waardt. "26x42.8-Gbit/s DQPSK Transmission with 0.8-bit/s/Hz Spectral Efficiency over 4,500-km SSMF using Optical Phase Conjugation", in *Proceedings of the European Conference on Optical Communication, ECOC'05,* Glasgow, Scotland, Paper Th4.1.5, September 2005.

[26] B. Huettl, A. G. Coca, H. Suche, R. Ludwig, C. Schmidt-Langhorst, H. G. Weber, W. Sohler, and C. Schubert. "320 Gbit/s DQPSK All-Optical Wavelength Conversion Using Periodically Poled $LiNbO_3$", in *Technical Digest of the Conference on Lasers and Electro-Optics, CLEO'07,* Baltimore, Maryland, U.S.A., Paper CThF1, May 2007.

[27] Y. Geng, P. A. Andersen, T. Tokle, C. Peucheret, and P. Jeppesen. "Wavelength Conversion of a 6 x 40 Gb/s DPSK WDM Signal using FWM in a Highly Non-linear Photonic Crystal Fiber", in *Proceedings of the European Conference on Optical Communication, ECOC'05,* Glasgow, Scotland, Paper Tu.3.3.4, September 2005.

[28] T. Tokle, Y. Geng, C. Peucheret, and P. Jeppesen. "Wavelength conversion of 80 Gbit/s optical DQPSK using FWM in a highly non-linear fibre", in *Technical Digest of the Conference on Lasers and Electro-Optics, CLEO'05,* Baltimore, Maryland, U.S.A., pp. 1708–1710, Paper JThE50, May 2005.

[29] M. Galili, B. Huettl, C. Schmidt-Langhorst, A. G. i Coca, R. Ludwig, and C. Schubert. "320 Gbit/s DQPSK All-Optical Wavelength Conversion Using Four Wave Mixing", in *Technical Digest of the Optical Fiber Communication Conference, OFC'07,* Anaheim, California, U.S.A., Paper OTuI3, March 2007.

[30] J. Hansryd and P. A. Andrekson. "Broad-Band Continuous-Wave-Pumped Fiber Optical Parametric Amplifier with 49-dB Gain and Wavelength-Conversion Efficiency", *IEEE Photonics Technology Letters*, vol. 13, no. 3, pp. 194–196, March 2001.

[31] W. Wang, L. Rau, and D. Blumenthal. "160Gb/s High Extinction Ratio Raman-Enhanced FWM Wavelength Converter with Highly-Nonlinear-Fiber", in *Technical Digest of the Conference on Lasers and Electro-Optics, CLEO'04,* San Francisco, California, U.S.A., Paper CPDC6, May 2004.

[32] S. Watanabe, G. Ishikawa, T. Naito, and T. Chikama. "Generation of Optical Phase-Conjugate Waves and Compensation for Pulse Shape Distortion in a Single-Mode Fiber", *Journal of Lightwave Technology*, vol. 12, no. 12, pp. 2139–2146, December 1994.

[33] J. Hansryd, F. Dross, M. Westlund, P. A. Andrekson, and S. N. Knudsen. "Increase of the SBS threshold in a short highly nonlinear fiber by applying a temperature distribution", *Journal of Lightwave Technology*, vol. 19, no. 11, pp. 1691–1697, November 2001.

[34] J. M. Chavez, J. D. Marconi, and H. L. Fragnito. "8 dB increase of the SBS threshold in an optical fiber by applying a stair ramp strain distribution", in *Technical Digest of the Conference on Lasers and Electro-Optics, CLEO'04,* San Francisco, California, U.S.A., Paper CThT30, May 2004.

[35] K. Shiraki, M. Ohashi, and M. Tateda. "SBS threshold of a fiber with a Brillouin frequency shift distribution", *Journal of Lightwave Technology*, vol. 12, no. 1, pp. 50–57, January 1996.

[36] S. K. Korotky, P. B. Hansen, L. Eskildsen, and J. J. Veselka. "Efficient Phase Modulation Scheme for Sppressing Stimulated Brillouin Scattering", in *International Conference on Integrated Optics and Optical Fiber Communication, IOOC'95,* Hong Kong, pp. 109–111, Paper WD2-1, 1995.

[37] H. Kim and P. J. Winzer. "Robustness to laser frequency offset in direct-detection DPSK and DQPSK systems", *Journal of Lightwave Technology*, vol. 21, no. 9, pp. 1887–1891, September 2003.

[38] S. Ferber, S. Watanabe, R. Ludwig, C. Boerner, C. Schmidt-Langhorst, L. Molle, K. Habel, M. Rohde, H. G. Weber, and F. Futami. "160 Gb/s regenerating conversion node", in *Technical Digest of the Optical Fiber Communication Conference, OFC'04,* Los Angeles, California, U.S.A., Paper ThT2, February 2004.

[39] K. Mishina, A. Maruta, S. Mitani, T. Miyahara, K. Ishida, K. Shimizu, T. H. andKuniaki Motoshima, and K. ichi Kitayama. "All-optical format conversion from NRZ-OOKto RZ-BPSK using SOA-MZI wavelength converter", in *Technical Digest of the Optical Fiber Communication Conference, OFC'06,* Anaheim, California, U.S.A., Paper OThB2, March 2006.

[40] C. Schmidt-Langhorst, R. Ludwig, M. Galili, B. Huettl, F. Futami, S. Watanabe, and C. Schubert. "160 Gbit/s all-optical OOK to DPSK in-line format conversion", in *Proceedings of the European Conference on Optical Communication, ECOC'06,* Cannes, France, Paper Th4.3.5, September 2006.

[41] M. Galili, B. Huettl, C. Schmidt-Langhorst, R. Ludwig, F. Futami, S. Watanabe, and C. Schubert. "All-Optical Combination of DPSK and OOK to 160 Gbit/s DQPSK Data Signals", in *Technical Digest of the Optical Fiber Communication Conference, OFC'07,* Anaheim, California, U.S.A., Paper OThI5, March 2007.

[42] M. Jinno. "Effects of crosstalk and timing jitter on all-optical time-division demultiplexing using a nonlinear fiber Sagnac interferometer switch", *IEEE Journal of Quantum Electronics*, vol. 30, no. 12, pp. 2842–2853, December 1994.

[43] A. T. Clausen, J. Bennike, L. K. Oxenlowe, J. Seoane, A. I. Siahlo, and P. Jeppesen. "Pilot tone modulation used for channel identification in OTDM networks", in *Technical Digest of the Conference on Lasers and Electro-Optics, CLEO'04,* San Francisco, California, U.S.A., Paper CThQ7, May 2004.

[44] M. Kagawa, H. Murai, H. Tsuji, and K. Fujii. "160 Gbit/s OTDM channel identification using optical phase index with 40 Gbit/s clock recovery circuit", in *Proceedings of the European Conference on Optical Communication, ECOC'05,* Glasgow, Scotland, pp. 441–442, Paper We3.2.4, September 2005.

[45] C. Boerner, C. Schubert, C. Schmidt, E. Hilliger, V. Marembert, J. Berger, S. Ferber, E. Dietrich, R. Ludwig, H. G. Weber, and B. Schmauss. "160 Gbit/s clock recovery with electro-optical PLL using a bidirectionally operated electroabsorption modulator as phase comparator", in *Technical Digest of the Optical Fiber Communication Conference, OFC'03,* Atlanta, Georgia, U.S.A., pp. 670–671, Paper FF3, March 2003.

[46] T. Shimizu, H. Kurita, and H. Yokoyama. "All-optical clock extraction performance of a mode-locked diode laser with a novel external-cavity configuration", in *Technical Digest of the IEEE Lasers and Electro-Optics Society Annual Meeting, LEOS'98,* Orlando, Florida, U.S.A., pp. 8–9, December 1998.

[47] M. Galili, L. K. Oxenløwe, A. T. Clausen, and P. Jeppesen. "320 Gbit/s Simultaneous Clock Recovery and Channel Identification", in *Proceedings of the European Conference on Optical Communication, ECOC'07,* Berlin, Germany, September 2007.

[48] L. Jie, B. E. Olsson, M. Karlsson, and P. A. Andrekson. "OTDM demultiplexer based on XPM-induced wavelength shifting in highly nonlinear fiber", *IEEE Photonics Technology Letters*, vol. 15, no. 12, pp. 1770–1772, December 2003.

[49] K. Uchiyama and T. Morioka. "All-optical signal processing for 160 Gbit/s/channel OTDM/WDM systems", in *Technical Digest of the Optical Fiber Communication Conference, OFC'01,* Anaheim, California, U.S.A., Paper ThH2, March 2001.

[50] M. Nakazawa, T. Hirooka, F. Futami, and S. Watanabe. "Ideal distortion-free transmission using optical Fourier transformation and Fourier transform-limited optical pulses", *IEEE Photonics Technology Letters*, vol. 16, no. 4, pp. 1059–1061, April 2004.

[51] L. K. Oxenløwe, M. Galili, A. T. Clausen, and P. Jeppesen. "Generating a square switching window for timing jitter tolerant 160 Gb/s demultiplexing by the optical Fourier transform technique", in *Proceedings of the European Conference on Optical Communication, ECOC'06,* Cannes, France, pp. 73–74, Paper We2.3.4, September 2006.

[52] L. K. Oxenløwe, M. Galili, H. C. Mulvad Hansen, A. T. Clausen, and P. Jeppesen. "Reduced timing sensitivity in all-optical switching

using flat-top control pulses obtained by the optical fourier transform technique", in *International Conference on Photonics in Switching,* Heraklion, Greece, Paper O9.3, October 2006.

[53] J. H. Lee, L. K. Oxenlwe, M. Ibsen, K. S. Berg, A. T. Clausen, D. J. Richardson, and P. Jeppesen. "All-optical TDM data demultiplexing at 80 Gb/s with significant timing jitter tolerance using a fiber Bragg grating based rectangular pulse switching technology", *Journal of Lightwave Technology*, vol. 21, no. 11, pp. 2518–2523, November 2003.

[54] L. K. Oxenløwe, F. Parmigiani, M. Galili, D. Zibar, A. T. Clausen, M. Ibsen, P. Petropoulos, D. J. Richardson, and P. Jeppesen. "160 Gb/s retiming using rectangular pulses generated using a superstructured fibre Bragg grating", in *Proceedings of the OptoElectronics and Communications Conference, OECC'07,* Yokohama, Japan, July 2007.

[55] F. Parmigiani, L. Oxenløwe, M. Galili, M. Ibsen, D. Zibar, P. Petropoulos, D. Richardson, A. Clausen, and P. Jeppesen. "All-optical 160 Gbit/s RZ data retiming system incorporating a pulse shaping fibre Bragg grating", in *Proceedings of the European Conference on Optical Communication, ECOC'07,* Berlin, Germany, September 2007.

[56] M. Kulishov, Y. Park, J. Azaña, and R. Slavík. "(Sub-)Picosecond Flat-Top Waveform Generation using a Single Uniform Long-Period Fiber Grating", in *Proceedings of the European Conference on Optical Communication, ECOC'06,* Cannes, France, Paper We2.3.7, September 2006.

[57] R. Slavík, Y. Park, M. Kulishov, R. Morandotti, and J. Azaña. "Ultrafast all-optical differentiators", *Optics Express*, vol. 14, no. 22, pp. 10699–10707, October 2006.

[58] L. K. Oxenløwe, R. Slavik, M. Galili, H. Mulvad, Y. Park, J. Azaña, and P. Jeppesen. "Flat-top pulse enabling 640 Gb/s OTDM demultiplexing", in *Technical Digest of the European Conference on Lasers and Electro-Optics, CLEO Europe'07,* Munich, Germany, Paper CI8-1, June 2007.

[59] L. K. Oxenløwe, M. Galili, R. Slavík, H. C. H. Mulvad, A. T. Clausen, Y. Park, J. Azaña, and P. Jeppesen. "400 fs flat-top pulse for error-free timing jitter tolerant 640 Gb/s demultiplexing using a long-period grating", in *Proceedings of the European Conference on Optical Communication, ECOC'07,* Berlin, Germany, September 2007.

[60] F. Parmigiani, P. Petropoulos, M. Ibsen, and D. J. Richardson. "All-optical pulse reshaping and retiming systems incorporating pulse shaping fiber Bragg grating", *Journal of Lightwave Technology*, vol. 24, no. 1, pp. 357–364, January 2006.

[61] P. Petropoulos, M. Ibsen, A. D. Ellis, and D. J. Richardson. "Rectangular pulse generation based on pulse reshaping using a superstructured fiber Bragg grating", *Journal of Lightwave Technology*, vol. 19, no. 5, pp. 746–752, May 2001.

[62] R. G. Smith. "Optical Power Handling Capacity of Low Loss Optical Fibers as Determined by Stimulated Raman and Brillouin Scattering", *Applied Optics*, vol. 11, no. 11, pp. 2489–2494, November 1972.

[63] G. P. Agrawal. *Fiber-Optic Communciation Systems.* Wiley, Second edition, 1997. ISBN 0-471-17540-4.